NASA CR-66277

ENGINEERING STUDY and EXPERIMENT DEFINITION for an APOLLO APPLICATIONS PROGRAM EXPERIMENT on VEHICLE DISTURBANCES DUE TO CREW ACTIVITY

MARCH 1967

J. R. Tewell
C. H. Murrish

Prepared under Contract No. NAS1-6713 by
MARTIN MARIETTA CORPORATION

For

National Aeronautics and Space Administration

NASA CR-66277

ENGINEERING STUDY AND EXPERIMENT DEFINITION FOR AN APOLLO APPLICATIONS PROGRAM EXPERIMENT ON VEHICLE DISTURBANCES DUE TO CREW ACTIVITY

By
J. R. Tewell
C. H. Murrish

Prepared under Contract No. NAS1-6713 by

MARTIN MARIETTA CORPORATION

for

NATIONAL AERONAUTICS AND SPACE ADMINISTRATION

FOREWORD

This final report was prepared under Contract No. NAS1-6713 and was approved for publication by NASA, Langley Research Center letter NAS1-6713(CEK).

This report is a result of a team effort in close cooperation with the NASA Technical Monitor Mr. Bruce Conway. The Martin Marietta Corporation's Denver Division overall effort was directed by Dr. Charles H. Murrish and ably seconded by J. Robert Tewell.

The implementation of the digital simulation was carried out by Charles H. Johnson and Larry D. Burrows. Richard A. Skidmore not only acted as the test subject but detailed the flight plan, designed the simulator mockups, and assisted in the actual preparation of this report.

Mr. Robert G. Brown and Fred J. Greeb detailed the digital attitude and attitude rate system, and Peter Corveleyn carried out the necessary modifications to the limb motion sensor.

CONTENTS

ENGINEERING STUDY AND EXPERIMENT DEFINITION FOR AN APOLLO APPLICATIONS PROGRAM EXPERIMENT ON VEHICLE DISTURBANCES DUE TO CREW ACTIVITY

By

J. R. Tewell and C. H. Murrish
Martin Marietta Corporation

SUMMARY

Because of the lack of data regarding the effects of man's activities in orbit in his spacecraft, an Apollo Applications Program (AAP) flight experiment has been proposed to investigate crew motion disturbances. As part of the overall experiment development, NASA Contract NAS1-6713 was awarded to the Martin Marietta Corporation's Denver Division to perform an engineering study to define an in-orbit experiment that would yield realistic data in this area. The study included both analysis and direct simulation. Typical crew motions were selected on the basis of frequency of occurrence during normal orbital operations and those activities associated with the AAP experiments.

This report is presented in two parts, a technical report and a data supplement. The technical report is self-contained in that it presents a complete technical description of the study program and a condensation of the most significant data as it affects a space vehicle.

In addition, a 16-mm silent movie was made of all the simulation studies and constitutes a significant contribution, in a qualitative way, to the numerical data.

The report itself outlines the selection of the crew motions studied, the analytic and direct simulation approaches, and defines the required instrumentation for an in-orbit experiment duplicating those activities studied. A detailed orbital experiment plan, including a NASA Form 1138, is also developed.

As an illustration of the significant results of this study, it was found that the simple process of raising and lowering one arm can produce a change in attitude angle of 0.00075° (approximately 3 arc-sec) in a matter of 1 sec for uncontrolled space vehicles typical of the AAP.

INTRODUCTION

The increased degree of sophistication of orbital experiments together with added emphasis on man's participation has placed severe requirements on the attitude stability of space vehicles. Realistic assessment of reaction control system fuel requirements, valid control system design and development, and knowledge of the ability to obtain precise attitude control are dependent on the knowledge of disturbances on the space vehicle. Not the least of these disturbances are those induced by crew activity.

The pointing accuracies required for certain AAP experiments are such that not only vehicle configuration and control system design but also crew activity must be given careful consideration. This study gives particular attention to the latter. The results of a review of AAP experiments, insofar as crew activity is considered, is used to develop an experiment to determine the effects of this activity on a space vehicle attitude. Certain typical activities common to a number of missions are then detailed and an orbital experiment defined. The experiment is defined in such a way as to enable the widest application of the results.

Paramount to the definition of this experiment is a realistic ground-based evaluation of man's activity in an orbital environment. This evaluation was based on the use of the Denver Division's six-degree-of-freedom servo-driven simulator programed with the dynamical equations of motion of man. A digital computer was used for data reduction and verification of the simulation results. In addition, a parallel digital study was made on man and the vehicle using three prominent Apollo vehicle configurations.

The ability to measure the effects of crew activity in orbit is a prerequisite to the experiment. A detailed analysis of the measurement requirements was made and an instrumentation plan developed. This instrumentation plan includes the measurement of vehicle attitude and attitude rate for rates below the threshold of presently defined systems for the Apollo program. In addition, direct measurement of the forces imposed on the vehicles by crew activity are provided for, where feasible. For these measurements to be meaningful, a method for accurately defining the crew motion is necessary. This definition is provided for by means of a limb motion sensor (LIMS) developed by the Denver Division. LIMS provides for definition of crew activity through a direct measurement of joint rotation of the principal body joints.

LIMS was extensively used in the simulation exercises to generate input data to the dynamical equations of motion as well as to provide limb motion history for correlation of the simulation results with those obtained from the actual flight experiment.

Previous studies of man's activities in a gravity-free environment have been performed in water with a neutral buoyancy condition, in a sling arrangement, or in large aircraft flying a Keplerian trajectory. The damping effects of the water, in underwater testing, severely restrict the effects of man's activity on any reacting body. The sling arrangements unduly restrict man's motion, and the aircraft flights for zero gravity are of such short duration that little useful information can be obtained. It is for these reasons that the capabilities of a servo-driven simulator were brought to bear on this problem.

A significant effort was made to reduce the raw data to a form most applicable to the stability control problem, in terms of pertinent force levels and their effects on three Apollo vehicle configurations. These configurations are:

Configuration 1 - Apollo command and service module;

Configuration 2 - Command and service module, multiple docking adapter, airlock module, and Saturn S-IVB workshop;

Configuration 3 - Apollo cluster configuration.

These vehicle configurations are illustrated in figures 1, 2, and 3, and their properties are listed in Table I.

TABLE I.-PHYSICAL PROPERTIES OF AAP VEHICLES

Configuration	Weight, lb	Location of center of mass, in.[a]			Inertia, slug ft^2		
		x	y	z	x	y	z
1	24 860	965.4	-2.3	7.1	13 862	46 870	47 840
2	68 833	1738.3	4.1	1.3	114 735	1 967 770	1 930 880
3	87 861	1770.8	3.3	-7.5	311 728	2 179 040	1 987 350

[a]See figures 30, 34, and 38 for center-of-mass reference axes.

Configuration 1 was included primarily because the effects of crew activity are most pronounced in this vehicle and the attitude control system fuel supply is somewhat limited. Configuration 2 was considered since this vehicle is the most likely candidate for the orbital experiment. Configuration 3 was treated since it is the configuration associated with the ATM experiment where precise attitude stability is required.

The problem of presenting data in a meaningful format to satisfy the needs of a wide audience was found to be extremely difficult. As a result, the most significant data, with regard to the effects on vehicle attitude, are presented in the body of this report. All of the disturbance force and moment data, as well as the digital tab runs, are included in an off-standard size supplement as Appendixes B, C, D, and E. In addition to the data, a 16-mm silent movie of all the direct simulation was made.

SPECIAL SYMBOLS AND ABBREVIATIONS

AAP	Apollo Applications Program
AM	airlock module
ATM	Apollo telescope mount
Astro	astronaut
C	capacitor or capacitance
CSM	command and service module
$C\psi$, $C\theta$, $C\varphi$	Cosine ψ, Cosine θ, Cosine φ
DAR	digital attitude and attitude rate sensing system
D	transformation matrix
DOF	degree-of-freedom
d	element of a transformation matrix
E	unit dyad

E_o	rms value of output voltage
EAI	Electronic Research Associates, Inc.
EVA	extravehicular activity
F	force, lb
FREQ. DISCR.	frequency discriminator
H	angular momentum vector
I	inertia dyad, slug-ft^2
I_T	rms value of input current in A
IVA	intravehicular activity
i	current in A
i, j, k	orthogonal unit vectors
LIMS	limb motion sensor
LM	lunar module
MDA	multiple docking adapter
M	moment, ft-lb
m	mass in slugs or subscript denoting model man
NRZ	nonreturn to zero
OSC.	oscillator
PCM	pulse code modulation
POT	potentiometer
p, q, r	body fixed roll, pitch, and yaw angular rates in deg/sec or rad/sec
Q	$m_m m_s / \left(m_m + m_s\right)$

R, r	position vectors in ft
R and R	rest and relaxation
R_i	the i-th resistance element in a circuit
RCVR	receiver
RGS	rate gyro system
RM	resupply module
S	Laplace transform operator
SAA or S/AA	Saturn Apollo Applications
S/C	spacecraft
SLA	Saturn launch adapter
$S\psi$, $S\theta$, $S\varphi$	sine ψ, sine θ, sine φ
SOS	space operations simulator
s	subscript denoting spacecraft
T	system time constant
TM	telemetry system
t	time in sec
V/F	voltage to frequency
W_i	angular frequency in rad/sec
w, W	subject weight in lb
XMTR	transmitter
x, y, z	coordinate axes
x_{ms}, y_{ms}, z_{ms}	displacement of the center of mass of man from the center of mass of the spacecraft along the appropriate axis

ρ	position vector in ft
φ, θ, ψ	roll, pitch, and yaw angles in deg or rad
ω	angular velocity in deg or rad/sec

TYPICAL CREW MOTIONS

The motions typical of crew activity in any space mission can be divided into three categories associated with three activity areas. The activity areas are those associated with routine flight, housekeeping and sanitation, and experiments. The categories are involuntary motions (breathing, coughing, etc), in-place motions (operations of controllers, switches, and knobs on a control panel, exercise, etc), and translational motions (walking, soaring, etc).

During the initial effort to define which of these crew motions would be considered, it was necessary to apply certain constraints. It was desired to be able to correlate the in-flight data with the data obtained through simulation. Thus, there existed three constraints applicable to the crew motions to be examined, namely space vehicle interior configuration (CSM-S-IVB workshop), AAP experiment activities, and limitations imposed by simulation techniques.

In examining vehicle configurations, NASA-Houston was visited to obtain details on the command module. The Houston mockup was examined, and several structural and crew station drawings and photographs were obtained. A full-scale drawing of the command module Block II console was obtained and used in the simulation mockup. Conferences were held with the Apollo design and human factors groups that assisted in developing a total picture of the Apollo vehicle configurations and in defining the orbital housekeeping tasks performed by the crew.

A review of the then defined AAP experiments revealed that the level of detail for each experiment was such that extraction of meaningful data with regard to discrete crew activities or movements was not possible. As a result, it was decided to define a series of "typical" movements, common not only to many of the experiment activities, but also common to routine flight operations. These typical crew activities range from normal breathing to gross body impacts against the vehicle structure.

The third constraint imposed on the experiment plan was to interpret the simulation limitations into the proposed crew activity list. Restrained crew activities, such as console operations, were conducted on a mockup of the Apollo couch. This limited the limb and body motions to simply those of the arms, legs, and head. Unrestrained activities were carried out on Martin Marietta's space operations simulator (SOS), which is described in detail in a later paragraph. In simulating these activities, the test subject is mounted on a six-degree-of-freedom servo-driven head. Structural mockups were constructed so that the safety of the test subject was not jeopardized.

In actually carrying out the crew motions associated with this experiment, it was assumed that the crew members not performing the typical motions were immobilized. Those motions deemed representative are delineated in Table II, which constitutes the crew motion matrix.

TABLE II.-CREW MOTION MATRIX

Activity	Activity description	Frequency of occurrence	Location in spacecraft where activity can occur
Breathing/heart action	Normal and deep breathing, obviously heart action must be included since it is measurable	Continuous, will only affect vehicle attitude when astronaut is restrained	Anywhere in the total cluster where an astronaut can be restrained or can react against the vehicle
Coughing	Self-evident	Intermittent (low frequency), will only affect vehicle attitude when astronaut is restrained	Anywhere in the total cluster where an astronaut can be restrained or can react against the vehicle
Sneezing	Self-evident	Intermittent (low frequency), will only affect vehicle attitude when astronaut is restrained	Anywhere in the total cluster where an astronaut can be restrained or can react against the vehicle
Pure arm movements	Right and left arm movements in the frontal and sagittal planes with minimum elbow bending	Only applicable to TO-13 experiment	S-IVB workshop where experiment TO-13 is conducted
Typical console operations	Right and left arm movements to the main console in the CM, all three couch locations were used	Continuous for one astronaut during watch, intermittent for EVA and experiment activities	Main and auxiliary control panels in CM and LM, auxiliary panels in AM and S-IVB workshop
Exercise	Cardiovascular stimulus using Gemini/Apollo elastic cord exerciser or Apollo ergometer; arms, right leg, left leg, and both legs	Three 10-minute exercise periods per man per day, two men can exercise at the same time	Exercise in CM couch until S-IVB workshop is activated
Soaring and impacts	Translational movements where the astronaut pushes away from vehicle structure and must stop at a new location, can be applied to IVA and EVA	Any time astronaut translation takes place	Generally applicable to large areas as in S-IVB workshop
Tunnel translation	Translational movements through enclosed areas such as the CM to LM tunnel, AM to LM tunnel, and through the AM	Intermittent, probably several times per day	CM to LM tunnel, AM to LM tunnel, translation through AM
Guided soaring	Activities where a structure-to-structure bouncing translation may take place	Intermittent, but with a high frequency	LM, AM, MDA, and S-IVB workshop
Compressive walking	Activities where the astronaut can support himself with hands and feet between structure and translate	Intermittent, but with a high frequency	CM, LM, AM, MDA, S-IVB, and RM
Velcro walking	Activities where Velcro is used to restrain or support an astronaut, some translation can take place	Intermittent, with moderate frequency	CM, LM, AM, MDA, and S-IVB
Mass transfer	Transfer of equipment by astronauts within the individual vehicles and throughout the cluster	Intermittent, with moderate frequency	CM, LM, AM, MDA, RM, and S-IVB

CREW DISTURBANCE SIMULATION

The crew disturbance simulation was divided into two parts, each requiring a different simulation setup. The first setup was used for restrained (nontranslational) crew activities, while the second satisfied the translational activities.

Restrained Crew Activity and Simulation

The restrained crew activities such as breathing, exercising, and console operations were conducted on an Apollo couch mockup mounted rigidly to a load cell array as shown in figure 4. As activity is performed, the load cells measure the forces and moments generated. The load cell geometry and the equations required are found in Appendix A.

As an integral part of the simulation, a unique instrumentation system was developed to enable the recording of limb motion history. The LIMS can be seen on the astronaut in figure 5. The LIMS is a skeletal structure with pivots located at the major joints of the human body and allows almost unlimited freedom of motion (fig. 6). Each pivot contains a linear potentiometer supplied with direct voltage, so that the output voltage is directly proportional to joint rotation. Therefore, the knowledge of these angles provides instantaneous limb position.

Involuntary actions.- The subject was restrained in a horizontal position on the Apollo couch mockup and was instructed to be as relaxed and immobile as possible. Normal breathing disturbance levels were recorded and are shown in figure 7. The heart beat disturbance is the 5-cups pulse train generated approximately every second, and the breathing disturbance is the low-frequency signal superimposed with the heart beat signal.

Accelerated breathing, figure C-2 (complete data recordings for restrained crew activities, figure C-2 etc, are contained in Appendix C), produced a more random signal and, the disturbance levels increased by a factor of two above normal breathing. Simulated sneezes and coughs were performed to the best of the subject's ability and are shown in figures C-3 and C-4, respectively.

Voluntary actions.- Pure arm motions in the sagittal and frontal planes were made and data recorded as shown in figures C-5 thru C-8. These motions were used to provide baseline data. The simulation

curves generally follow those that are theoretically expected (for example, refer to figure C-5). As the right arm is initially raised in the sagittal plane, the arm accelerates in the negative z direction. This produces a positive 10-lb reaction force on the load cell. This is followed by a negative 10-lb force developed from the centrifugal forces due to outward arm motion. The final positive pulse results from decleration in the positive z direction. Similarly, the x component of force clearly shows those forces developed as the arm is accelerated and then decelerated in the x-z plane. Pure sagittal plane motion should not develop any y-force component; however, the simulation data show a y component. This indicates variations from a pure arm motion and may also be due to a nonrigid torso, as was theoretically assumed. The curves obtained when the arm is lowered are the reverse to those obtained when the arm is raised. The forces and moments have an average value of zero, as expected.

The left arm pure motions are similar to those of the right with M_{sx} and M_{sz} out of phase for the sagittal plane motion.

Exercise.- The exercise motions were also conducted in the Apollo couch mockup. The scheduled exercise sequence prescribed for the Gemini and first Apollo flights consists of pulling an elastic cord exercise device (an actual exerciser was borrowed from Nasa Houston for the study) extending from the hands to the feet as shown in figure 8. Several combinations of arm and leg motions are used with each exercise series. A series consists of one pull per sec for approximately 45 sec. The exerciser requires 70 lb to achieve maximum extension.

The test subject was instructed to exercise first using only the arms, then each leg individually, and finally both legs. These disturbance characteristics are shown in figures C-9 thru C-12.

The vehicle disturbances created during the exercises result from the accelerations of the subject's center of mass. This is illustrated by the forces in the x direction that progressively increase from 15 lb during the arm exercise to 40 lb while exercising both legs.

Console operation.- The typical control console arm movements were made with the arm moving from a rest position near the body to the face of the control console. The subject was instructed to reach out from the rest position to a designated area on the console, make switching and rotary type motions, and then return

to the rest position. Three typical panel segments used in one astronaut location are shown in figure 9. The left arm was used for panel 12 and the right arm for panels 17 and 19. These disturbance traces are shown in figures C-13 thru C-15.

Translational Activity Simulation

The translational activities were simulated on the SOS which was recently modified and configured for EVA or IVA simulation. Figure 10 shows an artist's concept of the SOS that incorporates a servo-driven six-degree-of-freedom (DOF) moving base controlled by analog computers. The moving base, figure 11, consists of a 3-DOF translational carriage (longitudinal, lateral, elevation) and a 3-DOF attitude head (yaw, pitch, roll). The elevation carriage is supported by a set of negator springs that exert a constant force independent of extension, and thus effectively counterbalance the weight of the elevation carriage and attitude head. Figure 12 shows the gimbaling system of the movable head. The entire installation is housed in a volume 130 ft long, 60 ft wide, and 25 ft high. Performance characteristics are shown in Table III.

TABLE III.-PERFORMANCE CHARACTERISTICS OF SPACE OPERATIONS SIMULATOR

Parameter	x	y	z	Roll	Pitch	Yaw
Max travel, ft or rad	60	±9	±6	±3	±0.3	±0.75
Maximum velocity, fps^2 or rad/sec^2 (step function input)	3.05	2.58	2.44	0.428	0.57	0.39
Maximum acceleration, fps^2 or rad/sec^2 (step function input)	1.03	2.16	3.36	----	3.58	2.0
Bandwidth, cps (displacement input)	0.5	0.5	0.5	0.5	1.2	0.5
Phase shift, deg	45	16	90	12	90	90
Initial lag, sec	0.25	0.063	0.063	0.063	0.063	0.063

For zero-g simulation, the astronaut is on the 3-DOF gimbaled head (fig 13). A worksite containing full-scale mockups of spacecraft structural components is mounted to one wall through a set of load cells. When EVA/IVA is performed on the worksite, the forces and moments generated by contact are measured by the load cell array. This information is conveyed to the computer, which solves the equations of relative motion between the work task area and the astronaut. The computer also generates command voltages that position the servo-driven moving base and gimbal system to provide the proper zero-g reactions on the astronaut. In addition, if the astronaut is wearing the LIMS, complete knowledge of limb positions is available. With the assumption of simple geometric models for the individual anthropometric links, one can formulate dynamic equations of the model man to program on the computer. The LIMS then provides inputs to the computer, which generates the proper self-induced reactions to the astronaut through the simulator servocommands. The functional operation of the simulation is illustrated in figure 14, and the equations of motion appear in Appendix A.

Note that while the complete equations of motion for a spacecraft-astronaut system were developed using a nine-segment model man, the required computer capacity exceeded that of the four EAI 231 R computers available for the simulation. Therefore, the equations of motion were simplified to allow programing on the four computers.

Free soaring and impacts.- This series of activities simulates gross translations of the astronaut from point to point and are also representative of disturbances generated by the astronaut bumping into the spacecraft while donning or doffing the space suit. The soaring sequence was initiated with the subject located 5 ft from the load cell array. An initial velocity was imparted to the SOS carriage towards the load cells. The subject would reach forward, make contact with the plate, decelerate, and stabilize. After stabilization, he pushed off and drifted away (fig. 15). Typical landing and pushoff forces are recorded. A series of trial runs were made to determine typical soaring velocities. The subject indicated what he considered to be slow, medium, and fast inpact velocities. These velocities were established as 0.25, 0.50, and 0.75 fps, respectively.

The disturbance data for typical runs at these soaring velocities are shown in figures 16 thru 19 (complete disturbance data for translational activity are contained in Appendix B). The deceleration pulses, F_{sx}, appear to be flat topped half-cycle sinusoids

of 1.5-sec duration. The maximum values of these pulses are compared with two sets of theoretical values in fig. 20. The first shows the level of force necessary to decelerate the astronaut assuming a constant applied force, while the second assumes a half-cycle sinusoidal deceleration force. The deceleration period was maintained at 1.5 sec.

The simulation results compare favorably. The higher values obtained in the simulation for the 0.75-fps landing was due to the tendency of the test subject to apply more force than necessary for a smooth landing. He would then drift back slowly and apply a negative force to stabilize.

The maximum pushoff force developed was 16 lb, which imparted a velocity of 3.5 fps to the subject. This value is expected to be the upper limit on free soaring rates in space where pure translational control is difficult.

Guided soaring.- Guided soaring is a crew transfer technique where the astronaut bounces from the floor to the ceiling while translating through the spacecraft. The locomotion technique was simulated using a mockup that provided two 2x8-ft reaction surfaces 7 ft apart and mounted to the load cell array. The mockup is shown in figure 21. The guided soaring was conducted between these reaction surfaces and found to be quite easy to control after an initial learning period. Directional control was quite sensitive; in particular, roll was developed as lateral translation was performed.

Figure 22 shows the time history of the disturbances developed, and figure 23 shows the effects of these disturbances on the "cluster" vehicle. The disturbance frequency (subject bounce rate) is 0.25 cps. The 5-cps low amplitude variation represents the mockup resonant frequency. The force trace, F_{sz}, shows that more sensitive control was effected by the hands as compared with that of the feet. The reversal of vertical translation using the hands was provided by a 6-lb force of 2.5- to 3-sec duration, while the feet developed a 10-lb force for 1.5 sec. The F_{sy} pulse is generated by the feet to provide lateral translation and a roll pulse is developed at the same time.

The major mass motion is the vertical displacement given by

$$z_{ms}\ (\text{ft}) = 0.6 \sin 2\pi (0.25)t$$

Differentiating twice and multiplying by the mass of the 180-lb subject yields

$$F_{sz} \text{ (lb)} = 8.3 \sin \pi /2t$$

This sinusoidal disturbing force represents a mean value between the positive 10-lb and negative 6-lb peak of F_{sz}.

Tunnel transfer.- Crew transfer through a tunnel will occur between the CSM and the LM. Since the simulator head will not allow a test subject to translate through an enclosed tunnel, it was necessary to construct the tunnel mockup so that the enclosed portion encircled approximately 200°. This mockup was mounted on the load cell array as shown in figures 24 and 25. The carriage translation in the x direction was inactivated so that the subject would not drift away from the mockup. The subject started by placing his hands on the lower end of the mockup and gently propelled himself through the 6-ft tunnel using only fingers and toes to stabilize and propel himself. Only contact areas inside the tunnel were used. It was found that if an exceptionally good initial pushoff were made, the subject could soar completely through the tunnel with minimal contact (fig. B-5). Figures B-5 and B-6 are in Appendix B, Data Supplement. Other tries required considerable stabilization during the translations (fig. B-6).

The LIMS was not worn during runs plotted in figure B-6, as the potentiometers on the LIMS reduced the amount of room available in the tunnel.

Compressive walking.- The reaction surfaces (fig. 26) used for the guided soaring study were placed closer together so that the subject's hands and feet touched both surfaces at the same time. The task consisted of simply translating laterally between the reaction surfaces while maintaining a stable attitude. This task was not difficult. The test subject could remain stable with only one hand and simulate work tasks with the other.

Velcro walking.- The mockup remained the same as in the compressive walking task except that Velcro pile was bonded to the lower surface of the mockup and Velcro hook to the bottoms of the subject's shoes. These translations were considerably more difficult to control than those without Velcro. Peeling the foot up to take a step created considerable subject instability. Even though these movements were quite sensitive the translations could readily be made. The Velcro bond on the subject's feet was adequate to hold the subject at a worksite so that both hands could

be free. Translations were also made without using the hands for stabilizing. These were accomplished but with considerable difficulty. This translation mode could not be recommended for a space vehicle.

Mass transfer.- The same reaction surface mockup used in the compressive waling and Velcro walking study was used to perform the mass transfer study. Figure 27 shows the configuration. The task simulated was the transfer of a LiOH canister in the CSM from a storage area against the aft equipment bay to the environmental control unit in the left-hand equipment bay. The task consisted of the subject stabilizing in the center of the reaction surfaces, translating to the right-hand end of the mockup, grasping and removing the LiOH canister, translating to the far left-hand end of the mockup with the canister in one hand, returning to the right-hand end, stabilizing and inserting the canister. This task was done both with and without Velcro. Again Velcro made the task more difficult.

A summary of the accumulated data is given in Table IV. These data also include the approximate fundamental frequency associated with the particular crew activity for later comparison with the natural modes of any given vehicular configuration.

TABLE IV.-MAXIMUM FORCES AND MOMENTS

Activity	F_x, lb	F_y, lb	F_z, lb	M_x, ft-lb	M_y, ft-lb	M_z, ft-lb	Frequency, Hz
Soaring, fps							
0.25	8.0	1.0	2.0	0.75	-1.0	-1.2	0.33
0.50	16.0	-1.1	2.25	-4.3	-3.25	4.5	0.40
0.75	2.0	0.5	2.0	1.0	1.0	1.0	0.33
Guided soaring	6.6	4.8	14.0	-22.0	24.0	7.0	0.25
Tunnel transfer	-3.6	2.5	-12.0	-9.1	-8.0	-4.5	0.67
Compressive walking	3.75	2.75	10.0	-8.5	11.25	4.5	0.72
Velcro walking	6.7	-4.5	11.0	-18.0	19.5	14.0	1.0
Velcro compressive walking	10.0	6.5	23.0	19.5	23.0	-8.5	0.72
Canister operation							
Compressive walking	2.5	2.0	5.0	5.5	7.5	2.0	0.72
Velcro Compressive walking	4.5	5.0	9.5	-8.0	18.5	7.5	0.83
Velcro walking	4.5	3.5	10.0	-8.0	19.0	5.0	0.91
Normal breathing	0.75	0.075	0.85	0.12	1.0	0.15	0.83
Accelerated breathing	2.1	1.5	4.5	1.4	3.5	2.3	4.0
Coughing	19.0	-5.5	32.0	-8.0	-30.0	6.0	1.0
Sneezing	6.0	2.5	15.0	3.0	-20.0	3.1	1.0
Pure arm movements							
Right arm Sagittal	16.0	-9.0	11.5	14.0	25.0[a]	20.0	1.0
Frontal	26.0	9.5	8.0	10.5	9.0[a]	19.5	0.83
Left arm Sagittal	17.5	12.5	-13.0	15.5	14.0[a]	-23.0	1.0
Frontal	10.0	7.2	7.5	-16.0	12.0[a]	-20.0	1.0
Panel operations Panel 1	-6.0	1.2	-5.2	-4.3	-5.0[a]	2.6	0.50
Panel 2	5.0	2.6	6.5	5.0	5.0[a]	-2.6	0.50
Panel 3	2.6	1.0	5.0	4.0	3.4[a]	2.2	0.50
Exercise Arms	24.0	5.0	13.0	7.0	31.0[a]	6.5	0.830
Right leg	22.0	12.0	13.0	18.0	24.0[a]	8.5	0.83
Left leg	22.0	12.0	6.0	20.0	30.0[a]	12.5	0.83
Both legs	29.0	18.0	11.0	14.0	28.0[a]	7.0	0.830

[a]Moment in y direction subject to variation from given value due to mass of segment in different locality.

Digital Program

A digital computer program has been developed to simulate astronaut activities and to calculate the resulting forces and moments causing spacecraft angular rates and deflections. The equations used in the program are derived in Appendix A and the program itself is presented in Appendix D. All results from the program are presented in Appendix E. The program is written in Fortran IV and was run on a Control Data 6400 computer.

Although the program was designed to be as flexible and general as possible, only arm angle motions have been used to obtain the results presented in this report. Also, it has been assumed that the torso is fixed rigidly to the spacecraft as is the case when the astronaut is strapped into the couch.

The forces and moments appearing in the results section are calculated at a point corresponding approximately to the spacecraft/astronaut interface, which is also the approximate location of the load cell centroid for the couch study. Forces and moments were also calculated at the spacecraft center of mass.

Two sets of forces and moments are shown on the computer printouts. The "effective" forces and moments are those required to rotate and translate the spacecraft at the calculated rates without the astronaut. These are the forces and moments that would be measured by load cells if they were placed at the spacecraft/astronaut interface. The "actual" forces and moments shown in the results are those required to move the spacecraft plus that part of the astronaut which is not moving relative to the spacecraft. These forces and moments would be measured by load cells if they could be placed, for example, at the right shoulder joint, assuming that the right arm only is moving relative to the spacecraft.

The program also prints out a time history of the arm motions and the spacecraft angular rates and positions. The total instantaneous inertia dyad for the man as a function of arm position is shown on the last page of each run. All angular rates, positions, forces, moments, and the inertia dyad have been calculated in torso coordinates. However, for all runs the spacecraft axes have been aligned with the torso axes so that all printed results can be considered in either torso on spacecraft coordinates.

During checkout of the digital program, simple arm motions following a cosine curve were used as inputs. Examples of results

from the digital program using this type of motion as input are shown in Appendix E under Run A. The equation for the angle variation is given by

$$\varphi_2 = 45^\circ \ (1 - \cos \pi t)$$

where t = 0 to 1 sec and φ_2 is the angle that would be measured by the right upper arm roll potentiometer on LIMS. This arm motion represents a movement of the right arm from the astronaut's side upwards, in a plane 45° between the frontal and sagittal planes, to a horizontal position. The spacecraft chosen for this run has a weight of 40 000 lb, and inertia values of

$$I_{xx} = 40\ 000,\ I_{yy} = 200\ 000, \text{ and } I_{zz} = 200\ 000 \text{ slug-ft}^2$$

The first two sets of results under Run A use identical inputs for arm motions but use a different time interval for the numerical differentiation and integration processes. The first set of results (pp. E-2 thru E-5) was obtained with an 0.0001-sec time interval and the second set with 0.001 sec. Comparison of results shows a negligible difference in angular rates and positions and, at worst, a 6 to 7% difference in forces and moments. These differences were considered too small to justify using a time increment smaller than 0.001 sec (an 0.001-sec interval requires about 3 minutes computer time for one run, while the 0.0001-sec interval requires about 30 minutes).

The remaining results under Run A show the effects of varying the x distance between the spacecraft center of mass and the man's torso center of mass. Peak spacecraft disturbances as a function of separation distances are shown in figures 28 and 29. As expected, roll angeles and rates are not affected, while pitch and yaw angles and rates linearly increase with increasing separation distance.

Run B results were obtained using the Configuration 1 spacecraft and arm motions that more closely approximate an actual arm motion (fig. 30 thru 33). A simple cosine curve fit of an analog trace of a right arm upward motion in a plane between the frontal and sagittal planes was used. These equations are

$$\varphi_2 = -85° \div 65° \cos (2.8t)$$

where

$t = 0$ to 1.2 sec

$$\theta_2 = -15° + 15° \cos (5.6t)$$

where

$t = 0$ to 1.2 sec

$$\psi_2 = 45°$$

$$\theta_4 = 36°$$

where φ_2, θ_2, and ψ_2 correspond to angle measurements of the roll, pitch, and yaw potentiometers respectively of the right upper arm on LIMS, and θ_4 to the pitch potentiometer on the right forearm. Peak angular rates reached 0.0078 (roll), -0.0071 (pitch), and 0.0049 (yaw) °/sec, and peak angular displacements reached 0.0053 (roll), -0.0044 (pitch), and -0.0016 (yaw)°.

For comparison, a run was made using the same angular variation but at one-half the rate of the previous run (fig. 34). The angle equations for this case are

$$\varphi_2 = -85° + 65° \cos (1.4t)$$

where

$t = 0$ to 1.2 sec

$$\theta_2 = 15° + 15° \cos (5.6t)$$

where

$t = 0$ to 1.2 sec

$$\psi_2 = 45°$$

$$\theta_4 = 36°$$

As expected, the peak angular rates are one-half of the above rates, but the peak angular displacements are the same. These results show that the angular displacement due to a disturbance is independent of the time in which the disturbance takes place, and likewise, the angular rates vary in the same manner as the disturbance time varies.

The results of Run B pertain to an astronaut located approximately at the center couch.

Further attempts to obtain more realistic input angles resulted in the method used for Runs C, D, and E. For these runs, actual analog signals from LIMS were digitized by an analog-to-digital converter for a right arm motion, upward in a plane between the frontal and sagittal planes. Although only the right arm moved significantly, signals from all eight arm potentiometers were recorded, and the results appear in Appendix E beginning on p. E-36. The signals were sampled at a rate of 400 samples/sec/channel.

The sampled data (for only the right arm) were then fed into a least-squares curve-fitting computer program to arrive at a polynomial equation analytically describing the data. The following equations, which fit all the data to within a few percent, were obtained:

$$\varphi_2 = -18.725 - 179.867t - 160.146t^2 - 211.411t^3 + 801.373t^4$$

$$\theta_2 = -8.069 + 52.397t - 271.518t^2 - 709.51t^3 - 1037.95t^4 + 5150.5t^5 - 4477.18t^6$$

$$\psi_2 = 47.106 + 72.436t - 1112.04t^2 + 6098.18t^3 - 14654.2t^4 + 13813.1t^5 - 3137.46t^6$$

$$\theta_4 = 25.693 + 47.514t - 953.563t^2 + 6177.4t^3 - 17034.6t^4 + 19860.4t^5 - 7546.65t^6$$

All angles are given in degrees.

Using the above equations for angle inputs, results shown in Appendix E, Run C, D, and E, were obtained. Run C uses the Configuration 1 spacecraft, Run D the Configuration 2 spacecraft, and run E the Configuration 3 spacecraft. For all these runs, the separation distance between the spacecraft center of mass and the torso center of mass was varied along the x and z axes. Also, a run using Configuration 1 was made placing the astronaut approximately in the right command module couch (p. E-63).

The peak spacecraft angular rates and maximum angular deflections (roll, pitch, and yaw) are shown in figures 35 thru 37 as a function of x, y, and z separation distances. The separation distances covered include the approximate duty location of the astronaut in each of the three configurations.

As expected, the results show there is little difference between the effective and actual forces and moments calculated at the astronaut/spacecraft interface. This is due to the fact that the mass and inertia of the man are small compared to the mass and inertia of the spacecraft. The forces that cause spacecraft translations vary very little from run to run and never exceed a magnitude of about 10 lb for the cases considered in this report. The moments causing spacecraft rotations, applied at the astronaut/spacecraft interface, also vary little from run to run and never exceed a magnitude of about 25 ft-lb for the cases considered in this report. The total moments applied to the spacecraft center of mass, however, vary considerably as the separation distances increase. This, of course, is due to the increasing force lever arm. Spacecraft center-of-mass moments approached 300 ft-lb for the cases considered in this report.

For further information concerning the Configuration 3 spacecraft, see figures 38 thru 44.

FLIGHT INSTRUMENTATION ANALYSIS

Prior to the development of the in-orbit experiment instrumentation requirements, it was necessary to detail a flight experiment plan. This plan was developed and a NASA Form 1138, which appears in Appendix F, was prepared.

Flight Experiment Plan

Program.- The data contained in the experiment functional description, timelines, and total flight integration must be considered preliminary, since at the time this integration was made, the S-IVB workshop configuration, cluster configuration, and the total flight timelines were in the process of being developed.

Preliminary assumptions, flight experiment ground rules.- The ground rules are:

Any orbit providing zero g is acceptable for this experiment.

The S-IVB workshop, AM, and MDA will contain a two-gas EC system containing 3.5 psi of O_2 and 1.5 psi of N_2 with a total pressure of 5 psi. The CSM will contain 100% O_2 at 5 psi.

The total experiment will be conducted (once) in the S-IVB workshop.

There is no requirement for pressure suits or EVA during this experiment.

All experimental equipment will be stowed in the MDA or airlock section.

This experiment will make maximum use of equipment assembled in the S-IVB workshop for use on other experiments, such as, communication links, cameras (35-mm still, 16- and 8-mm movie), lights, recorders, electrical power, control and display panels, personnel anchoring tethers, and a personnel chair.

The flight experiment will duplicate the ground simulation as closely as possible and will include:

Involuntary actions (breathing, coughing, and sneezing);

Console operations (restrained activities);

Exercise;

Soaring and impacts;

Crew transfer (tunnel, guided soaring, compressive walking, Velcro walking, and mass transfer).

Experimental data will be recorded and telemetered to the ground at tracking station overpasses for future evaluation.

Basic flight experimental hardware will include LIMS, load cells (minimum of 2, preferably 3), digital attitude rate sensing package, data recording equipment not available from other experiments, and interface equipment (cabling etc).

Preliminary flight experiment assumptions.- Experiment assumptions are:

The experiment will be conducted on Flight AAP-2, day 29, between hr 674.5 and 678. It was necessary to delay preparation for return to earth 3 hr and use 0.5 hr of rest and relaxation time. See fig. 45 and 46.

Two astronauts are located in the S-IVB workshop before the start of the experiment.

All of the experimental equipment, LIMS, DAR package, load cells, recorders, and cameras have been transferred from the MDA to the S-IVB workshop and placed in temporary storage as part of experiment N-487 (the initial workshop setup).

The total experiment can be run once in AAP-2, or once in AAP-2 and once in AAP-4, or only once in AAP-4.

Total flight experiment, functional description.- The total flight experiment functional description outlines all of the activities that must take place before and after the experiment. Two astronauts are required to conduct this experiment. One must assist the experimental astronaut but must remain restrained and immobile during the experiment unless a specific task is required of him, such as to change camera film. Tasks such as turning the cameras and recorders on and off will be done with a hand-held switch.

The third astronaut will conduct his normal watch activities in the CM; however, during the experiment he must remain restrained and as immobile as possible.

The detailed experiment functional description contains a step-by-step detailed description of the actual experiment. Times given in the following functional descriptions are preliminary and probably can be shortened considerably.

	Approximate time, minutes
1. Take experimental equipment out of temporary storage in S-IVB.	10
2. Unpackage and mount experimental equipment (including cameras) at worksite in S-IVB.	10
3. Attach interface wiring to load cells, DAR package, and recording equipment.	3
4. Turn on and calibrate above equipment.	10
5. Turn on DAR package (20-minute warmup).	0.2
6. Assemble LIMS.	15
7. Don LIMS, attach interface cabling, and calibrate potentiometers.	20
8. Activate minimum impulse stability mode (at CSM). Allow 10 to 15-minute stabilization time.	10
9. Position astronaut at experiment location.	2

10.	Activate all experimental equipment and place cameras on standby.	2
11.	Restrain astronauts not in experiment.	3
12.	Disable spacecraft attitude thrusters.	0.2
13.	Record total spacecraft drift and attitude rate in all axes.	2
14.	Activate cameras (intermittent operation).	0.2
15.	Perform experimental sequence, partial and total body movements (see detailed description).	101
16.	Deactivate cameras and recorders.	0.4
17.	Verify data collection accuracy.	3
18.	Turn off all experimental equipment.	0.5
19.	Activate spacecraft stabilization system.	1
20.	Remove LIMS and restrain in S-IVB workshop.	4
21.	Stow movie film in CSM.	7
	Total*	204.5

Detailed experiment functional description.- The following detailed tasks are performed:

		Astronaut†	Time, minutes
1.	Activate vehicle attitude rate recorders (DAR) and record for 30 sec.	2	0.5

*As a more accurate timeline evolves, this total time will be shortened, since several tasks can be done simultaneously by the astronaut.

†Astronaut 1 in CSM, Astronaut 2 experiment assistant, Astronaut 3 performs experiments.

2.	Activate LIMS, load cell recorders, and cameras.	2	0.1
3.	Experiment astronaut breaths normally for one minute.	3	1.0
4.	Turn off cameras.	2	0.1
5.	Record vehicle rates for 15 sec.	2	0.3
6.	Turn on cameras.	2	0.1
7.	Experiment astronaut breaths heavy for 30 sec.	3	0.5
8.	Turn off cameras.	2	0.1
9.	Record vehicle rates for 15 sec.	2	0.3
10.	Turn on cameras.	2	0.1
11.	Experiment astronaut coughs twice with 5-sec interval	3	0.2
12.	Turn off cameras.	2	0.1
13.	Record vehicle rates for 15 sec.	2	0.3
14.	Experiment astronaut coughs twice with 5-sec interval.	3	0.2
15.	Record vehicle rates for 15 sec.	2	0.3
16.	Experiment astronaut coughs twice with 5-sec interval.	3	0.2
17.	Record vehicle rates for 15 sec.	2	0.3
18.	Turn on cameras.	2	0.1
19.	Experiment astronaut sneezes twice with 5-sec interval.	3	0.2
20.	Turn off cameras	2	0.1
21.	Record vehicle rates for 15 sec.	2	0.3

22.	Experiment astronaut sneezes twice with 5-sec interval.	3	0.2
23.	Record vehicle rates for 15 sec.	2	0.3
24.	Experiment astronaut sneezes twice with 5-sec interval.	3	0.2
25.	Record vehicle rates for 15 sec.	2	0.3
26.	Turn on cameras.	2	0.1
27.	Experiment astronaut extends and retracts right arm in frontal plane.	3	0.1
28.	Turn off cameras.	2	0.1
29.	Record vehicle rates for 15 sec.	2	0.3
30.	Turn on cameras.	2	0.1
31.	Experiment astronaut extends and retracts right arm in frontal plane.	3	0.1
32.	Turn off cameras.	2	0.1
33.	Record vehicle rates for 15 sec.	2	0.3
34.	Turn on cameras.	2	0.1
35.	Experiment astronaut extends and retracts right arm in frontal plane.	3	0.1
36.	Turn off cameras.	2	0.1
37.	Record vehicle rates for 15 sec.	2	0.3
38.	Turn on cameras.	2	0.1
39.	Experiment astronaut extends and retracts left arm in frontal plane.	3	0.1
40.	Turn off cameras.	2	0.1
41.	Record vehicle rates for 15 sec.	2	0.3

42.	Turn on cameras.	2	0.1
43.	Experiment astronaut extends and retracts left arm in frontal plane.	3	0.1
44.	Turn off cameras.	2	0.1
45.	Turn off recorders.	2	0.1
46.	Replace film in cameras.	2	2.0
47.	Turn on vehicle rate recorders and record for 30 sec.	2	0.5
48.	Turn on load cell and LIMS recorders.	2	0.1
49.	Turn on cameras.	2	0.1
50.	Experiment astronaut extends and retracts left arm in frontal plane.	3	0.1
51.	Turn off cameras.	2	0.1
52.	Record vehicle rates for 15 sec.	2	0.3
53.	Turn on cameras.	2	0.1
54.	Experiment astronaut extends and retracts right arm in sagittal plane.	3	0.1
55.	Turn off cameras.	2	0.1
56.	Record vehicle rates for 15 sec.	2	0.3
57.	Turn on cameras.	2	0.1
58.	Experiment astronaut extends and retracts right arm in sagittal plane	3	0.1
59.	Turn off cameras.	2	0.1
60.	Record vehicle rates for 15 sec.	2	0.3
61.	Turn on cameras.	2	0.1

62.	Experiment astronaut extends and retracts right arm in sagittal plane.	3	0.1
63.	Turn off cameras.	2	0.1
64.	Record vehicle rates for 15 sec.	2	0.3
65.	Turn on cameras.	2	0.1
66.	Experiment astronaut extends and retracts left arm in sagittal plane.	3	0.1
67.	Turn off cameras.	2	0.1
68.	Record vehicle rates for 15 sec.	2	0.3
69.	Turn on cameras.	2	0.1
70.	Experiment astronaut extends and retracts left arm in sagittal plane.	3	0.1
71.	Turn off cameras.	2	0.1
72.	Record vehicle rates for 15 sec.	2	0.3
73.	Turn on cameras.	2	0.1
74.	Experiment astronaut extends and retracts left arm in sagittal plane.	3	0.1
75.	Turn off cameras.	2	0.1
76.	Record vehicle rates for 15 sec.	2	0.3
77.	Turn on cameras.	2	0.1
78.	Experiment astronaut extends right arm to prepositioned control console, makes switching action, and retracts arm.	3	0.2
79.	Turn off cameras.	2	0.1
80.	Record vehicle rates for 15 sec.	2	0.3
81.	Turn off cameras.	2	0.1

82.	Repeat Step 78.	3	0.2
83.	Turn off cameras.	2	0.1
84.	Record vehicle rates for 15 sec.	2	0.3
85.	Turn on cameras.	2	0.1
86.	Repeat Step 78.	3	0.2
87.	Turn off cameras.	2	0.1
88.	Record vehicle rate for 15 sec.	2	0.3
89.	Turn on cameras.	2	0.1
90.	Experiment astronaut extends left arm to prepositioned control console, makes switching action, and retracts arm.	3	0.2
91.	Turn off cameras.	2	0.1
92.	Record vehicle rates for 15 sec.	2	0.3
93.	Turn off recorders.	2	0.1
94.	Replace film in cameras.	2	2.0
95.	Turn on vehicle rate recorders and record for 30 sec.	2	0.5
96.	Turn on load cell and LIMS recorder.	2	0.1
97.	Turn on cameras.	2	0.1
98.	Repeat Step 90.	3	0.2
99.	Turn off cameras.	2	0.1
100.	Record vehicle rates for 15 sec.	2	0.3
101.	Turn on cameras.	2	0.1
102.	Repeat Step 90.	3	0.2

103.	Turn off cameras.	2	0.1
104.	Record vehicle rates for 15 sec.	2	0.3
105.	Experiment astronaut unstows exerciser and assumes position for both leg exercises.	3	0.5
106.	Turn on cameras.	2	0.1
107.	Experiment astronaut conducts both leg exercises for 15 sec.	3	0.3
108.	Turn off cameras.	2	0.1
109.	Record vehicle rates for 30 sec.	2	0.5
110.	Turn on cameras.	2	0.1
111.	Repeat Step 107.	3	0.3
112.	Turn off cameras.	2	0.1
113.	Record vehicle rates for 30 sec.	2	0.5
114.	Turn on cameras.	2	0.1
115.	Repeat Step 107.	3	0.5
116.	Turn off cameras.	2	0.1
117.	Record vehicle rate for 30 sec.	2	0.5
118.	Experiment astronaut assumes position between load cells.	3	1.5
119.	Turn on cameras.	2	0.1
120.	Experiment astronaut conducts three pushoffs, stops, and stabilizes.	3	2.0
121.	Turn off cameras.	2	0.1
122.	Record vehicle rates for 30 sec.	2	0.5
123.	Turn off recorders.	2	0.1

124.	Replace film in cameras.	2	2.0
125.	Activate recorders and record vehicle rate for 30 sec.	2	0.5
126.	Turn on cameras.	2	0.1
127.	Repeat Step 120.	3	2.0
128.	Turn off cameras.	2	0.1
129.	Record vehicle rates for 30 sec.	2	0.5
130.	Turn on cameras.	2	0.1
131.	Repeat Step 120.	3	2.0
132.	Turn off cameras.	2	0.1
133.	Record vehicle rate for 30 sec.	2	0.5
134.	Turn off recorders.	2	0.1
135.	Replace film in cameras.	2	2.0
136.	Position experiment astronaut in S-IVB crew transfer tunnel.	3	1.0
137.	Turn on recorders and record vehicle rates for 30 sec.	2	0.5
138.	Turn on LIMS recorder.	2	0.1
139.	Experiment astronaut translates full length of S-IVB crew transfer tunnel, returns, and stabilizes	3	2.0
140.	Record vehicle rates for 30 sec.	2	0.5
141.	Repeat Step 139.	3	2.0
142.	Record vehicle rates for 30 sec.	2	0.5
143.	Repeat Step 139.	3	2.0
144.	Record vehicle rates for 30 sec.	2	0.5

145.	Turn off recorders.	2	0.1
146.	Reposition cameras.	2	1.5
147.	Record vehicle rates for 30 sec.	2	0.5
148.	Turn on cameras.	2	0.1
149.	Experiment astronaut translates width of S-IVB workshop using floor to ceiling bounces, and returns.	3	2.0
150.	Turn off cameras.	2	0.1
151.	Record vehicle rates for 30 sec.	2	0.5
152.	Turn on cameras.	2	0.1
153.	Repeat Step 149.	3	2.0
154.	Turn off cameras.	2	0.1
155.	Record vehicle rates for 30 sec.	2	0.5
156.	Turn off recorders.	2	0.1
157.	Replace camera film.	2	2.0
158.	Record vehicle rates for 30 sec.	2	0.5
159.	Turn on cameras.	2	0.1
160.	Repeat Step 149.	3	2.0
161.	Turn off cameras.	2	0.1
162.	Record vehicle rates for 30 sec.	2	0.5
163.	Turn off recorders.	2	0.1
164.	Reposition experiment astronaut at compressive walking task.	3	1.0
165.	Turn on recorders and record vehicle rates for 30 sec.	2	0.5

166.	Turn on cameras.	2	0.1
167.	Experiment astronaut translates (walks) width of S-IVB workshop using hands and feet (floor to ceiling) for support, returns, and stabilizes.	3	2.0
168.	Turn off cameras.	2	0.1
169.	Record vehicle rates for 30 sec.	2	0.5
170.	Turn off recorders.	2	0.1
171.	Replace camera film.	2	2.0
172.	Record vehicle rates for 30 sec.	2	0.5
173.	Turn on cameras.	2	0.1
174.	Repeat Step 167.	3	2.0
175.	Turn off cameras.	2	0.1
176.	Record vehicle rates for 30 sec.	2	0.5
177.	Turn on cameras.	2	0.1
178.	Repeat Step 167.	3	2.0
179.	Turn off cameras.	2	0.1
180.	Record vehicle rates for 30 sec.	2	0.5
181.	Turn off recorders.	2	0.1
182.	Replace camera film.	2	2.0
183.	Experiment astronaut repositions to Velcro walking pad.	3	1.0
184.	Turn on recorders and record vehicle rates for 30 sec.	2	0.5
185.	Turn on cameras.	2	0.1

186.	Experiment astronaut translates (walks) length of Velcro pad without using hands and returns using hand support.	3	2.0
187.	Turn off cameras.	2	0.1
188.	Record vehicle rates for 30 sec.	2	0.5
189.	Turn on cameras.	2	0.1
190.	Repeat Step 186.	3	2.0
191.	Turn off cameras.	2	0.1
192.	Record vehicle rates for 30 sec.	2	0.5
193.	Turn off recorders.	2	0.1
194.	Replace camera film.	2	2.0
195.	Turn on recorders and record vehicle rates for 30 sec.	2	0.5
196.	Turn on cameras.	2	0.1
197.	Repeat Step 186.	3	2.0
198.	Turn off cameras.	2	0.1
199.	Record vehicle rates for 30 sec.	2	0.5
200.	Reposition experiment astronaut at mass transfer task.	3	1.0
201.	Record vehicle rates for 30 sec.	2	0.5
202.	Turn on cameras.	2	0.1
203.	Experiment astronaut unlatches equipment container, translates, and secures container.	3	1.5
204.	Turn off cameras.	2	0.1
205.	Record vehicle rates for 30 sec.	2	0.5

206.	Turn off recorders.	2	0.1
207.	Replace camera film.	2	2.0
208.	Turn on recorders and record vehicle rates for 30 sec.	2	0.5
209.	Turn on cameras.	2	0.1
210.	Repeat Step 203.	3	1.5
211.	Turn off cameras	2	0.1
212.	Record vehicle rates for 30 sec.	2	0.5
213.	Turn on cameras.	2	0.1
214.	Repeat Step 203.	3	1.5
215.	Turn off cameras.	2	0.1
216.	Record vehicle rates for 30 sec.	2	0.5
	Total		101.1

Sensor Requirements and Preliminary Design

There are three classes of sensors required to fully instrument this experiment: those associated with the motion of the astronaut; those dealing with the direct measurement of the actual forces and movements imposed on the vehicle due to astronaut body contact; and those concerned with the measurement of the vehicle attitude and attitude rate.

In addition to these sensors are the interface components required to render the basic sensor outputs compatible with the onboard data management and telemetry equipment. These interface components were not examined in this study. Rather, consideration was given only to the fact that the sensor system outputs could be made compatible with the existing data systems.

Astronaut motion sensors.- The limb motion sensor (LIMS) was developed as an integral part of the SOS. LIMS is fundamentally an external skeleton carrying joint rotation sensors. These sensors are simply linear potentiometers fed by a direct voltage

source and yielding a voltage output proportional to shaft or joint rotation. Part of this study was devoted to the development of a simplified LIMS in which a five-joint shoulder complex was reduced to a three-joint configuration without significantly reducing the mobility of the shoulder. This 3-joint shoulder simplifies the mathematical transformations presented in Appendix A.

The laboratory unit, as seen in the photographs throughout this report, has both a linear and sine-cosine potentiometer at each joint. The sine-cosine potentiometers were used to mechanize some of the transformation matrices, thus reducing the burden on the computing facility. The orbital model would require only the linear potentiometers. The degree of mobility attained by the wearer of LIMS is demonstrated by figure 47, which is a triple exposure of a test subject.

In developing the space-qualified LIMS, certain modifications are required. Particular attention should be given to: redesigning the structural members so as to conceal all electrical wiring; and reducing the size of the potentiometers used at all joints. Consideration should be given to attempt to make the potentiometer integral with the joint.

Two methods of data readout from the LIMS were considered. These consisted of an electrical umbilical and an RF link between the LIMS and the spacecraft. It is recommended that the RF link between the LIMS and the spacecraft be used for the flight experiment, since the umbilical could result in spurious disturbing forces and present a hazard to the test subject as he performs certain of the prescribed exercises.

Two RF systems have been considered during the course of the study program: an FM/FM system and PCM system. Either system would employ an RF transmitter link mounted on the astronaut. A central receiver mounted in the spacecraft would then supply the data in voltage or NRZ form to the main data subsystem.

Figure 48 shows the FM/FM system schematically. The FM/FM subsystem would require 14 subcarrier oscillators, a mixer, a low-power FM transmitter, and an FM receiver with appropriate subcarrier discriminators.

Figure 49 is a schematic of the PCM system. This system is basically a digital encoding system in which each of the 14 potentiometer output values are converted to an 8-bit word, and these data, together with a synchronizing word, are used to modulate

the PCM transmitter. The PCM receiver accepts the data and sends it to the main data system over a hardwire line.

The problem of locating the astronaut within the spacecraft has not yet been adequately solved. It is felt that by restricting the experiment site to the aft compartment of the S-IVB workshop and using motion picture records of actual experiment, position locations can be made with reasonable accuracy. Several more precise schemes have been examined and have been abandoned as impractical. Should the need for more precise location of the astronaut arise, a triangulation scheme, using one sort of energy radiator mounted on the head of the test subject and three strategically located tracking sensors, should be considered.

Direct force and moment sensors.- The measurement of body impact forces and the resulting moments will be made using a load cell array rigidly attached to the spacecraft. An array suitable for this experiment consists of six semiconductor strain gage bridges (Schaevitz-Bytrex JP series) rigidly mounted between two plates. It may be necessary to provide a high-frequency (several hundred cps) dither to this array to overcome the possibility of stiction as indicated in the simulation data run (fig. C-14a).

In addition to the six load cells in each array, a power supply capable of delivering 5 Vdc 1.5 A will be required. A signal conditioner/amplifier complex may also be needed to render the load cell outputs compatible with the onboard data system (fig. 50).

Vehicle attitude and attitude rate system.- In determining the vehicle attitude rate, it was found that the attitude sensing package contained in the vehicle attitude control system had a threshold of 40 °/hr. Since this rate threshold is far in excess of the predicted rates and of those rates required to satisfy the requirements of the ATM experiment, a preliminary design of a digital rate gyro system capable of meeting these requirements was carried out. The threshold of the system designed was 0.1 °/hr, and the saturation level was slightly in excess of 40 °/hr. This system was selected because it represents off-the-shelf space qualified hardware and permits acquisition of both attitude angles and attitude rates. The elements of this system are shown in figure 51.

The rate gyro system (RGS) develops a dc voltage proportional to vehicle rates. The approximate mean value (drift rate) of this signal is removed by an adjustable bias. The different of these signals is converted to a pulse train by the voltage-to-frequency converter. The pulse repetition rate of this pulse train is proportional to the input voltage.

The binary counter counts the number of pulses for a fixed increment of time. The contents of the register represent the total angular change since the last reset. The total number of pulses divided by the time per reset equals the average input or vehicle rate per reset. The total number of pulses per reset (i.e., the counter contents) is set into the storage register.

The storage register serves as an intermediate storage device to provide a suitable interface between the counter and the tape unit or telemetry system. It allows readout and write times up to 30 msec for compatibility with permanent storage.

Rate gyro system* and interface to digital output circuitry.- A single axis of the system consists of a floated integrating gyro with a torque to balance the loop closed around the gyro as shown in figure 52. The analog current i is proportional to the input rate W_i.

The present scaling of the RGS is 0.5 V/deg/sec. For measuring the desired low rates, the scale factor will be changed to 1 V/40°/hr. This can be done by shunting the torquer coil to decrease the torquer sensitivity or by increasing the value of the load resistor. A combination of these two techniques will be used to achieve the desired scale factor and transient response.

Preliminary analysis of the system indicates that a shunt resistor (R_1) of approximately 53 ohms, a load resistor (R_2) of 5000 ohms, and a capacitor of 1 μF will result in the desired scale factor of 1 V/40°/hr (fig. 53).

Referring to figure 52, two elements will saturate. The RGS will saturate if input rates exceed output capability, and the voltage-to-frequency converter will saturate if the input exceeds 1 V.

The proposed method of scaling the RGS causes saturation when input rates exceed 0.28°/sec.

---

*A detailed description of the rate gyro system is given in: Investigation of Titan III Rate Gyro System Dynamic Response. TM-0451-7-65, 1965. Martin Marietta Corporation, Denver, Colorado.

The voltage-to-frequency converter saturates when the input voltage exceeds the average voltage of the pulse train. This occurs at 1-Vdc input. One volt is 40°/hr or 0.011°/sec.

In conclusion, the system will saturate if input rates exceed 0.28°/sec or if input rates change more than 0.011°/sec after dc biasing is completed.

The astronaut will apply a step body rate of short duration for many normal body motions. For this reason, the response of the system to a step input was investigated. An electrical step input into the test torquer can be used to evaluate the response of the system.

The system transfer function is of the form

$$\frac{E_O}{I_T} = \frac{1}{(1 + T_e S)\left(1 + \frac{Z_e}{W_e} S + \frac{S^2}{W_e^2}\right)}$$

With the scale factor set to 1 V/40°/hr as previously discussed, the values of T_e, W_e, and Z_e are

$$T_e = \frac{1}{333} \text{ sec}$$

$$W_e = 88 \text{ rad/sec}$$

$$Z_e = 0.85$$

For a unit step input, the output is of the form

$$I_o = 1 - k_1 e^{-t/T_e} + k_2 e^{-Z_e W_e t} \sin(wt + \varphi)$$

The second term decays to less than 10^{-2} at 0.01 sec and can, therefore, be eliminated for all but very small values of time. The rise time of the output is very short since it is controlled by this rapidly decaying exponential term.

Eliminating the second term and inserting the proper values, the response of the system, for all but very small values of time, reduces to

$$I_o = 1 + 2.42e^{-74.8t} \sin (45.5\ t + 0.38)$$

The total system has a fast response time with very little overshoot. The error in measured rate is less than 0.1%, 0.1 sec after the unit step is applied.

This bias is a dc voltage which cancels the average output of the RGS. The bias is adjusted prior to conducting experiments and will null out vehicle rates. Figure 54 shows the basic scheme.

The ten-turn potentiometer will be adjusted by the astronaut to turn out a light or null a meter. The light or meter null indicates that the vehicle rates have been nulled out to a sufficient level to conduct the experiment.

A battery will be used to supply excitation to the potentiometer. Stability of 0.1% of the supply will contribute errors that are less than 0.03°/hr. This accuracy is an order of magnitude below the accuracies required.

The voltage-to-frequency converter input is the difference between the RGS output and the bucking circuit. It converts this voltage into a pulse rate which is proportional to the input. The converter scaling is 1800 parts/sec/V. The converter functions as shown in figure 55.

When the integrator (1/S) output exceeds the level of the threshold detector, the pulse source is connected through the pulse switch to the input of the integrator. The pulse switch sets the polarity of the pulse so as to drive the integrator output towards zero. The output of the integrator is as shown in figure 56.

The ramp output of the integrator is due to E_{in}, assuming that E_{in} is constant with respect to the pulse rate involved. When the ramp output exceeds the threshold voltage, a pulse is fed back to restore the integrator output to near zero. Thus, the pulse frequency is determined by the rate of rise of the integrator output. This is determined by the gain of the integrator, $\frac{1}{RC}$, and E_{in}. The frequency/V is determined by pulse area, threshold value, and integrator gain. If c = threshold voltage and k = integrator gain in V/sec, the time per pulse is kt = c and t = c/k.

This equation shows that, if in design c is small with respect to k, output frequency will be independent of small variations in c, the error being c/k.

The pulse size is determined by pulse amplitude x duty cycle x scale factor = maximum output, and pulse amplitude x time per pulse = resolution.

Additional design constraints are that the threshold should be small with respect to variations in E_{in}. The proposed frequency converter delivers 1800 parts/sec/V.

As previously discussed, the mean voltage out of the integrator is zero so that

$$\int E_{in}\, dt = \int \text{pulses}\, dt$$

The $\int$ pulses dt = pulse area $/\frac{1}{\text{pulse repetition rate}}$ = average pulse voltage. The average pulse voltage = 1 V for pulse repetition rates of 1800 parts/sec so that the pulse area = 1 V $\left(\frac{1}{1800}\right)$ = 1/1800 V-sec.

The RGS will be scaled so that 1 V is 40°/hr, thus, the pulse area = 1/1800 V-sec x 40°/hr/V = 6.2 x 10^{-6}°. If 1800 parts/sec = 40°/hr, 45 parts/sec = 1°/hr.

The total number of pulses per unit of time will indicate the change in vehicle attitude, and the pulse rate will be a measure of body rate. Thus, the counter indicates body attitude and rate as desired.

Estimates of body movements indicate that a data sample interval of 0.1 sec is adequate for data analysis.

Since the maximum input rate is equivalent to 1800 parts/sec, the maximum counter size requires a capability to count 180 pulses plus a sign.

The counter required is an eight-bit counter plus a sign bit.

As is the case with nonlinear systems, the frequency response of the system is a function of input amplitude as well as frequency.

Intuitively, it can be seen that for a particular frequency w, if the amplitude of E_{in} is below a certain value, the integrator output will not exceed the threshold and there will be no pulse output.

Let the input E_{in} = A sin wt. The output of the integrator with no pulse feedback is A/W cos wt. Pulse output will occur when A/W exceeds the threshold. The low-frequency gain of the integrator ensures that low-amplitude low-frequency inputs will be detected.

The RGS is space qualified for the Titan IIIC launch vehicle. Analysis of available data indicates that the vibration and shock levels in the Apollo command module are below the levels for which the RGS is qualified (figs. 57, 58). The RGS should be operating during launch to ensure survival of the environmental conditions. The system can be shut down following launch to reduce power consumption.

System accuracy is tabulated:

VOLTAGE-TO-FREQUENCY CONVERTER

Error source	Error
Gain of integrator	
Calibrated	0.05%
Fixed	0.1%
Pulse area	
Height (dc supply = 0.01%)	0.01%
Capacitor (40 parts/million dc)	0.03%
Quantizing error	±1 pulse, 6.2 μdeg
Integrator drift (20 μV)	0.002%
Pulse area (due to repetition rate)	<0.005%
Switch leakage (10 nano A)	0.004%
RSS error	0.06%

ADJUSTABLE DC BIAS

0.01% dc stability	0.01%

RATE GYRO SYSTEM

Uncalibrated

Frequency	0.5%
Torquer scale factor	1.0%
Torquer linearity	0.5%
RSS error	1.23%

Calibrated

Frequency	20 parts/ million
Torquer scale factor	0.1%
Torquer linearity	0.1%
RSS error	0.1%

TOTAL RSS ACCURACY

Uncalibrated	1.3%
Calibrated	0.11%

Vehicle perturbations due to aerodynamic drag, magnetic disturbances, and spurious vehicle torques encountered in space will be noise input to the system.

Effects of these inputs on overall accuracy is difficult to estimate from available information. Since the system is very sensitive, external inputs could cause near-saturation conditions. All available facts will be used in data reduction to achieve the best estimates possible. Knowledge of when the experiment was started and stopped and the expected waveform can be used to advantage in the data reduction.

A block diagram showing the functional aspects of the digital output is shown in figure 59.

The control element gates the counter and provides signals in sequence to the reset, data transfer, and tape unit in the following way every 0.1 sec.

1) It opens the gate to the counter and stops the count for 100 μsec;

2) Simultaneously with Step 1), data transfer from the storage register to tape is inhibited;

3) It transfers the counter contents to the storage register;

4) It resets the counter to zero and closes the gate, which restarts the counter;

5) Simultaneously with Step 4), a transfer instruction causes the contents of the storage register to be written on tape. Thus, the number of pulses per 0.1 sec generated by the voltage-to-frequency converter are recorded on the tape unit.

The control element consists of circuitry generating the waveform shown in figure 60. This circuitry is composed of a 10-cps astable multivibrator. The onboard signal of 1 cps is used to reset the multivibrator every 0.5 sec. In a sense, the multivibrator is synchronized with the 1-cps base frequency.

During the 100-μsec period, the contents of the counter will be transferred to an auxiliary register, and the counter will be reset to zero. The remainder of the 0.1-sec period is used to count the incoming rate signal and transfer the data in the auxiliary register to permanent storage on magnetic tape.

The signal input to the control element comes from the voltage-to-frequency converter. The voltage-to-frequency converter output is on two lines. One line indicates positive body rates and the other indicates negative body rates.

The signal on either of these lines is as shown in figure 61.

Input pulses are 100 μsec long. If data transfer time is kept below 100 μsec, there is a possibility that a pulse will be counted twice, and if the data transfer time is longer than 100 μsec, one pulse could be missed. Either event will have negligible effect on the output since digital filtering will smooth the data. The data transfer time was chosen as 100 μsec. During this interval, the counter will be stopped. When restarted, the counter will not have missed any pulses unless a pulse occurred at precisely the same 100-μsec interval that the counter was stopped. The probability of this occurrence is near zero.

Assuming no crew motions, the output of the voltage-to-frequency converter will be near zero since the vehicular rates will have been nulled out by the adjustable dc bias.

The astronaut is capable of inducing either positive or negative rates on the spacecraft. Therefore, there is a distinct possibility that the output of the voltage-to-frequency converter will change in sign due to crew-induced vehicle disturbances.

Since the up counter counts positive or negative rates in the same manner, the counter will indicate a higher average rate than is actually present during the interval when the sign change occurs. Analysis of the data will require that the information obtained during the interval of sign transition be disregarded. This interval will be indicated by a change in the sign bit of the counter.

The sign bit will change either in the interval in which the sign changes, or in the following interval, depending on the direction of the sign change and the method of implementing the sign indicating bit.

Since the counting interval is 0.1 sec, very little information will be lost by rate sign changes. If necessary, approximate information can be obtained by determining the rate before and after the sign change and approximating the sign change interval to result in a smooth transition.

The up counter requires fewer components than an up-down counter, which will result in size and weight savings and increased reliability.

The counter is a nine-bit binary counter (fig. 62). Eight bits are used to count incoming pulses and the ninth bit indicates the sign of the input. The counter is initially set at zero. After each 0.1-sec counting interval, the register is reset to zero. If the input rate is negative, a one appears in the ninth bit. The eight bits of the counter are cascaded triggers.

Inverters and nand gates are used to implement the use of DT micrologic components.

The data transfer circuitry accomplishes two functions. First, it transfers data from the counter to the auxiliary register. Second, it transfers the data in the auxiliary register to magnetic tape.

The transfer of data from the counter to the auxiliary register occurs after counting has been stopped. Transfer of data from the auxiliary register to the tape occurs during the counting phase.

The method of data transfer is shown in figure 63. Ten μsec after the control signal has stopped counting (the 10-μsec delay) a 30-μsec transfer pulse is generated. This pulse causes the contents of the counter to be transferred to the auxiliary register.

The control signal then restarts the counter and transfers the contents of the auxiliary register onto magnetic tape.

After the contents of the counter has been transferred to the auxiliary register, the counter must be reset to zero. Figure 64 is a block diagram of the reset mechanism. The control signal is delayed 10 μsec to allow adequate time to stop the counter and inhibit the transfer of data from the auxiliary register where magnetic tape. Next, a 30-μsec pulse is generated to transfer the counter contents of the counter to the auxiliary register where it is stored until transfer to tape. Ten μsec later another 30-μsec pulse is generated to reset the counter to zero. The 10-μsec delay is necessary to provide adequate time to complete the transfer of the counter data to the auxiliary register.

The final stage in this system is the tape recorder. The recorder is used to store the digital output of the counter. The recorder used must be capable of recording a minimum of 108 000 words, each of nine-bit size. Information on recorders indicates a maximum bit storage of 1000 bits/in. of tape. The output of the system is 30 bits/sec, which necessitates a minimum tape speed of 0.03 in./sec.

The features of the tape recorders under consideration are listed in Table V. At the present time, a recorder has not been selected. Available information indicates that the recorders which will meet the requirements of the system are available as off-the-shelf items or may be available as onboard equipment.

The possibility of using magnetic core storage was also considered. The size of this type storage unit prohibits its use.

TABLE V.-SPACE-QUALIFIED TAPE RECORDERS

Manufacturer	Model	Size, in.	Tape capacity, ft	Recording speed, in./sec	Recording time	Playback speed, in./sec	Channel	Features
Kinelogic Corp.	B	10x13x3	1800	24	900 sec @ 24 in./sec	0.48	14	Separate synchronous temporary storage loop
Kinelogic Corp.	C	$6x4\frac{1}{4}x3\frac{1}{8}$	500	30	200 sec @ 30 in./sec	0.3	14	Record and playback speeds interchangeable
Kinelogic Corp.	CM	$6x6x3\frac{1}{4}$	650	0.01 to 12.8	600 sec @ 12.8 in./sec	0.01 to 12.8	14	Playback-to-record speed ratio is 1280 to 1 (tape size 1/4, 1/2, and 1 in.)
Kinelogic Corp.	CJ	$6x7\frac{3}{4}x4$	500	0.5 and 15	400 sec @ 15 in./sec	0.5 and 15		Weighs 6 lb
RCA		11 (diam.) x 8	1200	0.297	12 hr	18.9	9	OGO recorder stores 43 million bits
Raymond Engineering	1849	4 (diam.) x 9	113	$3\frac{3}{4}$ to 30	360 sec @ $3\frac{3}{4}$ in./sec	$3\frac{3}{4}$ to 30	14	Reel-to-reel
Raymond Engineering	1897	10x10x7	550	1.5	4400 sec	1.5	16	Reel-to-reel, Gemini

TABLE VI.-PHYSICAL PROPERTIES OF ATTITUDE, ATTITUDE RATE SYSTEM

Item	Weight, lb	Dimensions, in.
Rate gyro system	15	12x12x7
Voltage-to-frequency converter	6	4x5x8
Tape recorder	10	8x8x8
Electronics	5	9x6x4

It is possible to eliminate the tape recorder from the system by telemetering the data to ground stations on a real-time basis. However, this limits the performance of the experiments to time periods when the spacecraft is over ground stations with telemetry facilities. This limitation is not considered desirable, and is eliminated by inclusion of the tape recorder in the system.

A summary of physical properties of the attitude rate system is given in Table VI. These components will be packaged on a single mount. Estimated overall dimensions will not exceed 12x12x16 in. Estimated system weight will be less than 40 lb.

Summaries of system and gyro parameters are given in Tables VII and VIII.

DATA ACQUISITION, STORAGE, REDUCTION, AND ANALYSIS

In considering the acquisition of the orbital experiment data, two approaches were examined. One involved storing all the data on magnetic tape to be returned to earth with the command module. Such a procedure would reduce the interface problems with the existing data management/telemetry system. It might, however, require the use of an additional tape recorder and require provision for tape storage for the reentry maneuver. In addition, it would provide little opportunity for in-flight data processing and any desired repetition of certain exercises.

A second procedure involved collecting all the data at a central point in the spacecraft, identified in figure 65 as the telemetry interface. This interface equipment will require temporary storage prior to transmission to the ground.

The data reduction could then take place immediately upon receipt at the ground station, at a later time while the flight is still in orbit, or the data could be stored on tape for reduction at any later time. The reduction process, if carried out while the flight is still in orbit, would permit repetition of any desired exercise at the discretion of the mission control officer.

The reduction process, outlined in figures 66 thru 69 may involve only the readout and comparison of flight data with previously determined analytical and simulation data either visually or automatically. It could also involve an actual computation of spacecraft attitude and attitude rates based on the actual in-flight limb motion history for comparison purposes.

TABLE VII.-ATTITUDE, ATTITUDE RATE SYSTEM PROPERTIES

Range	
Rate	0.1°/hr to 40°/hr rate change from nominal inputs of 0°/hr to 1000°/hr absolute range
Attitude	1.11×10^{-3} °/counting interval, maximum angle unlimited
Resolution	
Rate	0.1°/hr
Attitude	6.2×10^{-6}°
Accuracy	0.11% full-scale (0.044°/hr)
Output form	digital
Operating life	2000 hr minimum
Power requirements	120 W maximum
	250 W maximum during warmup
Warmup time	20 minutes maximum
Size	12x12x16 in.
Weight	40 lb maximum

TABLE VIII.-GYRO PARAMETERS

Gimbal damping	2.3×10^{4} dyne-cm/sec
Wheel momentum	5.13×10^{4} dyne-cm/sec
Angular pickoff	10 V/rad
Torquer sensitivity	134 dyne-cm/ma

CONCLUSIONS AND RECOMMENDATIONS

This study has shown that an initially stable space vehicle with zero-drift rates can acquire drift rates of low, but significant amplitude, through the effects of crew activity. These low drift rates can conceivably impair the effectiveness of those space experiments requiring precise attitude orientations. For example, as is well known, the usual AAP vehicles are equipped with an attitude control system whose rate threshold is of the order of 0.011°/sec or 40 arc-sec/sec. The Apollo ATM experiment requires a pointing accuracy of ±2 arc-sec for periods up to 15 minutes. The data accumulated in this study indicate that very simple crew motions can introduce a roll rate in the cluster configuration vehicle (Configuration 3) of the order of 0.0015°/sec (5.4 arc-sec/sec). The force producing this rate was of the order of 10 lb acting at a distance of about 15 ft from the vehicle center of mass. It would further appear that the activities of a crew member standing watch at the control console can induce uncontrolled vehicle rates of the order of 0.008°/sec (about 30 arc-sec/sec). The simple act of breathing can induce vehicle rates of the order of 0.00012°/sec (about 0.45 arc-sec/sec). The cyclic nature of these disturbances can impose a significant burden on the spacecraft attitude control system and is an area that requires further investigation with orbital verification.

In defining an orbital experiment, preliminary designs of the necessary instrumentation were carried out, and the feasibility of all the necessary sensors and the associated instrumentation was established. The total orbital experiment design is reflected in the NASA Form 1138 in Appendix F.

It is recommended that an investigation to improve the mathematical model of man be made and his orbital characteristics set forth. In particular, a study should be initiated on the basic effects of limb motion on man's dynamic characteristics. Such a study could result in a significant modification of LIMS by reducing the number of joints required to provide the significant limb motion history.

In particular, the model of man requires further study. As assumed for this study, the model consisted of nine rigid homogeneous segments with relatively simple joints. No attempt was made to account for visceral shifts or displacements of fatty tissues. While these effects may be small, we are concerned with small effects. It is necessary to verify the results of this

study and the model of man by an actual orbital flight. To gain maximum benefit of the orbital data to the ATM experiment and other experiments requiring precise attitude control, it is recommended that an early orbital experiment be planned.

Martin Marietta Corporation,
Denver Division,
Denver, Colorado, March 23, 1967.

APPENDIX A

EQUATIONS OF MOTION

INTRODUCTION

The purpose of this appendix is to derive the equations that describe the general motions of a spacecraft-astronaut system where forces and moments causing spacecraft translations and rotations are produced by astronaut translations and limb movements. The coordinate systems used in the derivation are shown in figures A-1 and A-2, and a description of a nine-segment model is given. The segment reference numbers are shown in figure A-3. The equations for the digital program are then derived followed by the analog program equations.

NOTATION

A method of notation for vectors, dyads, and transformation matrices has been devised in an attempt to define completely all variables and constants used in the analysis.

A single bar or dot appearing above a quantity indicates a vector or a first-time derivative, respectively. Two bars or two dots appearing above a quantity indicate a dyad or second-time derivative, respectively. If the dots appear above the bars, a total or true-time derivative is indicated, i.e., derivatives of unit vectors must be accounted for if the quantity is resolved in a rotating coordinate system. Dots appearing below the bars indicate that the quantity is to be treated as if seen by an observer in the rotating coordinate system.

A subscript apperaring to the left of a quantity (vectors or dyads) indicates the coordinate system in which the components are resolved. The first subscript to the right of a quantity refers the quantity to either the spacecraft or a specific body segment. The subscript s refers to the spacecraft while 1 through 9 refer to body segments as shown in figure A-3. The subscript m refers to the combined center of mass of the model man, and o refers to the inertial reference, i.e., the combined center of mass of the man and spacecraft. The subscript sm has been used to indicate a position vector locating the man's combined center of mass relative to the spacecraft center of mass.

Appendix A

SPACECRAFT

The coordinate system, in which the governing equations are written, and the problem geometry are shown in figure A-1. The spacecraft in any configuration is considered to be a rigid body with mass m_s. A right-hand set of orthogonal axes, X_s, Y_s, and Z_s are rigidly imbedded in the spacecraft with the origin at the spacecraft center of mass.

The vector ${}_s\bar{R}_s$ denotes the location of the spacecraft center of mass with respect to the inertial reference, and ${}_s\bar{\omega}_{so}$ denotes the inertial angular velocity of the spacecraft. Denoting the spacecraft inertia dyad by ${}_s\bar{\bar{I}}_s$, the angular momentum ${}_s\bar{H}_s$ of the spacecraft written about the origin of the inertial reference is then given by

$$ {}_s\bar{H}_s = {}_s\bar{\bar{I}}_s \cdot {}_s\bar{\omega}_{so} + m_s\left({}_s\bar{R}_s \times {}_s\dot{\bar{R}}_s\right) \tag{1} $$

The first term in equation (1) represents the angular momentum of the spacecraft about its own center of mass, and the second term represents the angular momentum of the spacecraft center of mass about the origin of the inertial reference.

The vector ${}_1\bar{r}_{sm}$ locates the center of mass of the astronaut with reference to the spacecraft center of mass. Then, from the definition of the total system center of mass

$$ +{}_s\bar{R}_s(m_m + m_s) = {}_s\bar{r}_{sm}(m_m) $$

or

$$ {}_s\bar{R}_s = \left(\frac{+m_m}{m_m + m_s}\right) {}_s\bar{r}_{sm} \tag{2} $$

Substituting equation (2) into (1) gives

$$ {}_s\bar{H}_s = {}_s\bar{\bar{I}}_s \cdot {}_s\bar{\omega}_{so} + \frac{m_s m_m^2}{(m_m + m_s)^2}\left({}_s\bar{r}_{sm} \times {}_s\dot{\bar{r}}_{sm}\right) \tag{3} $$

For example, $_1\bar{R}_4$ is a position vector resolved in the coordinate system of the torso and locating the right forearm; $_1\bar{\bar{I}}_2$ is the inertia dyad resolved in torso coordinates of the upper right arm.

A second subscript to the right has been used for the angular velocity to denote the spacecraft or body segment that the quantity is measured relative to. For example, $_2\bar{\omega}_{21}$ is the angular velocity vector, resolved in the coordinate system of and referring to the right upper arm, and measured relative to the angular velocity of the torso.

Coordinate transformation matrices will be denoted by D and will be subscripted by two numbers to the right, indicating the two segments or bodies the transformation is to take place between. For example, D_{21} is the transformation from the right upper arm to the torso. This notation allows writing $D_{21} = D_{12}^{-1}$. The small letter d will be used to denote an element of a matrix, with two subscripts to the left indicating the specific element. For example, $_{13}d_{41}$ is the element in the first row, third column, of the transformation matrix from the right forearm to the torso.

DIGITAL EQUATIONS

This section presents the derivation of the equation of motion of the spacecraft-astronaut system for solution on a digital computer. It is assumed that no net external forces or moments (e.g. from thrusters) are applied to the system. Therefore, the combined center of mass of the system is considered the inertial reference. The equations of motion are obtained from the conservation of angular momentum principle, which states that the total angular momentum of the system about the combined center of mass is constant with respect to time.

Appendix A

ASTRONAUT

For this analysis, the astronaut is approximated by a model man consisting of nine rigid body segments. The model man is shown in figures A-2 and A-3, and the equations giving mass and inertia properties of each body segment are given in the section of this appendix entitled, Math Model of Man. Each segment mass is denoted by m_i, and $\sum_{i=1}^{9} m_i = m_m$ where m_m denotes the total mass of the model. A right-hand set of orthogonal axes X_i, Y_i, and Z_i are rigidly imbedded in the ith body segment with origin at the center of mass of the ith segment.

The vector ${}_1\bar{R}_i$ denotes the ith segment center-of-mass location relative to the inertial reference origin, and ${}_1\bar{\omega}_{io}$ denotes the inertial angular velocity of the ith segment. Denoting the inertia dyad of the ith segment by ${}_1\bar{\bar{I}}_i$, the angular momentum ${}_1\bar{H}_m$ of the model man written about the origin of the inertial reference is given by

$$ {}_1\bar{H}_m = \sum_{i=1}^{9} \left[{}_1\bar{\bar{I}}_i \cdot {}_1\bar{\omega}_{io} + m_i \left({}_1\bar{R}_i \times {}_1\dot{\bar{R}}_i \right) \right] \tag{4} $$

The first term in brackets in equation (4) represents the angular momentum of the ith segment about its own center of mass, and the second term represents the angular momentum of the ith segment center of mass about the origin of the inertial reference.

The vector ${}_1\bar{r}_i$ locates the ith segment center of mass with reference to the model man combined center of mass, and ${}_1\bar{R}_m$ locates the combined center of mass with reference to the inertial origin.

Thus,
$$ {}_1\bar{R}_i = {}_1\bar{R}_m + {}_1\bar{r}_i \tag{5} $$

Appendix A

As mentioned previously, the vector $_1\bar{r}_{sm}$ locates the model man center of mass relative to the spacecraft and command module. Then, again from the definition of the total system center of mass

$$+ {}_1\bar{R}_m(m_m + m_s) = m_s({}_1\bar{r}_{sm})$$

or

$${}_1\bar{R}_m = \left(\frac{+ m_s}{m_m + m_s}\right) {}_1\bar{r}_{sm} \tag{6}$$

Also, by definition of the model man center of mass

$$\sum_{i=1}^{9} m_i({}_1\bar{r}_i) = 0 \tag{7}$$

Substituting equations (5), (6), and (7) into equation (4) gives

$${}_1\bar{H}_m = \sum_{i=1}^{9} \left[{}_1\bar{\bar{I}}_i \cdot {}_1\bar{\omega}_{io} + m_i\left({}_1\bar{r}_i \times {}_1\dot{\bar{r}}_i\right)\right] + \frac{m_m m_s^2}{(m_m + m_s)^2}\left({}_1\bar{r}_{sm} \times {}_1\dot{\bar{r}}_{sm}\right) \tag{8}$$

TOTAL SYSTEM

The total angular momentum of the system about the system combined center of mass is obtained by adding equations (3) and (8). Writing equation (3) in segment 1 coordinates and adding to equation (8) gives

$${}_1\bar{H}_T = {}_1\bar{\bar{I}}_s \cdot {}_1\bar{\omega}_{so} + \frac{m_s m_m^2}{(m_m + m_s)^2}\left({}_1\bar{r}_{ms} \times {}_1\dot{\bar{r}}_{ms}\right)$$

$$+ \sum_{i=1}^{9} \left[{}_1\bar{\bar{I}}_i \cdot {}_1\bar{\omega}_{io} + m_i\left({}_1\bar{r}_i \times {}_1\dot{\bar{r}}_i\right)\right] + \frac{m_m m_s^2}{(m_m + m_s)^2}\left({}_1\bar{r}_{sm} \times {}_1\dot{\bar{r}}_{sm}\right)$$

or

$$1\bar{H}_T = 1\bar{\bar{I}}_s \cdot 1\bar{\omega}_{so} + \sum_{i=1}^{9} \left[1\bar{\bar{I}}_i \cdot 1\bar{\omega}_{io} + m_i \left(1\bar{r}_i \times 1\dot{\bar{r}}_i \right) \right] + Q\left(1\bar{r}_{sm} \times 1\dot{\bar{r}}_{sm} \right) \quad (9)$$

where $$Q = \frac{m_m m_s}{m_m + m_s}$$

The inertial angular rotation of each segment can be written as

$$1\bar{\omega}_{io} = 1\bar{\omega}_{so} + 1\bar{\omega}_{1s} + 1\bar{\omega}_{i1} \quad (10)$$

where $1\bar{\omega}_{so}$ is the inertial spacecraft angular velocity, $1\bar{\omega}_{1s}$ is the angular velocity of segment 1 relative to the spacecraft, and $1\bar{\omega}_{i1}$ is the angular velocity of the i<u>th</u> segment relative to segment 1. Equation (9) can now be written as

$$1\bar{H}_T = \left(1\bar{\bar{I}}_s + \sum_{i=1}^{9} 1\bar{\bar{I}}_i \right) \cdot 1\bar{\omega}_{so} + \sum_{i=1}^{9} 1\bar{I}_i \cdot \left(1\bar{\omega}_{1s} + 1\bar{\omega}_{i1} \right) + \sum_{i=1}^{9} m_i \left(1\bar{r}_i \times 1\dot{\bar{r}}_i \right) + Q\left(1\bar{r}_{sm} \times 1\dot{\bar{r}}_{sm} \right) \quad (11)$$

Since the position vectors $1\bar{r}_i$ and $1\bar{r}_{sm}$ are resolved in a rotating coordinate system, the total or true-time derivatives of these vectors are

$$1\dot{\bar{r}}_i = 1\bar{\dot{r}}_i + 1\bar{\omega}_{1o} \times 1\bar{r}_i \quad (12a)$$

and

$$1\dot{\bar{r}}_{sm} = 1\bar{\dot{r}}_{sm} + 1\bar{\omega}_{1o} \times 1\bar{r}_{sm} \quad (12b)$$

where

$$1\bar{\omega}_{1o} = 1\bar{\omega}_{so} + 1\bar{\omega}_{1s}$$

Appendix A

Substituting equation (12) into (11) gives

$$
\begin{aligned}
{}_1\bar{\bar{H}}_T = & \left({}_1\bar{\bar{I}}_s + \sum_{i=1}^{9} {}_1\bar{\bar{I}}_i \right) \cdot {}_1\bar{\omega}_{so} + \sum_{i=1}^{9} {}_1\bar{\bar{I}}_i \cdot \left({}_1\bar{\omega}_{1s} + {}_1\bar{\omega}_{i1} \right) \\
& + \sum_{i=1}^{9} m_i \left({}_1\bar{r}_i \times {}_1\dot{\bar{r}}_i \right) + Q \left({}_1\bar{r}_{sm} \times {}_1\dot{\bar{r}}_{sm} \right) \\
& + \sum_{i=1}^{9} m_i \left[{}_1\bar{r}_i \times \left({}_1\bar{\omega}_{so} \times {}_1\bar{r}_i \right) \right] + Q \left[{}_1\bar{r}_{sm} \times \left({}_1\bar{\omega}_{so} \times {}_1\bar{r}_{sm} \right) \right] \\
& + \sum_{i=1}^{9} m_i \left[{}_1\bar{r}_i \times \left({}_1\bar{\omega}_{1s} \times {}_1\bar{r}_i \right) \right] + Q \left[{}_1\bar{r}_{sm} \times \left({}_1\bar{\omega}_{1s} \times {}_1\bar{r}_{sm} \right) \right] \qquad (13)
\end{aligned}
$$

Using a vector identity, the vector triple product terms can be written as

$$
\bar{r} \times (\bar{\omega} \times \bar{r}) = \left[(\bar{r} \cdot \bar{r}) \bar{\bar{E}} - \bar{r}\bar{r} \right] \cdot \bar{\omega}
$$

where $\bar{\bar{E}}$ is the unit dyad defined by

$$
\bar{\bar{E}} = \begin{bmatrix} ii & ij0 & ik0 \\ ji0 & jj & jk0 \\ ki0 & kj0 & kk \end{bmatrix}
$$

Making this substitution into equation (13) gives

$$
\begin{aligned}
{}_1\bar{H}_T = &\left\{ {}_1\bar{\bar{I}}_s + \sum_{i=1}^{9} {}_1\bar{\bar{I}}_i + \sum_{i=1}^{9} m_i \left[\left({}_1\bar{r}_i \cdot {}_1\bar{r}_i \right) \bar{\bar{E}} - {}_1\bar{r}_i \left({}_1\bar{r}_i \right) \right] \right. \\
&\left. + Q \left[\left({}_1\bar{r}_{sm} \cdot {}_1\bar{r}_{sm} \right) \bar{\bar{E}} - {}_1\bar{r}_{sm} \left({}_1\bar{r}_{sm} \right) \right] \right\} \cdot {}_1\bar{\omega}_{so} + \sum_{i=1}^{9} {}_1\bar{\bar{I}}_i \cdot {}_1\bar{\omega}_{i1} \\
&+ \sum_{i=1}^{9} m_i \left({}_1\bar{r}_i \times {}_1\dot{\bar{r}}_i \right) + Q \left({}_1\bar{r}_{sm} \times {}_1\dot{\bar{r}}_{sm} \right) \\
&+ \left\{ \sum_{i=1}^{9} m_i \left[\left({}_1\bar{r}_i \cdot {}_1\bar{r}_i \right) \bar{\bar{E}} - {}_1\bar{r}_i \left({}_1\bar{r}_i \right) \right] + \sum_{i=1}^{9} {}_1\bar{\bar{I}}_i \right. \\
&\left. + Q \left[\left({}_1\bar{r}_{sm} \cdot {}_1\bar{r}_{sm} \right) \bar{\bar{E}} - {}_1\bar{r}_{sm} \left({}_1\bar{r}_{sm} \right) \right] \right\} \cdot {}_1\bar{\omega}_{1s}
\end{aligned}
\tag{14}
$$

If the spacecraft or astronaut have relative motions at time equal to zero, equation (14) can be used to find the initial total angular momentum, ${}_1\bar{H}_T\Big|_{t=0}$. After time zero, the spacecraft angular rates are given by [solving for ${}_1\bar{\omega}_{so}$ from equation (14)],

$$
{}_1\bar{\omega}_{so} = \left[\bar{\bar{A}} \right]^{-1} \cdot \bar{B} \tag{15}
$$

where

$$
\begin{aligned}
\bar{\bar{A}} = &\ {}_1\bar{\bar{I}}_s + \sum_{i=1}^{9} {}_1\bar{\bar{I}}_i + \sum_{i=1}^{9} m_i \left[\left({}_1\bar{r}_i \cdot {}_1\bar{r}_i \right) \bar{\bar{E}} - {}_1\bar{r}_i \left({}_1\bar{r}_i \right) \right] \\
&+ Q \left[\left({}_1\bar{r}_{sm} \cdot {}_1\bar{r}_{sm} \right) \bar{\bar{E}} - {}_1\bar{r}_{sm} \left({}_1\bar{r}_{sm} \right) \right]
\end{aligned}
$$

Appendix A

$$\bar{B} = {}_1\bar{H}_T\Big|_{t=0} - \sum_{i=1}^{9} m_i\left({}_1\bar{r}_i \times {}_1\dot{\bar{r}}_i\right) - Q\left({}_1\bar{r}_{sm} \times {}_1\dot{\bar{r}}_{sm}\right)$$

$$- \left\{\sum_{i=1}^{9} m_i\left[\left({}_1\bar{r}_i \cdot {}_1\bar{r}_i\right)\bar{\bar{E}} - {}_1\bar{r}_i\left({}_1\bar{r}_i\right)\right] + \sum_{i=1}^{9} {}_1\bar{\bar{I}}_i\right.$$

$$\left. + Q\left[\left({}_1\bar{r}_{sm} \cdot {}_1\bar{r}_{sm}\right)\bar{\bar{E}} - {}_1\bar{r}_{sm}\left({}_1\bar{r}_{sm}\right)\right]\right\} \cdot {}_1\bar{\omega}_{1s}$$

$$- \sum_{i=1}^{9} {}_1\bar{\bar{I}}_i \cdot {}_1\bar{\omega}_{i1}$$

With LIMS measuring segment angles on the astronaut, all the ${}_1\bar{r}_i$ and ${}_1\dot{\bar{r}}_i$ terms in equation (15) can be calculated (see expansion of these terms at end of this section). The terms remaining to be specified are ${}_1\bar{r}_{sm}$, ${}_1\dot{\bar{r}}_{sm}$, and ${}_1\bar{\omega}_{1s}$. These terms depend on whether or not the astronaut is in contact with the spacecraft. For the case where the astronaut is not touching the spacecraft, $\bar{r}_{sm}$ and $\dot{\bar{r}}_{sm}$ are known from initial conditions, i.e., $\dot{\bar{r}}_{sm} = \text{constant} = \dot{\bar{r}}_{sm}\Big|_{t=0}$ and $\bar{r}_{sm} = \int \dot{\bar{r}}_{sm}\Big|_{t=0} dt$. Also, there are no forces on the spacecraft, and thus ${}_1\bar{\omega}_{so}$ is known from initial conditions. Equation (15) can then be used to calculate ${}_1\omega_{1s}$, the angular velocity of the astronaut's torso due to his own limb motions.

The case of interest in this report is where the astronaut is in contact with the spacecraft. In this case, the terms $\bar{r}_{sm}$ and $\dot{\bar{r}}_{sm}$ can be determined by knowing the astronaut's point of contact on the spacecraft, relative to the spacecraft center of mass, and knowing the segment with which the astronaut contacts the spacecraft. For the results obtained in this report, it is assumed that the astronaut is restrained in a seat or harness by his torso such that the torso and spacecraft form a rigid body.

Appendix A

If $_1\bar{\rho}_1$ is a vector defining the center of mass location of the torso relative to the spacecraft center of mass, then

$$_1\bar{r}_{sm} = -_1\bar{\rho}_1 - _1\bar{r}_i$$

and

$$_1\dot{\bar{r}}_{sm} = -_1\dot{\bar{r}}_i$$

In the general case where the astronaut is in contact with the spacecraft, the $_1\bar{\omega}_{1s}$ term would have to be measured in some manner or obtained from analog simulation. For the specific case considered in this report where the torso is restrained from moving relative to the spacecraft, $_1\bar{\omega}_{1s} = 0$.

With these assumptions, the spacecraft inertial velocity in torso coordinates, $_1\bar{\omega}_{so}$, can then be calculated from equation (15). Most of the terms in equation (14) require further expansion in order to obtain them in segment 1 coordinates and in terms of known quantities such as segment inertias, segment rotations, or segment dimensions. These expansions are carried out at the end of this appendix.

From the solution to equation (15), all relative motions between the man and spacecraft are known as a function of time. The forces and moments at any point in the system causing these motions can then be calculated. Of prime interest are the forces and moments applied to the spacecraft mass by the astronaut. These forces and moments are called "effective" since they produce the rotation and translation given by equation (15) as though the astronaut were not in the spacecraft. At the spacecraft center of mass, these forces and moments are then given by

$$\left.\begin{aligned} _1F_{s_{cm}} &= m_s\left(-_1\ddot{\bar{R}}_s\right) \\ \text{and} \qquad _1M_{s_{cm}} &= {}_1\bar{\bar{I}}_s \cdot {}_1\dot{\bar{\omega}}_{so} \end{aligned}\right\} \text{(Effective)} \tag{16}$$

From equation (2), the force equation can be written as

$$_1F_{s_{cm}} = -Q\,\bar{r}_{ms} \quad \text{(Effective)} \tag{17}$$

In the computer program, the forces and moments given by these equations are calculated at the spacecraft center of mass. Also, they are transferred to a point representing the contact point between the astronaut and the spacecraft (this point is equivalent to the load cell location relative to the torso used in the couch study).

Another set of forces and moments calculated by the program are called "actual." These are the forces and moments required to rotate and translate the rigid system consisting of the spacecraft and that part of the man which is not moving relative to the spacecraft. These forces and moments are (see figure A-1 for definition of vectors)

$$\left.\begin{aligned} {}_1\bar{F}'_{s_{cm}} &= m' {}_1\ddot{\bar{R}}_F \\ \text{and} \qquad & \\ \bar{M}_{s_{cm}} &= {}_1\bar{\bar{I}}'_s \cdot {}_1\bar{\omega}_{so} \end{aligned}\right\} \quad \text{(Actual)} \tag{18}$$

where m' and ${}_1\bar{\bar{I}}'_s$ are the mass and total inertia, respectively of the spacecraft plus that part of the man that is not moving relative to the spacecraft. Defining ${}_1\bar{r}'_m$ as the vector locating the man's center of mass, minus his moving segments, relative to the torso center of mass (see fig. A-1), the force equation can be written as

$${}_1F'_{s_{cm}} = (m' - m_s)\left({}_1\ddot{\bar{r}}'_m - {}_1\ddot{\bar{\rho}}_1\right) + \frac{m' m_m}{m_m + m_s}\left({}_1\ddot{\bar{\rho}}_1 + {}_1\ddot{\bar{r}}_1\right) \tag{19}$$

ANALOG SIMULATION EQUATIONS

Translational Activity

This section is concerned with the set of equations describing the motion of an astronaut relative to the spacecraft.

Appendix A

The general equations are identical to those of the previously derived digital program. At the present time, the analog facility adjacent to the SOS is not able to implement the complete model. The four EAI 231 R computers are limited to the use of 144 multipliers. Therefore, the analog program was simplified to match the available computer capability. The following approximations were made:

The spacecraft may be considered an inertial body due to its large mass and inertias relative to the astronaut;

The astronaut is considered to have constant inertia and center of mass;

The major component of the angular momentum generated on the torso by the limbs is the $m_i \left({}_1\bar{r}_i \times {}_1\dot{\bar{r}}_i \right)$ term.

Equation (9) of the digital program with the above approximations results in

$$ {}_1\bar{H}_T = \bar{\bar{I}}_m \cdot {}_1\bar{\omega}_{ms} + \sum_{i=2}^{9} m_i \left({}_1\bar{r}_i \times {}_1\dot{\bar{r}}_i \right) + m_m \left({}_1\bar{r}_{ms} \times {}_1\dot{\bar{r}}_{ms} \right) \tag{20} $$

where I_m is the astronaut's inertia dyad. The first two terms represent the angular momentum of the astronaut about his center of mass and can be written as

$$ {}_1\bar{H}_T = \bar{\bar{I}}_m \cdot {}_1\bar{\omega}_{ms} + \sum_{i=2}^{9} m_i \left({}_1\bar{r}_i \times {}_1\dot{\bar{r}}_i \right) \tag{21} $$

The third term is the angular momentum of the mass about the spacecraft. Using the relationship

$$ \dot{\bar{H}} = \bar{M} = \bar{r} \times \bar{F} \tag{22} $$

yields

$$ {}_s\bar{F}_m = m_m \, {}_s\ddot{\bar{r}}_{ms} \tag{23} $$

where $\bar{F}_m$ are the external forces applied to the astronaut.

Appendix A

The external forces and moments are generated from contact with the spacecraft. In the simulation, the mockup is mounted on a load cell array which measures the forces, $\bar{F}_s$, and moments, $\bar{M}_s$, applied to the mockup relative to the load cell centroid. The equivalent set of forces and moments at the man's center of mass is given by

$$\bar{F}_m = -\bar{F}_s \tag{24}$$

and

$$\bar{M}_m = \bar{r}_{ms} \times \bar{F}_s - \bar{M}_s \tag{25}$$

Equation (24) combined with equation (23) provides the translational commands for the carriage

$$r_{ms} = \iint \frac{-\bar{F}_s}{m_m} \, dt \tag{26}$$

The rotational commands are obtained by transforming equation (25) into the astronaut body axis

$$\bar{M}_m = D_{sm} \bar{M}_m \tag{27}$$

Since the moment is equal to the time rate of change of the angular momentum,

$$\bar{M}_m = \dot{\bar{H}}_T + \bar{\omega}_{ms} \times \bar{H}_T \tag{28}$$

or

$$\bar{H}_T = \int \left(\bar{M}_m - \bar{\omega}_{ms} \times \bar{H}_T \right) dt \tag{29}$$

Rearranging equation (21),

$$\bar{\bar{I}}_m \cdot \bar{\omega}_{ms} = \bar{H}_T - \sum_{i=2}^{9} m_i \left(\bar{r}_i \times \dot{\bar{r}} \right) \tag{30}$$

enables $\bar{\omega}_{ms}$ to be determined.

Appendix A

For the gimbal sequence on the attitude head (yaw, roll, pitch), the Euler rates of the astronaut are given by

$$\left.\begin{aligned} \dot{\psi}_{ms} &= \frac{r_{ms} C\theta_{ms} - p_{ms} S\theta_{ms}}{C\varphi_{ms}} \\ \dot{\varphi}_{ms} &= r_{ms} S\theta_{ms} + p_{ms} C\theta_{ms} \\ \dot{\theta}_{ms} &= q_{ms} - \dot{\psi}_{ms} S\varphi_{ms} \end{aligned}\right\} \tag{31}$$

where

$$1\bar{\omega}_{ms} = {}_1p_{ms} i + {}_1q_{ms} j + {}_1r_{ms} k \tag{32}$$

and the Euler angles by

$$\left.\begin{aligned} \psi_{ms} &= \int \dot{\psi}_{ms}\, dt \\ \varphi_{ms} &= \int \dot{\varphi}_{ms}\, dt \\ \theta_{ms} &= \int \dot{\theta}_{ms}\, dt \end{aligned}\right\} \tag{33}$$

Restrained Activity Equations

The equations of motion for the restrained crew activity requires the proper combination of the individual load cell output. The load cell geometry is shown in figure A-4. By direct resolution

$$F_{Lx} = 0.6124\,(F_3 - F_4 - F_5 + F_6)$$

$$F_{Ly} = 0.7071\,(-F_1 + F_2 + 0.5\,F_3 - 0.5\,F_4 + 0.5\,F_5 - 0.5\,F_6)$$

$$F_{Lz} = 0.7071\,(F_1 + F_2 + F_3 + F_4 + F_5 + F_6)$$

$$M_{Lx} = 0.3062\,(F_3 + F_4 - F_5 - F_6)$$

$$M_{Ly} = 0.3536\,(-F_1 - F_2 + 0.5\,F_3 + 0.5\,F_4 + 0.5\,F_5 + 0.5\,F_6)$$

Appendix A

The center of mass shift of the subject will produce gravity moments on the load cell array. The actual forces and moments at the load cell centroid disturbing the spacecraft are given by

$$F_{sx} = F_{Lx}$$

$$F_{sy} = F_{Ly}$$

$$F_{sz} = F_{Lz}$$

$$M_{sx} = M_{Lx} - W \cdot Y_{cm}$$

$$M_{sy} = M_{Ly} + W \cdot X_{cm}$$

$$M_{sz} = M_{Lz}$$

where W is the subject weight.

DESCRIPTION OF LIMS ANGLES

The angular positions of the astronaut's limbs are measured by the LIMS shown and identified in figure A-5. Segment masses are numbered as shown in figure A-3.

If the origin of a right-handed set of orthogonal axes is placed at the joints between the segments, the angles measured by LIMS represents the following rotations about these axes:

φ rotation about x;

θ rotation about y;

ψ rotation about z;

where the positive sense of rotation is determined by the right-hand rule.

The initial axes orientation for each segment is determined from the "zero" position of LIMS, i.e., the position when all potentiometers read zero. This position is attained when the astronaut assumes a normal standing position. The axes centered at the segment center of mass (shown in fig. A-2) have the same orientation as the joint axes.

For segments 1, 6, 7, 8, and 9, the positive x axis points toward the front of the astronaut, the positive y toward the right, and the positive z downward. The axes orientation for segments 2 and 3 are shown in figure A-6 (the axes for 4 and 5 are parallel to 2 and 3). The positive z axis points toward the outer part of the segment and is coincident with the longitudinal axis of the segment. If the arm assumes an initial position at the astronaut's side, the forearm will rotate about an axis at the elbow which is yawed approximately 45° as shown in figure A-6. Therefore, the initial orientation of the x and y axes for segments 2 through 5 is defined as follows: for segments 2 and 4 (right arm) x and y axes are yawed -45°; and for segments 3 and 5 (left arm) x and y are yawed +45°. Angles in these yawed coordinates are measured by LIMS.

The sequence of angle rotations for the right upper arm, segment 2, going from the torso axes to the segment axes is a yaw of -45°, roll (φ_2), pitch (θ_2), and finally a yaw (ψ_2). The sequence of angle rotations for the left upper arm, segment 3, going from the torso axes to the segment axes is a yaw of +45°, roll (φ_3), pitch (θ_3), and finally a yaw (ψ_3). Segments 4 through 9 rotate only in pitch (θ_{4-9}) relative to an adjacent segment.

LIMS TRANSFORMATION MATRICES

The following transformation matrices are used to transform quantities measured in the segment axes to the torso axes. The angles φ, θ, and ψ are those measured by LIMS.

In general, transforming from segment to reference axes, the transformation for a rotation about the z axis is

$$D(\psi) = \begin{bmatrix} C\psi & -S\psi & 0 \\ S\psi & C\psi & 0 \\ 0 & 0 & 1 \end{bmatrix}$$

Appendix A

For the rotation about the y axis

$$D(\theta) = \begin{bmatrix} C\theta & 0 & S\theta \\ 0 & 1 & 0 \\ -S\theta & 0 & C\theta \end{bmatrix}$$

And for the rotation about the x axis

$$D(\varphi) = \begin{bmatrix} 1 & 0 & 0 \\ 0 & C\varphi & -S\varphi \\ 0 & S\varphi & C\varphi \end{bmatrix}$$

Based on the description of LIMS and definition of angles given previously, the total transformations from the jth segment into the body can be written. They are given by

$$D_{42} = D(\theta_4)$$

$$D_{21} = D(\psi = -45°)\ D(\varphi_2)\ D(\theta_2)\ D(\psi_2)$$

$$D_{53} = D(\theta_5)$$

$$D_{31} = D(\psi = +45°)\ D(\varphi_3)\ D(\theta_2)\ D(\psi_2)$$

$$D_{86} = D(\theta_8)$$

$$D_{61} = (\theta_6)$$

$$D_{97} = D(\theta_9)$$

$$D_{71} = D(\theta_7)$$

Appendix A

Defining the elements of the transformation matrices as

$$D_{j1} = \begin{bmatrix} 11^{d}_{j1} & 12^{d}_{j1} & 13^{d}_{j1} \\ 21^{d}_{j1} & 22^{d}_{j1} & 23^{d}_{j1} \\ 31^{d}_{j1} & 32^{d}_{j1} & 33^{d}_{j1} \end{bmatrix}$$

and expanding

Segment 2, Right Upper Arm

$$D_{21} = D(\psi = -45°)\ D(\varphi_2)\ D(\theta_2)\ D(\psi_2)$$

$$11^{d}_{21} = .7071\ (C\theta_2 C\psi_2 + S\varphi_2 S\theta_2 C\psi_2 + C\varphi_2 S\psi_2)$$

$$12^{d}_{21} = .7071\ (-C\theta_2 S\psi_2 + C\varphi_2 C\psi_2 - S\varphi_2 S\theta_2 S\psi_2)$$

$$13^{d}_{21} = .7071\ (S\theta_2 - S\varphi_2 C\theta_2)$$

$$21^{d}_{21} = .7071\ (-C\theta_2 C\psi_2 + S\varphi_2 S\theta_2 C\psi_2 + C\varphi_2 S\psi_2)$$

$$22^{d}_{21} = .7071\ (C\theta_2 S\psi_2 + C\varphi_2 C\psi_2 - S\varphi_2 S\theta_2\ S\psi_2)$$

$$23^{d}_{21} = .7071\ (-S\theta_2 - S\varphi_2 C\theta_2)$$

$$31^{d}_{21} = -C\varphi_2 S\theta_2 C\psi_2 + S\varphi_2 S\psi_2$$

$$32^{d}_{21} = S\varphi_2 C\psi_2 + C\varphi_2 S\theta_2 S\psi_2$$

$$33^{d}_{21} = C\varphi_2 C\theta_2$$

Appendix A

Segment 3, Left Upper Arm

$$D_{31} = D(\psi = +45°)\ D(\varphi_3)\ D(\theta_3)\ D(\psi_3)$$

$$_{11}d_{31} = .7071\ (C\theta_3 C\psi_3 - S\varphi_3 S\theta_3 C\psi_3 - C\varphi_3 S\psi_3)$$

$$_{12}d_{31} = .7071\ (-C\theta_3 S\psi_3 - C\varphi_3 C\psi_3 + S\varphi_3 S\theta_3 S\psi_3)$$

$$_{13}d_{31} = .7071\ (S\theta_3 + S\varphi_3 C\theta_3)$$

$$_{21}d_{31} = .7071\ (C\theta_3 C\psi_3 + S\varphi_3 S\theta_3 C\psi_3 + C\varphi_3 S\psi_3)$$

$$_{22}d_{31} = .7071\ (-C\theta_3 S\psi_3 + C\varphi_3 C\psi_3 - S\varphi_3 S\theta_3 S\psi_3)$$

$$_{23}d_{31} = .7071\ (S\theta_3 - S\varphi_3 C\theta_3)$$

$$_{31}d_{31} = -C\varphi_3 S\theta_3 C\psi_3 + S\varphi_3 S\psi_3$$

$$_{32}d_{31} = S\varphi_3 C\psi_3 + C\varphi_3 S\theta_3 S\psi_3$$

$$_{33}d_{31} = C\varphi_3 C\theta_3$$

Segment 4, Right Lower Arm

$$D_{41} = D_{21}\ D_{42}$$

where $D_{42} = D(\theta_4)$

$$
\begin{aligned}
{}^{11}d_{41} &= 0.7071\left[\left(C\theta_2 C\psi_2 + S\varphi_2 S\theta_2 C\psi_2 + C\varphi_2 S\psi_2\right) C\theta_4 - \left(S\theta_2 - S\varphi_2 C\theta_2\right) S\theta_4\right] \\
{}^{12}d_{41} &= 0.7071\left(-C\theta_2 S\psi_2 + C\varphi_2 C\psi_2 - S\varphi_2 S\theta_2 S\psi_2\right) \\
{}^{13}d_{41} &= 0.7071\left[\left(C\theta_2 C\psi_2 + S\varphi_2 S\theta_2 C\psi_2 + C\varphi_2 S\psi_2\right) S\theta_4 + \left(S\theta_2 - S\varphi_2 C\theta_2\right) C\theta_4\right] \\
{}^{21}d_{41} &= 0.7071\left[\left(-C\theta_2 C\psi_2 + S\varphi_2 S\theta_2 C\psi_2 + C\varphi_2 S\psi_2\right) C\theta_4 + \left(S\theta_2 + S\varphi_2 C\theta_2\right) S\theta_4\right] \\
{}^{22}d_{41} &= 0.7071\left(C\theta_2 S\psi_2 + C\varphi_2 C\psi_2 - S\varphi_2 S\theta_2 S\psi_2\right) \\
{}^{23}d_{41} &= 0.7071\left[\left(-C\theta_2 C\psi_2 + S\varphi_2 S\theta_2 C\psi_2 + C\varphi_2 S\psi_2\right) S\theta_4 - \left(S\theta_2 + S\varphi_2 C\theta_2\right) C\theta_4\right] \\
{}^{31}d_{41} &= \left(-C\varphi_2 S\theta_2 C\psi_2 + S\varphi_2 S\psi_2\right) C\theta_4 - \left(C\varphi_2 C\theta_2\right) S\theta_4 \\
{}^{32}d_{41} &= S\varphi_2 C\psi_2 + C\varphi_2 S\theta_2 S\psi_2 \\
{}^{33}d_{41} &= \left(-C\varphi_2 S\theta_2 C\psi_2 + S\varphi_2 S\psi_2\right) S\theta_4 + \left(C\varphi_2 C\theta_2\right) C\theta_4
\end{aligned}
$$

Segment 5, Left Lower Arm

$$D_{51} = D_{31}\, D_{53}$$

where

$$D_{53} = D(\theta_5)$$

$$
\begin{aligned}
{}^{11}d_{51} &= 0.7071\left[\left(C\theta_3 C\psi_3 - S\varphi_3 S\theta_3 C\psi_3 - C\varphi_3 S\psi_3\right) C\theta_5 - \left(S\theta_3 + S\varphi_3 C\theta_3\right) S\theta_5\right] \\
{}^{12}d_{51} &= 0.7071\left(-C\theta_3 S\psi_3 - C\varphi_3 C\psi_3 + S\varphi_3 S\theta_3 S\psi_3\right) \\
{}^{13}d_{51} &= 0.7071\left[\left(C\theta_3 C\psi_3 - S\varphi_3 S\theta_3 C\psi_3 - C\varphi_3 S\psi_3\right) S\theta_5 + \left(S\theta_3 + S\varphi_3 C\theta_3\right) C\theta_5\right] \\
{}^{21}d_{51} &= 0.7071\left[\left(C\theta_3 C\psi_3 + S\varphi_3 S\theta_3 C\psi_3 + C\varphi_3 S\psi_3\right) C\theta_5 - \left(S\theta_3 - S\varphi_3 C\theta_3\right) S\theta_5\right]
\end{aligned}
$$

$$_{22}d_{51} = 0.7071\ (-C\theta_3 S\psi_3 + C\varphi_3 C\psi_3 - S\varphi_3 S\theta_3 S\psi_3)$$

$$_{23}d_{51} = 0.7071\ \left[(C\theta_3 C\psi_3 + S\varphi_3 S\theta_3 C\psi_3 + C\varphi_3 S\psi_3)\ S\theta_5 + (S\theta_3 - S\varphi_3 C\theta_3)\ C\theta_5\right]$$

$$_{31}d_{51} = (-C\varphi_3 S\theta_3 C\psi_3 + S\varphi_3 S\psi_3)\ C\theta_5 - (C\varphi_3 C\theta_3)\ S\theta_5$$

$$_{32}d_{51} = S\varphi_3 C\psi_3 + C\varphi_3 S\theta_3 S\psi_3$$

$$_{33}d_{51} = (-C\varphi_3 S\theta_3 C\psi_3 + S\varphi_3 S\psi_3)\ S\theta_5 + (C\varphi_3 C\theta_3)\ C\theta_5$$

Segment 6, Right Upper Leg

$$D_{61} = D(\theta_6)$$

$$_{11}d_{61} = C\theta_6$$

$$_{12}d_{61} = 0$$

$$_{13}d_{61} = S\theta_6$$

$$_{21}d_{61} = 0$$

$$_{22}d_{61} = 1$$

$$_{23}d_{61} = 0$$

$$_{31}d_{61} = -S\theta_6$$

$$_{32}d_{61} = 0$$

$$_{33}d_{61} = C\theta_6$$

Segment 7, Left Upper Leg

$$D_{71} = D(\theta_7)$$

$$_{11}d_{71} = C\theta_7$$

$$_{12}d_{71} = 0$$

$$_{13}d_{71} = S\theta_7$$

$$_{21}d_{71} = 0$$

$$_{22}d_{71} = 1$$

$$_{23}d_{71} = 0$$

$$_{31}d_{71} = -S\theta_7$$

$$_{32}d_{71} = 0$$

$$_{33}d_{71} = C\theta_7$$

Appendix A

Segment 8, Right Lower Leg

$$D_{81} = D_{61}\, D_{86}$$

where

$$D_{86} = D(\theta_8)$$

$$_{11}d_{81} = C(\theta_6 + \theta_8)$$

$$_{12}d_{81} = 0$$

$$_{13}d_{81} = S(\theta_5 + \theta_8)$$

$$_{21}d_{81} = 0$$

$$_{22}d_{81} = 1$$

$$_{23}d_{81} = 0$$

$$_{31}d_{81} = -S(\theta_6 + \theta_8)$$

$$_{32}d_{81} = 0$$

$$_{33}d_{81} = C(\theta_6 + \theta_8)$$

Segment 9, Left Lower Leg

$$D_{91} = D_{71}\, D_{97}$$

where

$$D_{97} = D(\theta_9)$$

$$_{11}d_{91} = C(\theta_7 + \theta_9)$$

$$_{12}d_{91} = 0$$

$$_{13}d_{91} = S(\theta_7 + \theta_9)$$

$$_{21}d_{91} = 0$$

$$_{22}d_{91} = 1$$

$$_{23}d_{91} = 0$$

$$_{31}d_{91} = -S(\theta_7 + \theta_9)$$

$$_{32}d_{91} = 0$$

$$_{33}d_{91} = C(\theta_7 + \theta_9)$$

Appendix A

MATH MODEL OF MAN*

The astronaut is considered to be a nine-segment model as shown in figure A-7. The masses and inertias of the segments as a function of the weight, W, of the man are given by

$$k_m = \frac{W}{29.3\ W + 389}$$

$$m_1 = k_m(0.47m + 12)$$

$$m_2 = m_3 = k_m(0.04\ W - 1.45)$$

$$m_4 = m_5 = k_m(0.025\ W + 0.1)$$

$$m_6 = m_7 = k_m(0.09\ W + 1.6)$$

$$m_8 = m_9 = k_m(0.065\ W - 0.2)$$

$${}_1I_{1xx} = 0.0146\ W - 0.576$$

$${}_1I_{1yy} = 0.0137\ W - 0.536$$

$${}_1I_{1zz} = 0.00331\ W - 0.243$$

$${}_2I_{zxy} = {}_2I_{2yy} = {}_3I_{3xx} = {}_3I_{3yy} = 0.00022\ W - 0.0172$$

$${}_2I_{2zz} = {}_3I_{3zz} = 0.0000268\ W - 0.00243$$

$${}_4I_{4xx} = {}_4I_{4yy} = {}_5I_{5yy} = 0.000159\ W - 0.00781$$

$${}_4I_{4zz} = {}_5I_{5zz} = 0.0000112\ W - 0.000768$$

$${}_6I_{6xx} = {}_6I_{6yy} = {}_7I_{7xx} = {}_7I_{7yy} = 0.000656\ W - 0.0373$$

$${}_6I_{6zz} = {}_7I_{7zz} = 0.00019\ W - 0.0142$$

*Wooley, C. T.: Segment Masses, Centers of Gravity and Local Moments of Inertia for an Analytical Model of Man. Internal Document LWP-228. Langley Research Center, Langley Station, Hampton, Virginia.

Appendix A

$${}_8I_{8xx} = {}_9I_{9xx} = 0.000892\ W - 0.0544$$

$${}_8I_{8yy} = {}_9I_{9yy} = 0.000859\ W - 0.0534$$

$${}_8I_{8zz} = {}_9I_{9zz} = 0.0000797\ W - 0.00463$$

$${}_1r_1 = 0.00145\ W + 1.55$$

$${}_2r_2 = {}_3r_3 - 0.000145\ W + 0.355$$

$${}_2L_2 = {}_3L_3 = 0.00132\ W + 0.768$$

$${}_4r_4 = {}_5r_5 = 0.000658\ W + 0.456$$

$${}_6r_6 = {}_7r_7 = -0.0004\ W + 0.828$$

$${}_6L_6 = {}_7L_7 = 0.000729\ W + 1.324$$

$${}_8r_8 = {}_9r_9 = 0.00106\ W + 0.597$$

$${}_1S_1 = 0.00135\ W + 0.916$$

$${}_1S_2 = 0.00196\ W + 0.388$$

$$S_3 = 0.000422\ W + 0.208$$

$${}_1L_1 = 0.0038\ W + 2.117$$

Appendix A

EXPANSION OF TERMS

$$\sum_{i=1}^{9} {}_1\bar{\bar{I}}_1 = {}_1\bar{\bar{I}}_1 + D_{21}\ {}_2\bar{\bar{I}}_2\ D_{12} + D_{31}\ {}_3\bar{\bar{I}}_3\ D_{13}$$

$$+ D_{41}\ {}_4\bar{\bar{I}}_4\ D_{14} + D_{51}\ {}_5\bar{\bar{I}}_5\ D_{15}$$

$$+ D_{61}\ {}_6\bar{\bar{I}}_6\ D_{16} + D_{71}\ {}_7\bar{\bar{I}}_7\ D_{17}$$

$$+ D_{81}\ {}_8\bar{\bar{I}}_8\ D_{18} + D_{91}\ {}_9\bar{\bar{I}}_9\ D_{19}$$

where $${}_i\bar{\bar{I}}_i = \begin{bmatrix} {}_iI_{ixx} & 0 & 0 \\ C & {}_iI_{iyy} & 0 \\ C & C & {}_iI_{izz} \end{bmatrix}$$

$$\sum_{i=1}^{9} {}_1\bar{\bar{I}}_i \cdot {}_1\bar{\omega}_{ii} = D_{21}\left({}_2\bar{\bar{I}}_2 \cdot {}_2\bar{\omega}_{21}\right) + D_{31}\left({}_3\bar{\bar{I}}_3 \cdot {}_3\bar{\omega}_{31}\right)$$

$$+ D_{41}\ {}_4\bar{\bar{I}}_4 \cdot \left({}_4\bar{\omega}_{42} + D_{24}\ {}_2\bar{\omega}_{21}\right)$$

$$+ D_{51}\ {}_5\bar{\bar{I}}_5 \cdot \left({}_5\bar{\omega}_{53} + D_{35}\ {}_3\dot{\bar{\omega}}_{31}\right)$$

$$+ D_{61}\left({}_6\bar{\bar{I}}_6 \cdot {}_6\bar{\omega}_{61}\right) + D_{71}\left({}_7\bar{\bar{I}}_7 \cdot {}_7\bar{\omega}_{71}\right)$$

$$+ D_{81}\ {}_8\bar{\bar{I}}_8\left({}_8\bar{\omega}_{86} + D_{68}\ {}_6\bar{\omega}_{61}\right)$$

$$+ D_{91}\ {}_9\bar{\bar{I}}_9\left({}_9\bar{\omega}_{97} + D_{97}\ {}_7\bar{\omega}_{71}\right)$$

Appendix A

The vector ${}_1\bar{\rho}_{cm}$ defines the man's combined center of gravity location with reference to the top of the astronaut's head, i.e.,

$$ {}_1\bar{\rho}_{cm} = \frac{1}{m_m} \sum_{i=1}^{9} m_i \, {}_i\bar{\rho}_i $$

where ${}_i\bar{\rho}_i$ is in the position vector locating the center of mass of each segment relative to the top of the head.

Using the segment dimensions shown in figure A-7, the ${}_i\bar{\rho}_i$ vectors are

$$ {}_1\bar{\rho}_1 = is_2 $$

$$ {}_1\bar{\rho}_2 = is_2 + js_1 + D_{21} \, {}_2\bar{\ell}_2 $$

$$ {}_1\bar{\rho}_3 = is_2 - js_1 + D_{31} \, {}_3\bar{\ell}_3 $$

$$ {}_1\bar{\rho}_4 = is_2 + js_1 + D_{21} \left({}_2\bar{L}_2 + D_{42} \, {}_4\bar{\ell}_4 \right) $$

$$ {}_1\bar{\rho}_5 = is_2 - js_1 + D_{31} \left({}_3\bar{L}_3 + D_{53} \, {}_5\bar{\ell}_5 \right) $$

$$ {}_1\bar{\rho}_6 = iL_1 + js_3 + D_{61} \, {}_6\bar{\ell}_6 $$

$$ {}_1\bar{\rho}_7 = iL_1 - js_3 + D_{71} \, {}_7\bar{\ell}_7 $$

$$ {}_1\bar{\rho}_8 = iL_1 + js_3 + D_{61} \left({}_6\bar{L}_6 + D_{86} \, {}_8\bar{\ell}_8 \right) $$

$$ {}_1\bar{\rho}_9 = iL_1 - js_3 + D_{71} \left({}_7\bar{L}_7 + D_{97} \, {}_9\bar{\ell}_9 \right) $$

The vector ${}_1\bar{r}_i$ is then given by

$$ {}_1\bar{r}_i = {}_1\bar{\rho}_i - {}_1\bar{\rho}_{cm} $$

APPENDIXES B, C, D, AND E

ARE BOUND SEPARATELY

IN THE DATA SUPPLEMENT

Appendix F

APOLLO EARTH ORBITAL SCIENTIFIC EXPERIMENT PROPOSAL

TITLE OF EXPERIMENT

Vehicle Disturbances Due To Crew Activities

NAME OF INVESTIGATOR

P. R. Kurzhals
Bruce Conway

NAME OF SPONSORING INSTITUTION

Spacecraft Systems Branch, AMPD
Langley Research Center
Hampton, Virginia

1. TITLE OF EXPERIMENT

Vehicle Disturbances Due to Crew Activity

DATE OF SUBMISSION

29 December 1966

(For Headquarters use only.)

DATE RECEIVED BY SM

2. SPONSOR

NAME OF SPONSORING INSTITUTION

Spacecraft Systems Branch, AMPD
Langley Research Center

ADDRESS

Hampton, Virginia

TELEPHONE

722-7961

NAME OF PRINCIPAL ADMINISTRATOR RESPONSIBLE FOR EXPERIMENT

Peter R. Kurzhals, Spacecraft Systems Branch, AMPD

3. INVESTIGATORS

NAME OF PRINCIPAL INVESTIGATOR

Peter R. Kurzhals, Spacecraft Systems Branch, AMPD

ADDRESS

NASA - Langley Research Center
Hampton, Virginia

TELEPHONE

722-7961 X-2691

NAMES OF OTHER INVESTIGATORS	ADDRESS	TELEPHONE
Bruce A. Conway	NASA - Langley Research Center Hampton, Virginia	722-7961 X-2691
C. H. Murrish J. R. Tewell R. A. Skidmore R. G. Brown	Martin Marietta Corporation Denver Division Denver, Colorado 80201	303-794-5211 X-2736

SCIENTIFIC INFORMATION AND PROGRAM PLAN - PART I

1. PURPOSE AND OBJECTIVE OF THE EXPERIMENT

Purpose. - To determine to what extent crew movements affect the Apollo spacecraft stability and control systems.

Objectives. - Measure the effects of various crew motions on the dynamics of manned spacecraft. Specifically, partial and total body motion of the astronaut will be measured by actual body instrumentation (LIMS, limb motion sensor) and by motion picture photography. The resulting vehicle motion due to astronaut movement will be recorded by rate, acceleration, and position sensing devices in the spacecraft. These data will be telemetered to the earth to check the validity of information obtained from ground simulation experiments and to determine the effects of astronaut motion on vehicle attitude and control systems.

2. STATE OF PRESENT DEVELOPMENT IN THE FIELD:

A review of crew activities has been made and categorized as in-place motions and translation motions. The in-place motions include console operations and exercise. The translation motions are those involving adhesive walking, compressive walking, guided soaring, and free soaring. These motions have been studied both analytically and by simulation under Contract NAS 1-6713. The edited results of this study are not yet available but will be by 9 January 1967. In this study, the necessary instrumentation to determine vehicle attitude and attitude rates, body position thru joint rotation, and direct measurement of applied forces and moments with respect to a fixed point were developed. Details of this instrumentation will be included in the final report on this contract.

A functional analysis of the planned experiment and timeline estimate was also made in the aforementioned study.

(Attach additional sheets if necessary, identifying items by number.)

3. SPECIFY PARAMETERS TO BE MEASURED INCLUDING NUMERICAL VALUES EXPECTED AND OUTLINE THE RESEARCH PROGRAM:

The dynamic effects of man on a spacecraft are dependent on the change of his center of mass and his inertia products. The Denver Division has developed both a digital program and a six-degree-of-freedom gravity-free simulation of man and his vehicle including the effects of man's inertia products and center-of-mass change. The basic element in both techniques is the determination of the inertia products and center-of-mass changes as a function of man's limb position. The determination of limb position as a function of time is thus of paramount interest to the development of this experiment. It enables direct comparison of in-flight data, gravity-free simulation, and analytic data developed thru the digital program.

Therefore, one set of parameters to be measured are the principal joint rotations as measured by the limb motion sensor developed by the Denver Division. Certain modifications and refinements are required to ensure reliable, convenient, flight-qualified hardware as well as to simplify the model as feasible. It is anticipated that a 50-man-month program to develop an optimum model and a refined LIMS design will be necessary.

The expected scope of the joint solution measurement will involve 14 joint sensors or linear potentiometers, a 14-channel analog-to-digital converter, a PCM transmitter, a PCM receiver, and the appropriate Apollo telemetry interface electronics as well as the necessary structural and packaging hardware.

Direct measurements of applied forces and the resulting moments will be measured by a load cell array, power supply, and signal conditioning combination. It is estimated that off-the-shelf hardware and standard packaging techniques will be satisfactory to measure these forces and moments.

The vehicle attitude rates will be measured by a rate gyro system provided with an adjustable bias null out of residual rates prior to initiation of the experiment. The gyro outputs will be converted to digital pulses and counted for fixed increments of time to yield vehicle attitude angles as well as attitude rates. It is estimated that a 20-man-month program will be required to produce the necessary designs to enable hardware procurement.

The magnitudes of the parameters are estimated to be in the following ranges:

Joint rotations, $0 < \theta < 180°$;

Applied forces, $0 < F < 50$ lb;

Applied moments, $0 < M < 50$ ft-lb;

Attitude rate, $0.1°/hr < \dot{\theta} < 40°/hr$;

Attitude, $\theta > 1.11 \times 10^{-3°}$.

(Attach additional sheets if necessary, identifying items by number.)

4. PRESENT AN ANALYSIS OF THE PERFORMANCE OF THE PROPOSED EXPERIMENT *(e.g., dynamic range, signal to noise ratio, etc.)*

Direct simulation of crew activity indicates joint rotations at the rate of 180°/sec are possible. During the simulation studies, the LIMS signal voltages were, at peak values, of the order of 1000 times the peak noise voltages. This figure may be optimistic for the in-flight system since there was no analog-to-digital conversion in the simulation.

Preliminary analysis indicates that there may be some hysteresis problems associated with the load cell arrays. This problem was solved during simulation by the addition of small amounts of low-amplitude, high-frequency, mechanical dither. The output level of the individual load cells is 150 mV for maximum rated load. Buffer amplification is necessary to maintain linearity and adjustment of maximum output to be compatible with the onboard telemetry system. Under the simulation conditions, the signal-to-noise ratio was found to be greater than 10:1, and the sensitivity is of the order of 3 mV/lb. The sensitivity is a function of the load cell rating, the applied voltage, and the degree of amplification used.

The digital attitude and attitude rate system dynamic range has not yet been established. Estimates of its performance are included in the attached report. Movies of the in flight activity will be made for comparison with those made of the simulation.

(Attach additional sheets if necessary, identifying items by number.)

5. DISCUSS THE METHOD OR POSSIBLE METHODS FOR THE ANALYSIS AND INTERPRETATION OF THE DATA *(e.g., the statistical validity)*

All data will be reduced and analyzed on the ground. It may be done during the orbital flight or at some later date, depending on the advisability of repeating certain phases to increase the confidence level of the results. It is anticipated, however, that this will not be necessary. Since the raw data will be telemetered to a ground station, it will be received in a digital format. This digital data will then be fed into a general-purpose digital computer and reduced to a usable form, including the rotation angles of all joints, those directly measured forces and moments, and the measured attitude and attitude rate. The rotation angles of all joints will then form the input data for a program designed to compute the forces, moments, attitude, and attitude rate for comparison purposes. The measured forces and moments will be translated to yield the moments on the spacecraft for direct comparison with the computed values. The measured and computed data for the in-flight experiment will then be compared with the simulation data. The following block diagram indicates briefly the analysis scheme.

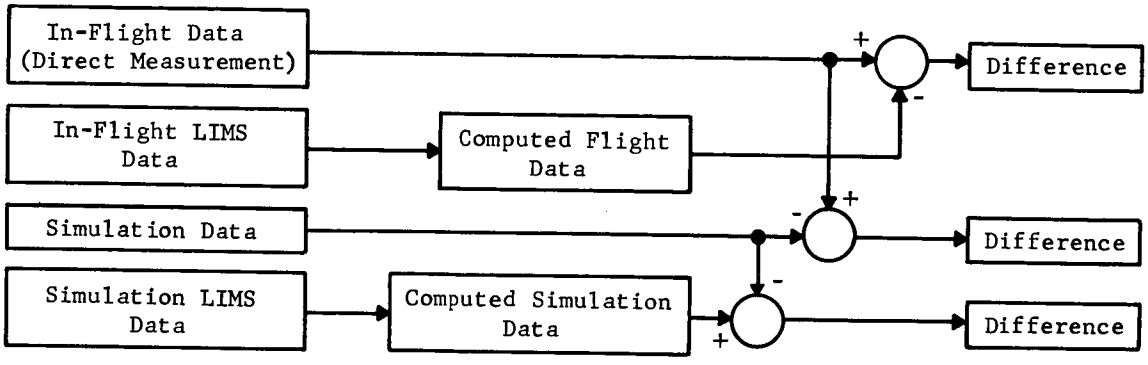

The direct comparison of in-flight data with simulation data is subject to question or at best only subjective analysis, since identical limb motion history is impossible to achieve.

(Attach additional sheets if necessary, identifying items by number.)

6. DESCRIBE THE EXPERIMENTAL PROCEDURE TAKING INTO CONSIDERATION THE ENVIRONMENT AND ORBITAL CHARACTERISTICS OF THE SPACECRAFT. INCLUDE ANY CONSTRAINTS ON SPACECRAFT ATTITUDE, POINTING ACCURACY, AND STABILITY. EXPLAIN WHY THE ASTRONAUT IS NECESSARY TO THE PERFORMANCE OF THIS EXPERIMENT. DESCRIBE IN DETAIL OPERATIONS PERFORMED BY THE ASTRONAUT AND TIME CONSUMED DURING EACH OPERATION. *(Include length of time the spacecraft must hold a given attitude.)*

Flight Experiment Ground Rules

1. Any orbit providing zero g is acceptable for this experiment.

2. The S-IVB workshop and MDA will contain a two-gas EC system containing 3.5 psi of O_2 and 1.5 psi of N_2 with a total pressure of 5 psi. The CSM will contain 100% O_2 at 5 psi.

3. The total experiment will be conducted (once) in the S-IVB workshop.

4. All experimental equipment will be stowed in the MDA or airlock section.

5. This experiment will make maximum use of equipment assembled in the S-IVB workshop for use on other experiments, such as, communication links, 35-mm-still and 16- and 8-mm-movie cameras, lights, recorders, electrical power, control and display panels, personnel anchoring tethers, and a personnel chair.

6. The in-flight experiment will duplicate the ground simulation as closely as possible. The flight experiment will include:

   Involuntary actions (coughing, sneezing, etc);
   Exercise;
   Console operations (restrained activities);
   Soaring and impacts;
   Torquing and assembly tasks;
   Crew transfer;
   Compressive walking;
   Velcro walking.

Ground Rules

7. Experiment data will be recorded and telemetered to the ground at tracking station overpasses for future evaluation.

8. Basic flight experimental hardware will include:

   LIMS (limb motion sensor);
   Load cells (minimum to two);
   Digital attitude rate sensor package (DARS);
   Data recording equipment not available from other experiments;
   Interface equipment (cabling, etc).

9. The experimental astronaut will not be in a pressure suit, and no EVA is required for this experiment.

(Attach additional sheets if necessary, identifying items by number.)

Item 6.-Continued

Experiment Function Description

Two astronauts are required in the S-IVB workshop to perform this experiment, and one astronaut is required in the CSM.

		Approximate time, minutes
1.	Two astronauts translate from CSM to MDA (open and close one hatch).	5
2.	Unstow experimental equipment, LIMS, DAR package, load cells, and recording equipment if not already in S-IVB from other experiments.	10
3.	Translate from MDA to S-IVB workshop with experiment equipment.	20
4.	Establish communication link to CSM.	3
5.	Mount experiment equipment in S-IVB workshop at experiment location.	5
6.	Attach interface wiring to load cells, DAR package, and recording equipment.	3
7.	Turn on and calibrate above equipment.	10
8.	Turn on DAR package (20-minute warmup).	0.2
9.	Assemble LIMS.	15
10.	Don LIMS, attach interface cabling, and calibrate potentiometers.	20
11.	Activate minimum impulse stability mode (at CSM) for 0.005°/sec, all axes. Allow 10-15 minute stabilization time.	10
12.	Position astronaut at experiment location.	2
13.	Activate all experiment equipment and recording devices, LIMS, DAR, load cells, and TM, and place cameras on standby.	2

Appendix F

Item 6.-Concluded

14.	Restrain nonexperiment astronauts (one in S-IVB workshop and one in CSM).	3
15.	Disable spacecraft attitude thrusters.	0.2
16.	Record total spacecraft drift (attitude rate) in 3 axes.	2
17.	Activate cameras.	0.2
18.	Perform experimental sequence, partial and total body movements.	45
19.	Deactivate cameras and recorders.	0.4
20.	Verify data collection accuracy.	3
21.	Turn off all experiment equipment.	0.5
22.	Activate spacecraft stabilization system.	1.0
23.	Remove LIMS and restrain in S-IVB workshop.	4
24.	Remove recorder tape and movie film.	3

Total = 2 hr 48 minutes

7. ASTRONAUT TIME REQUIREMENT SYNOPSIS

PREFLIGHT TIME	IN-FLIGHT TIME	POSTFLIGHT TIME
	Approximately 2 hr 48 minutes	None

8. DESCRIBE THE PREFLIGHT AND POSTFLIGHT REQUIREMENTS ON THE ASTRONAUT

No special preflight skills are required of the astronauts other than those obtained during training for the mission and equipment familiarization.

There are no postflight astronaut requirements associated with this experiment.

9. DISCUSS PREFLIGHT AND RECOVERY FACILITIES REQUIRED AND DATA HANDLING PROCEDURES

Preflight facilities will be minimal. It will be necessary only to check out the instrumentation packages prior to launch, and it is anticipated that whatever checkout equipment is required is already available.

Since it is planned that all data will be telemetered to ground stations, the only recovery facilities required will be those normally associated with the manned Apollo flights. The only special provisions will be suitable storage for the movie film taken during flight.

The telemetered data may be fed directly into a digital computer for reduction as outlined under Item 5 or stored on tape for subsequent reduction.

(Attach additional sheets if necessary, identifying items by number.)

ENGINEERING INFORMATION AND PROGRAM PLAN - PART II

1. DESCRIPTION OF EQUIPMENT *(Sketch major assemblies in Item 5.)*

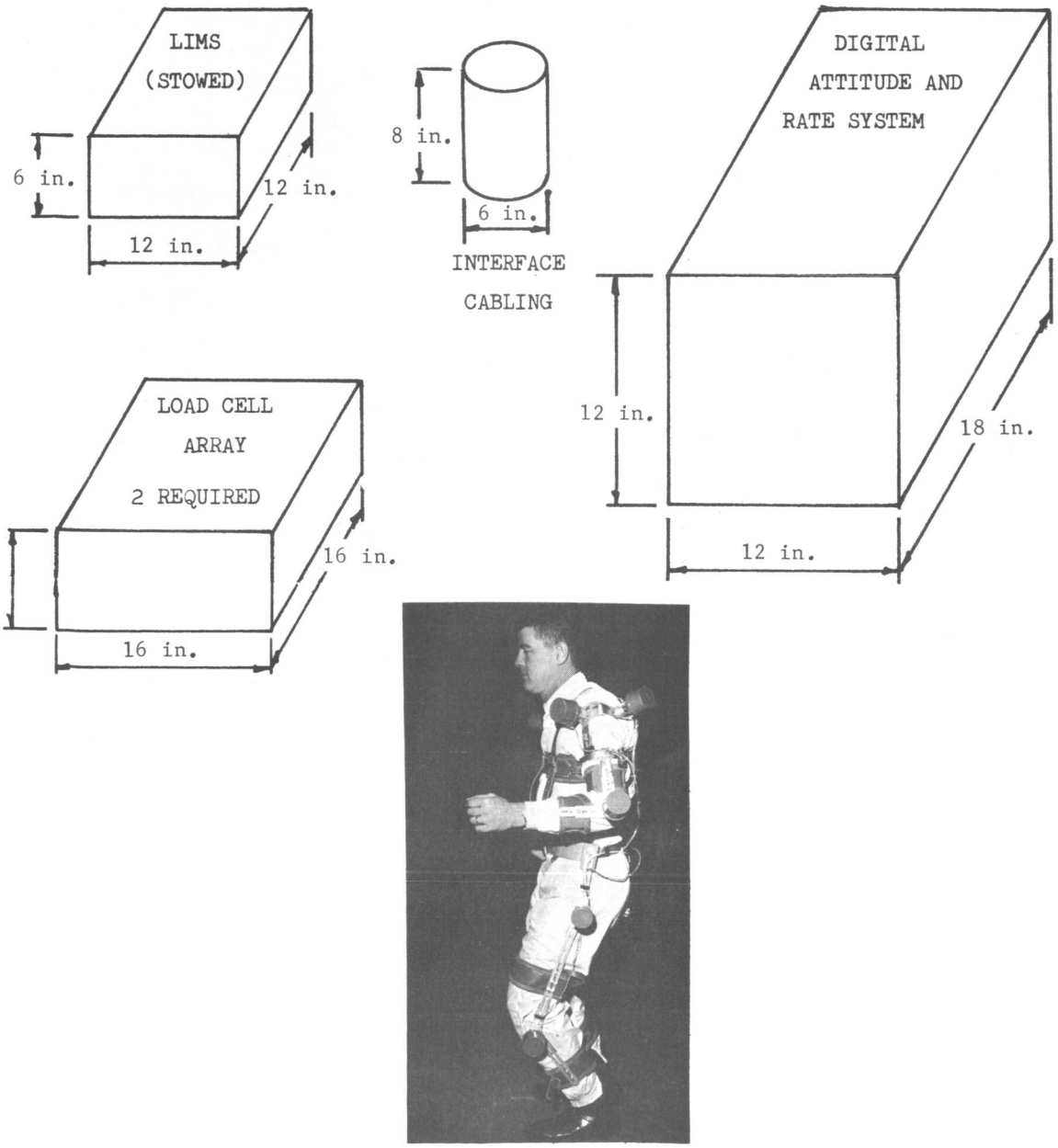

(Attach additional sheets if necessary, identifying items by number.)

ENGINEERING INFORMATION AND PROGRAM PLAN - PART II

1. DESCRIPTION OF EQUIPMENT *(Sketch major assemblies in Item 5.)*

(Attach additional sheets if necessary, identifying items by number.)

2. DESCRIBE SPACECRAFT MODIFICATIONS REQUIRED FOR ACCOMODATION OF EQUIPMENT. INDICATE PREFERRED MOUNTING CONFIGURATION HERE OR IN ITEM 5

No modifications to the CSM are anticipated.

Storage provisions for the above equipment must be provided either in the MDA or airlock.

Provisions for mounting the experimental equipment must be provided in the S-IVB workshop. The optimum location in the S-IVB and hardware required are yet to be defined.

(Attach additional sheets if necessary, identifying items by number.)

3. WEIGHT		4. VOLUME	
TOTAL WEIGHT:	95 lb	**TOTAL VOLUME:**	4 1/3 cu ft
WEIGHT OF SEPARATE ASSEMBLIES *(If any)*		VOLUME OF SEPARATE ASSEMBLIES *(If any)*	
ASSEMBLY #1 2 LOAD CELL ARRAYS	20 lb	ASSEMBLY #1	2 cu ft
ASSEMBLY #2 DIGITAL ATTITUDE AND RATE SYSTEM	40 lb maximum	ASSEMBLY #2	1 1/3 cu ft
ASSEMBLY #3 LIMS	Less than 35 lb	ASSEMBLY #3	Less than 1 cu ft

5. **ENVELOPE** *(Sketch each assembly (Designate 1, 2 or 3) indicate nominal and limiting values of each major dimension.)*

6.	POWER		
TOTAL POWER:	STANDBY 185 watts	AVERAGE 185 watts	MAXIMUM 315 watts
POWER CONSUMED BY SEPARATE ASSEMBLIES			
ASSEMBLY #1 2 load cell arrays	STANDBY 60	AVERAGE 60	MAXIMUM 60
DAR ASSEMBLY #2	STANDBY 120	AVERAGE 120	MAXIMUM 250 (during warmup)
LIMS ASSEMBLY #3	STANDBY 5 watts	AVERAGE 5 watts	MAXIMUM 5 watts

IF POWER CONSUMPTION IS NOT CONSTANT, INDICATE POWER PROFILES BELOW:

Assembly 2: 250 watts for 20-minute warmup time,
120 watts operating.

(Attach additional sheets if necessary, identifying items by number.)

7.	THERMAL CONSTRAINTS		
OPERATING TEMPERATURE LIMITS OF EACH ASSEMBLY			
Load cells	ASSEMBLY #1	MINIMUM -26 °C	MAXIMUM 94°C
DAR	ASSEMBLY #2	MINIMUM -4 °C	MAXIMUM 38°C
LIMS	ASSEMBLY #3	MINIMUM 0 °C	MAXIMUM 40°C
STORAGE TEMPERATURE LIMITS OF EACH ASSEMBLY			
Load cells	ASSEMBLY #1	MINIMUM -62 °C	MAXIMUM 100°C
DAR	ASSEMBLY #2	MINIMUM -37 °C	MAXIMUM 72°C
LIMS	ASSEMBLY #3	MINIMUM -40 °C	MAXIMUM 70°C

OTHER THERMAL CONSTRAINTS

8. OTHER ENVIRONMENTAL CONSTRAINTS *(List any remaining constraints such as preferred or prohibited orientation of assemblies with respect to direction of maximum vibration and acceleration, susceptibility to RFI, etc.)*

Digital attitude and attitude rate system must be aligned along vehicle body axes.

9. **TELEMETRY**

	OUTPUT 1	OUTPUT 2	OUTPUT 3	OUTPUT 4
FUNCTION	Limb motion history	Direct force measurement	Digital attitude	Digital attitude rate
MUST MEASUREMENT BE CONTINUOUS	During experiment only	During experiment only	During experiment only	During experiment only
MINIMUM NUMBER OF SAMPLES PER SECOND	500	500		
ACCURACY OF MEASUREMENT	1%	1%		0.11% or 0.044°/hr
MAXIMUM BIT RATE *(Digital only)*				
MINIMUM FREQUENCY RESPONSE *(Analog only)*	25 cps	25 cps		

ADDITIONAL INFORMATION

Limb motion history and direct force measurements are essentially analog measurements but will be ultimately formatted to be compatible with onboard telemetry system.

(Attach additional sheets if necessary, identifying items by number.)

10. **DEVELOPMENTAL PROGRAM**

ITEM	WHERE PERFORMED	BEGINNING DATE	COMPLETION DATE
PRELIMINARY ELECTRICAL DESIGN	Contractor		6 months from contract go-ahead
PRELIMINARY MECHANICAL DESIGN	Contractor		6 months from contract go-ahead
PRELIMINARY MOCK UP FABRICATION	Contractor		6 months from contract go-ahead
FINAL ELECTRICAL DESIGN	Contractor		9 months from contract go-ahead
FINAL MECHANICAL DESIGN	Contractor		9 months from contract go-ahead
EXACT MECHANICAL MOCK UP CONSTRUCTION	Contractor		10 months from contract go-ahead
PROTOTYPE FABRICATION	Contractor		12 months from contract go-ahead
PROTOTYPE ENVIRONMENTAL TEST	Undefined		
FLIGHT UNIT FABRICATION	Contractor		
FLIGHT UNIT ENVIRONMENTAL TEST	Undefined		
FLIGHT SPARE FABRICATION	Contractor		
FLIGHT SPARE ENVIRONMENTAL TEST	Undefined		

MANAGEMENT PLAN - PART III

(For Headquarters use only.)
DATE RECEIVED BY SM

TITLE OF EXPERIMENT

Vehicle Disturbances due to Crew Activity

SPONSORING INSTITUTION	ADDRESS
Spacecraft Systems Branch, AMPO	Langley Research Center Hampton, Virginia

1. **RESPONSIBILITIES**

INDIVIDUAL	NAME	ADDRESS
A. RESPONSIBLE ADMINISTRATOR	P. R. Kurzhals	NASA Langley Research Center Hampton, Virginia
B. PRINCIPAL INVESTIGATOR	Bruce Conway	NASA Langley Research Center Hampton, Virginia
C. CO-INVESTIGATOR(S)		

D. PRINCIPAL INVESTIGATOR'S ROLE IN RELATION TO THIS EXPERIMENT

E. RESPONSIBILITIES OF OTHER KEY PERSONS

(Attach additional sheets if necessary, identifying items by number.)

2. Estimated **COST BREAKDOWN** - Phase B

Attach a sheet (or sheets) giving the costs of the experiment for which NASA support will be required, in the following format, and in the detail specified. Separate cost breakdowns should be submitted for the three phases of experiment funding shown in Item 3, "Quarterly Funding Requirements".

ITEM	AMOUNT
DIRECT LABOR *(Separate by Labor Category; Rate per hour or man-month; Personnel involved, what they will do, etc.)*	$ 43 574
MANUFACTURING BURDEN *(Overhead)* RATE (%) *(Flight experiments normally will be supported by contracts rather than grants.)*	47 496
MATERIALS *(Total) (Bill of Material, including estimated cost of each major item.)*	25 000
PROFIT (10%)	17 503
SPECIAL EQUIPMENT *(Total) (List of lab equipment, proposed uses, and estimated cost.)* Computers Computers	36 480
TRAVEL *(Estimated number of individual trips, destinations, and costs.)*	
ANY OTHER ITEMS *(Total) (Explain in detail similar to the above.)* Direct Services	2 320
TOTAL COSTS	$ 172 373
GENERAL AND ADMINISTRATIVE RATE (0.13)	$ 19 862
TOTAL ESTIMATED COST	$ 192 235

Experimenters who request to conduct the proposed experiment as an extension of an existing grant or contract, should list the grant or contract number and the name and address of the NASA technical monitor below.

GRANT OR CONTRACT NO.	NAME AND ADDRESS OF NASA TECHNICAL MONITOR
NAS 1-6713	Bruce Conway, NASA-Langley Research Center Hampton, Virginia

3. **QUARTERLY FUNDING REQUIREMENTS** *(Dollars in thousands)*

Budgetary Estimates Only

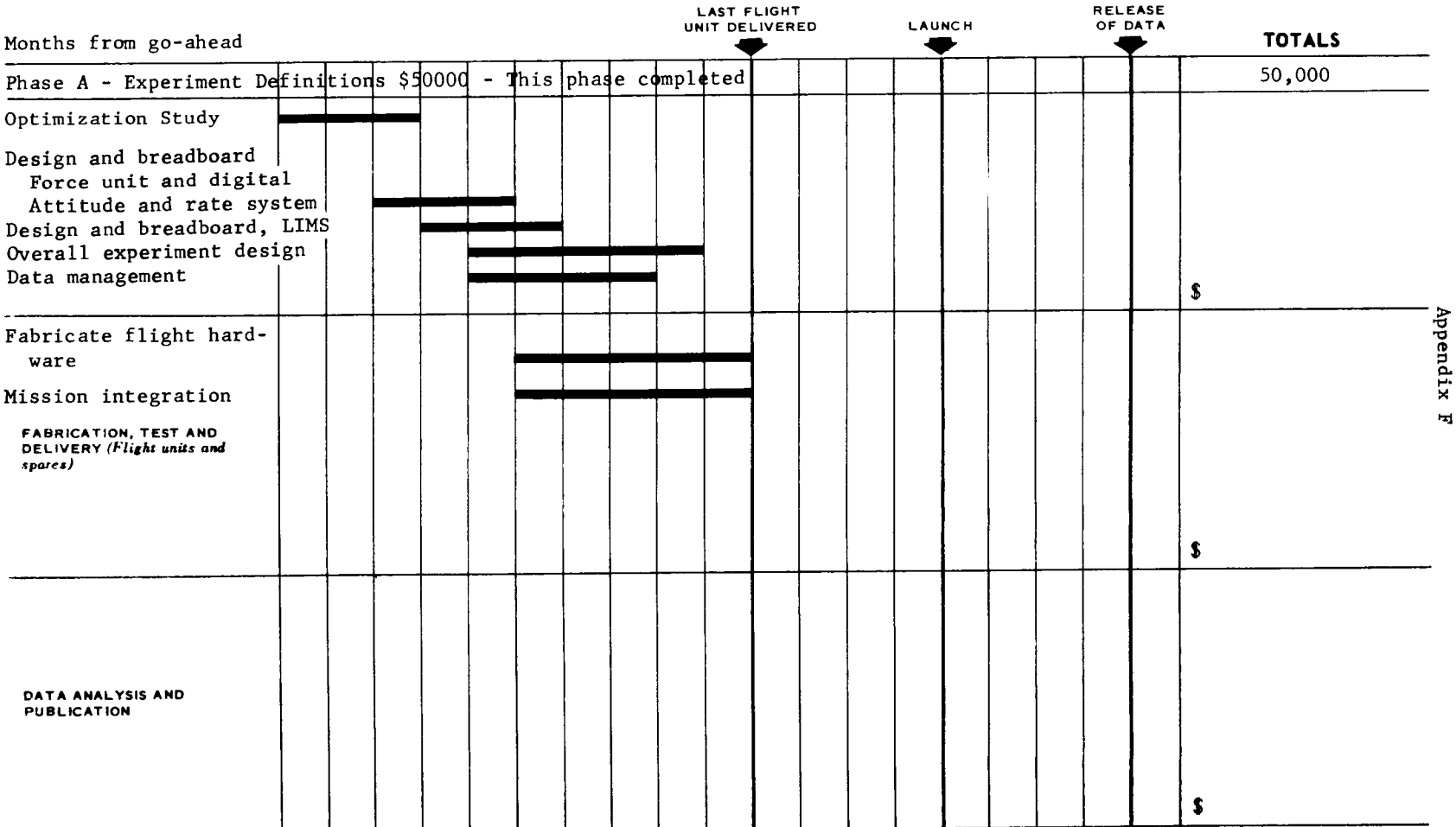

Appendix F

NASA FORM 1138c AUG 64

GPO 865-187

APPENDIX G

ANTHROPOMETRIC MEASUREMENTS OF TEST SUBJECT

In the simulation study, only one test subject was used. The anthropometric data (in in.) for this subject are tabulated below:

Ankle circumference	8.75
Axillary arm circumference	13.50
Buttock depth	9.75
Chest depth	10.13
Chest breadth	13.0
Elbow circumference	10.13
Fist circumference	11.5
Foot length	10.9
Head circumference	22.50
Hip breadth	13.13
Knee circumference	14.63
Lower arm length	10.25
Shoulder height	59.1
Sitting height	36.81
Sphyrion height	4.0
Stature	70.9
Substernale height	42.5
Thigh circumference	21.9
Tibiale height	19.9
Trochanteric height	42.5
Upper arm length	13.75
Waist breadth	11.25
Waist depth	8.5
Wrist circumference	6.75

Locations of those measurements not obvious by their title are shown in figure G-1.

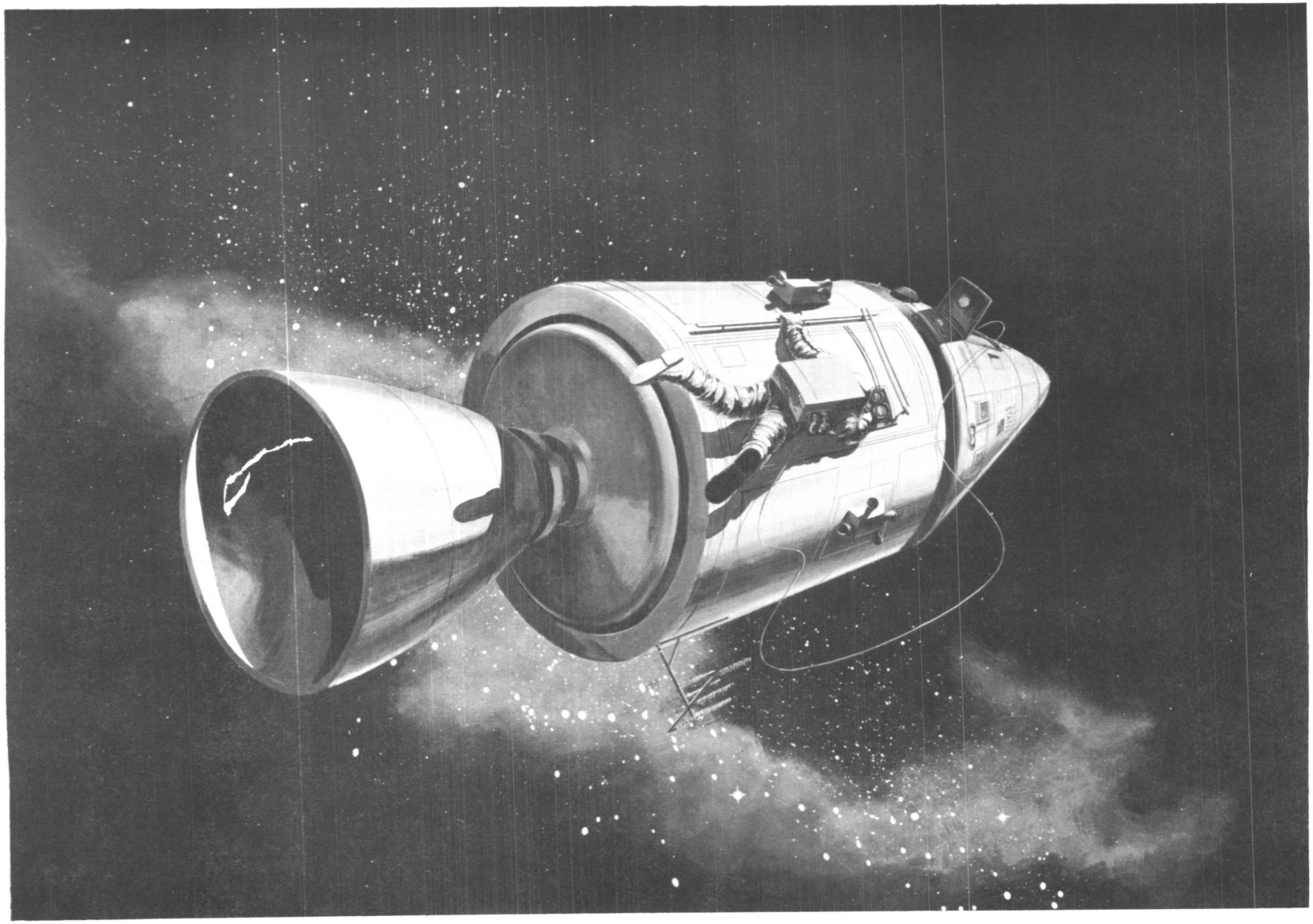

Figure 1.-Configuration 1, Apollo Command and Service Module

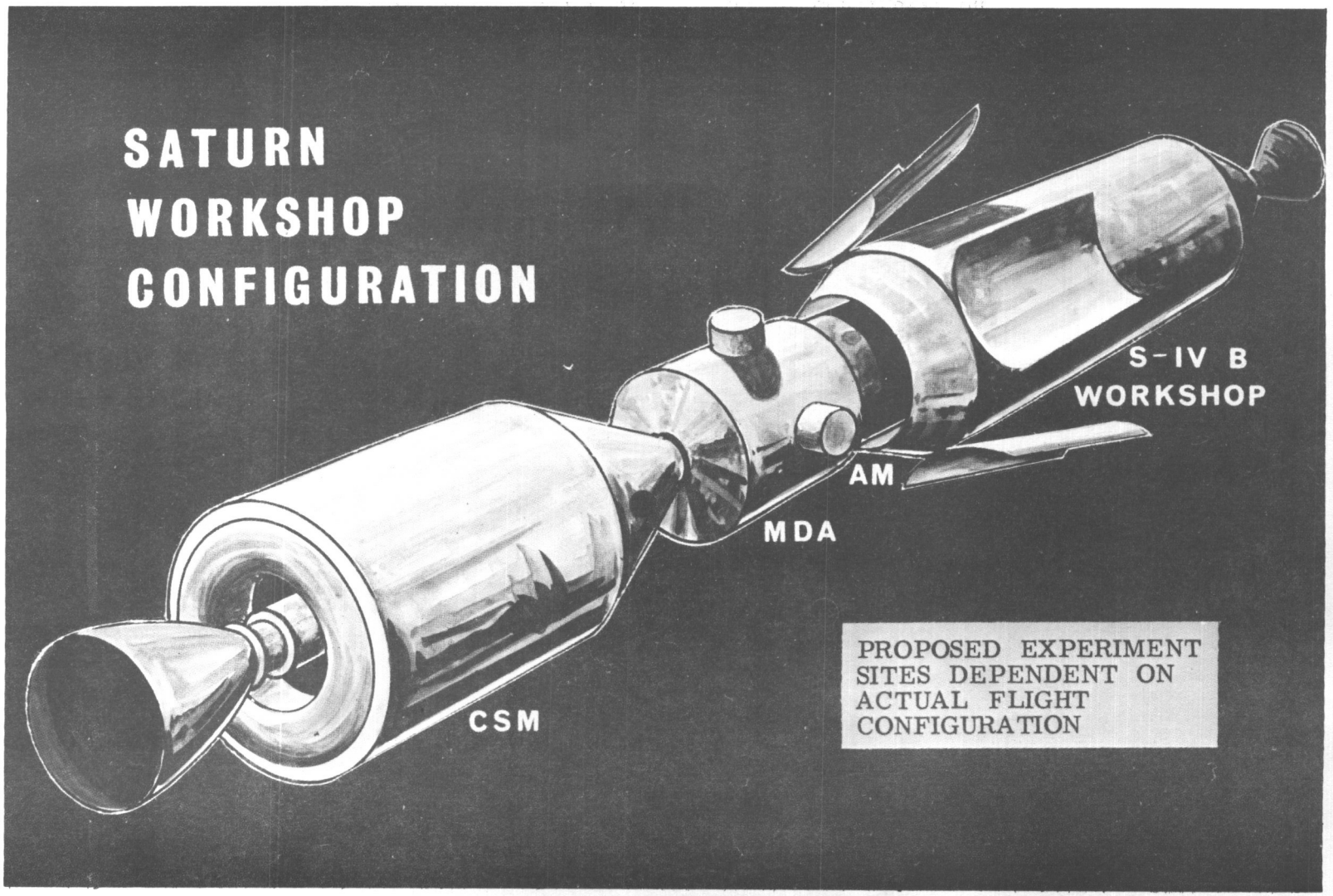

Figure 2.-Configuration 2, Saturn Workshop

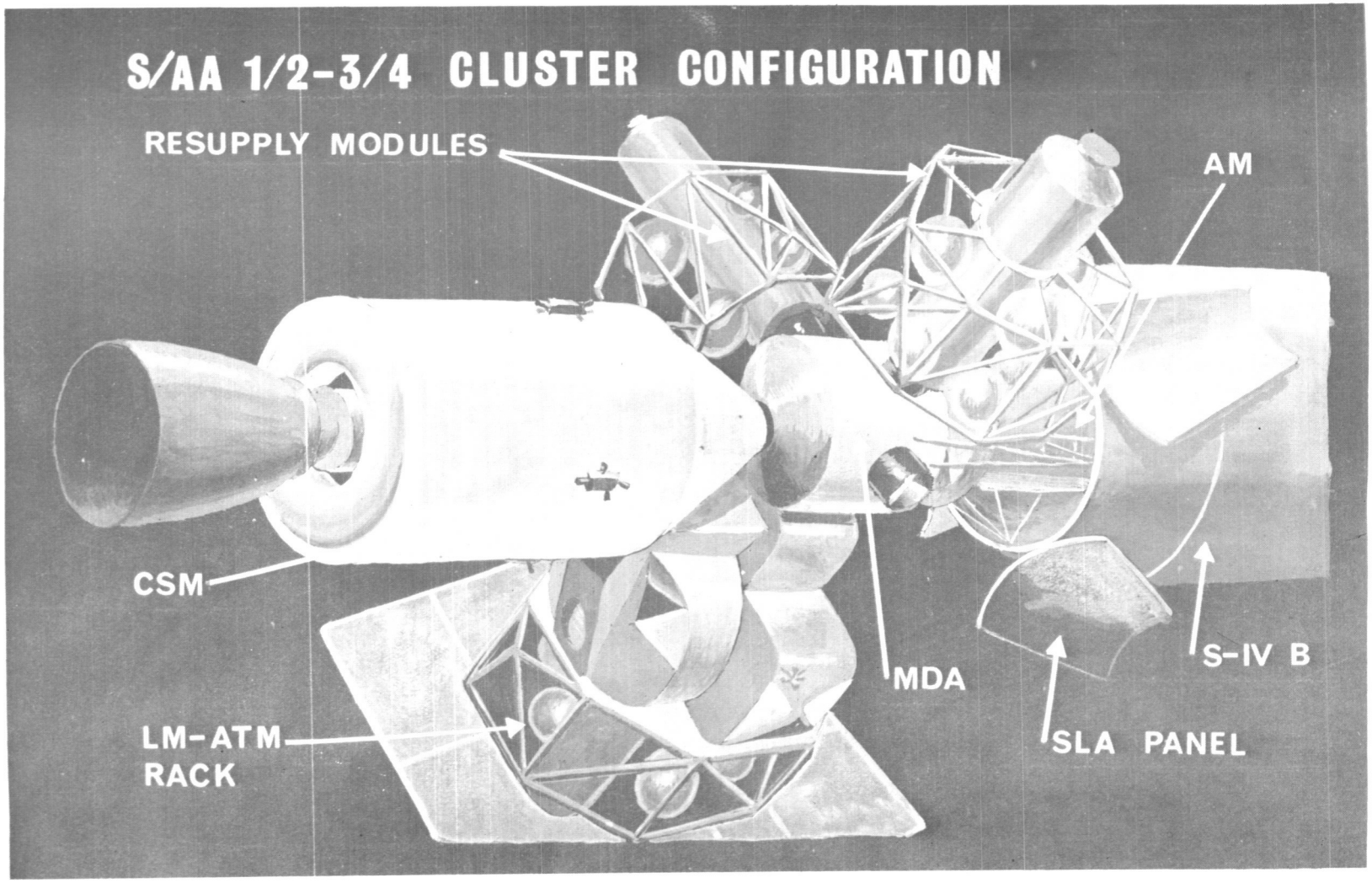

Figure 3.-Configuration 3, AAP Cluster Configuration

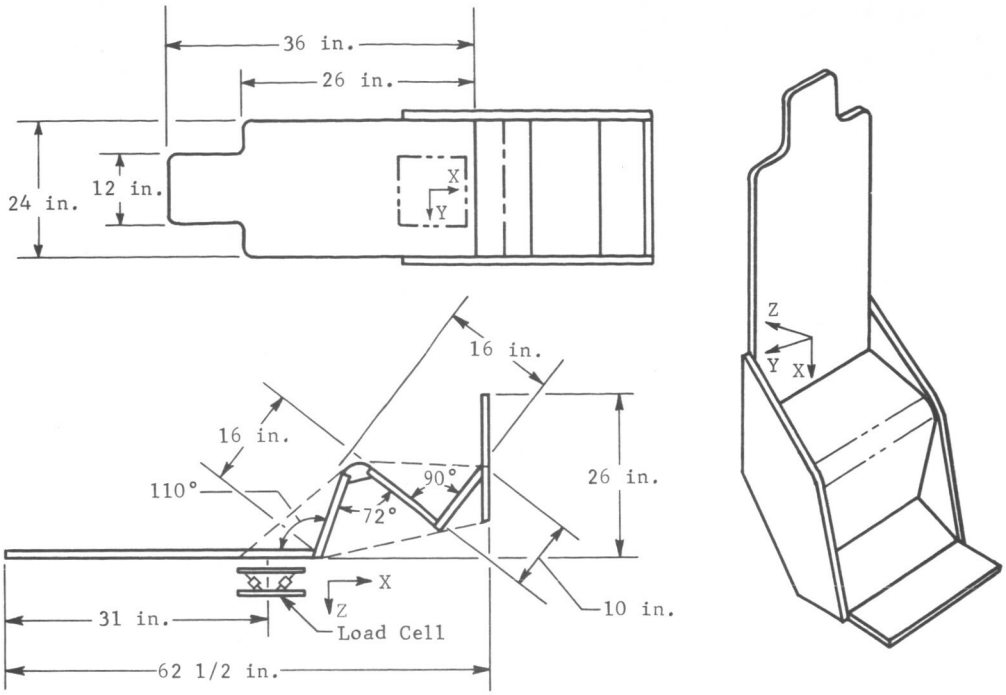

Figure 4.-Apollo Couch Mockup

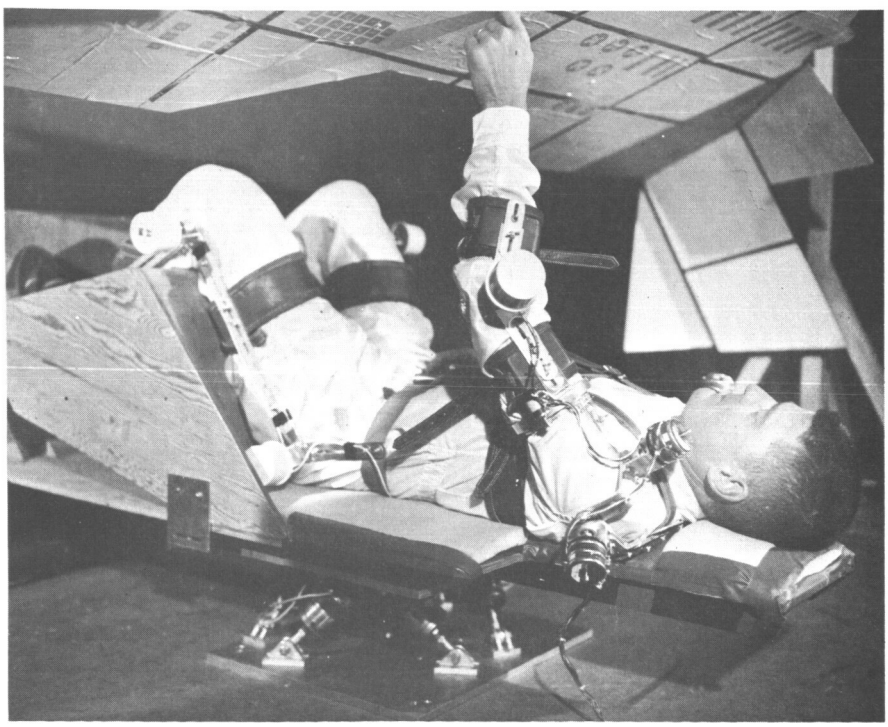

Figure 5.-Restrained Crew Activity Simulation

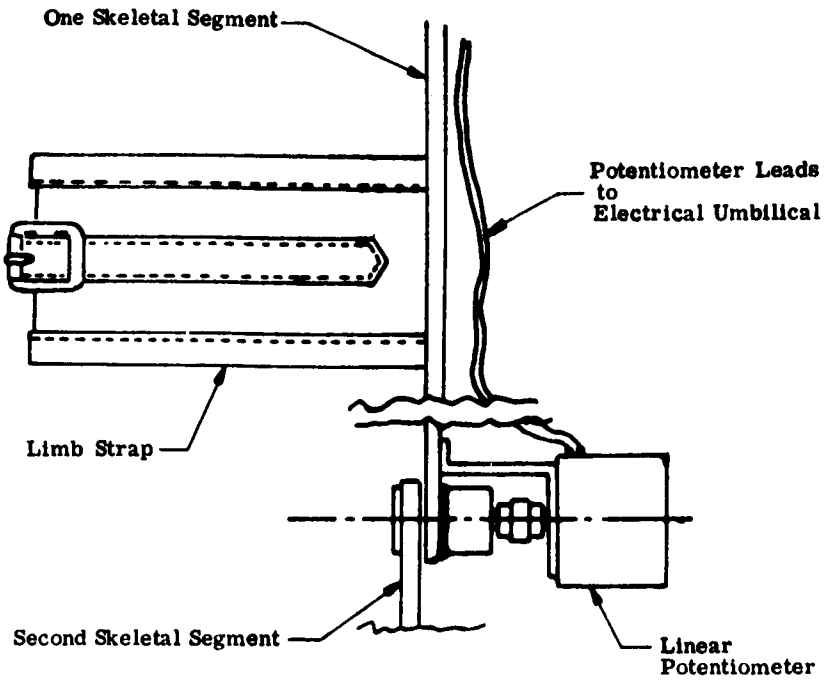

Figure 6.-Typical Joint Segment

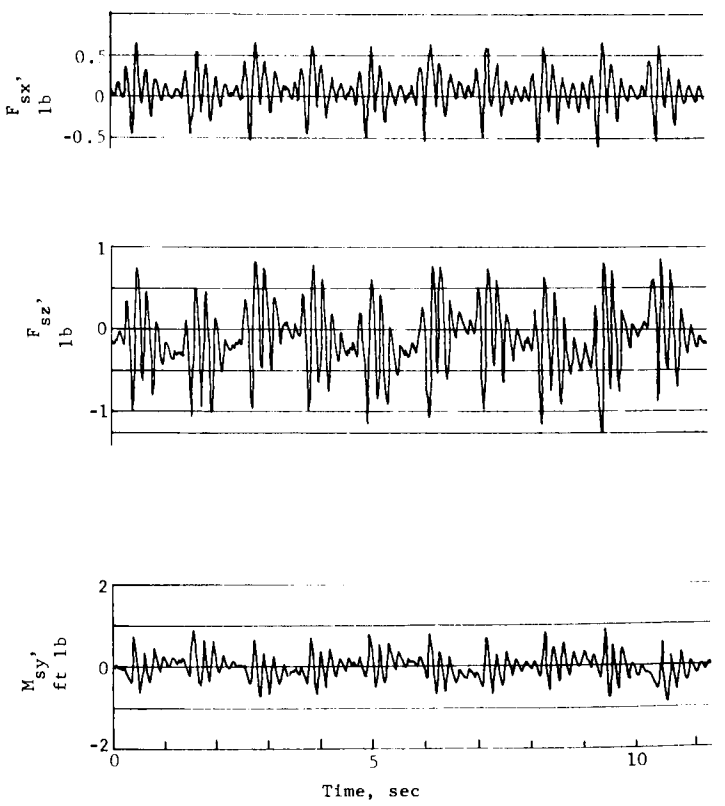

Figure 7.-Normal Breathing Disturbance Spectra

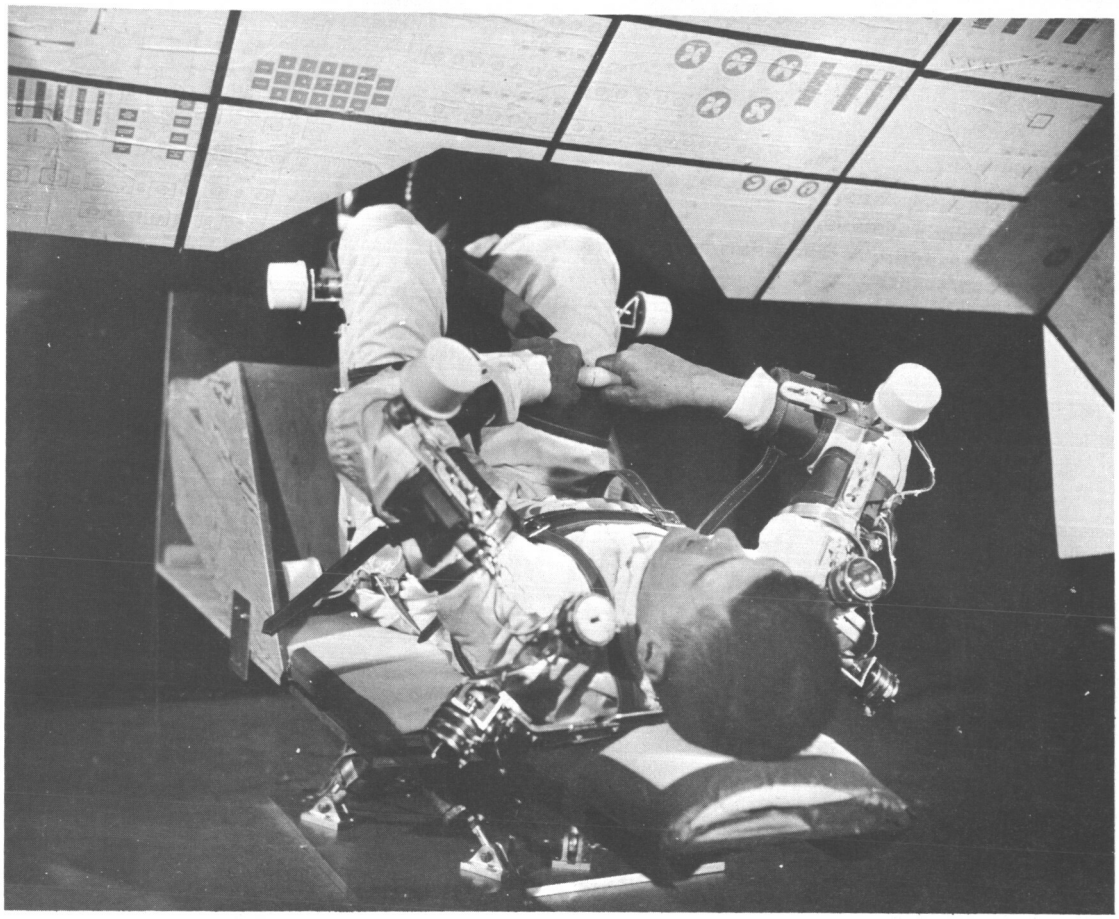

Figure 8.-Exercise

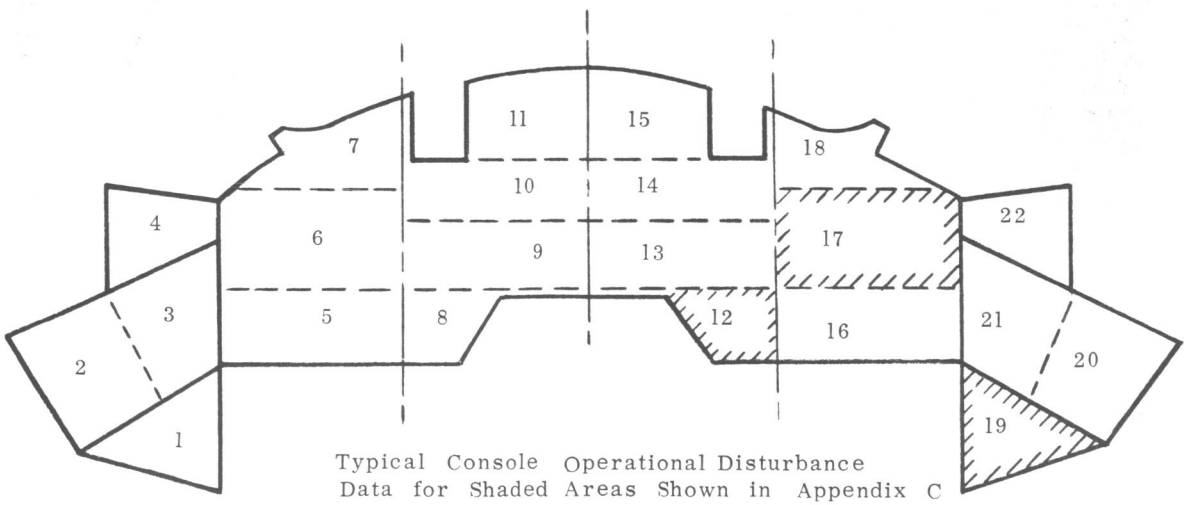

Figure 9.-Apollo Crew Module Console Mockup

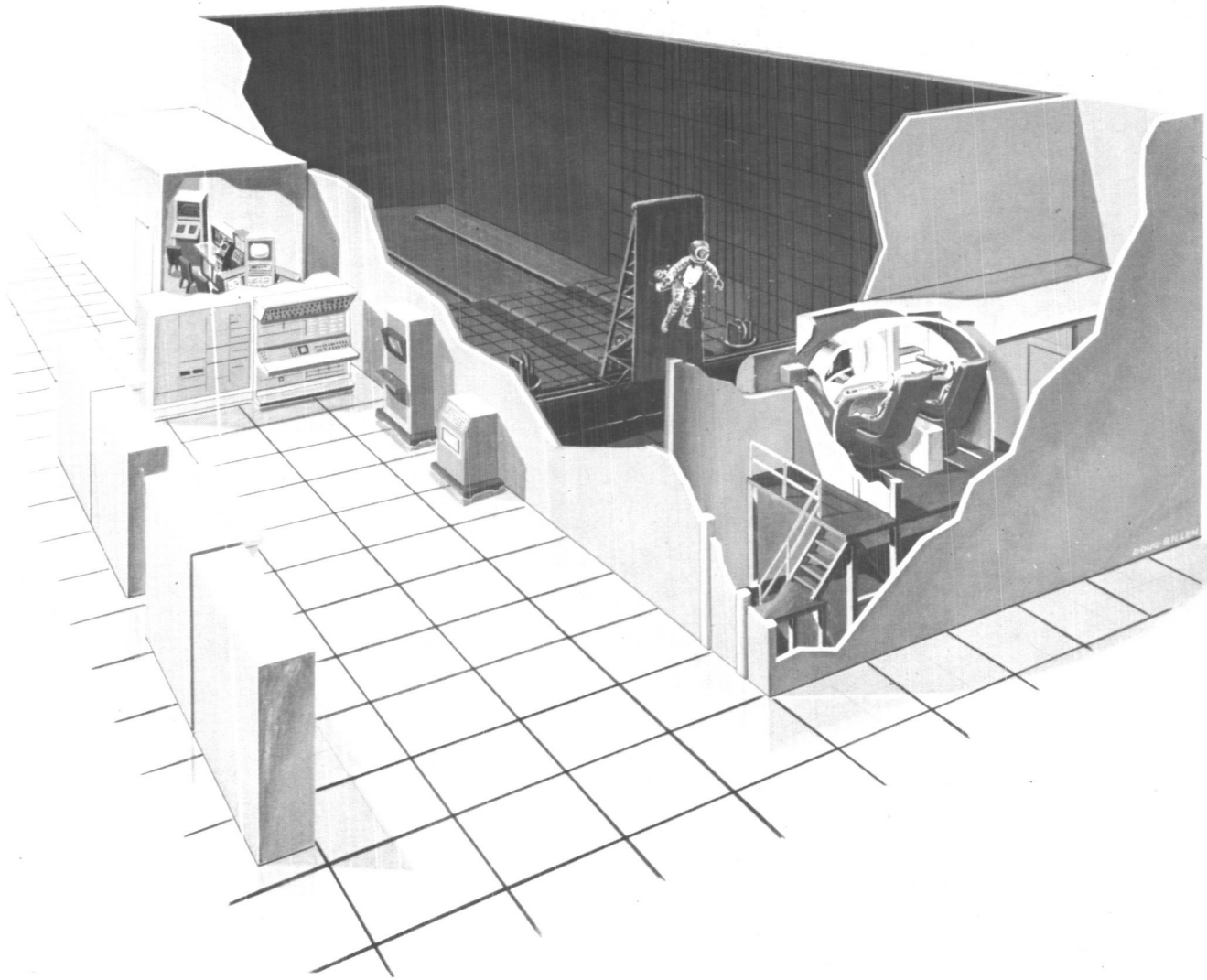

Figure 10.-Space Operations Simulator

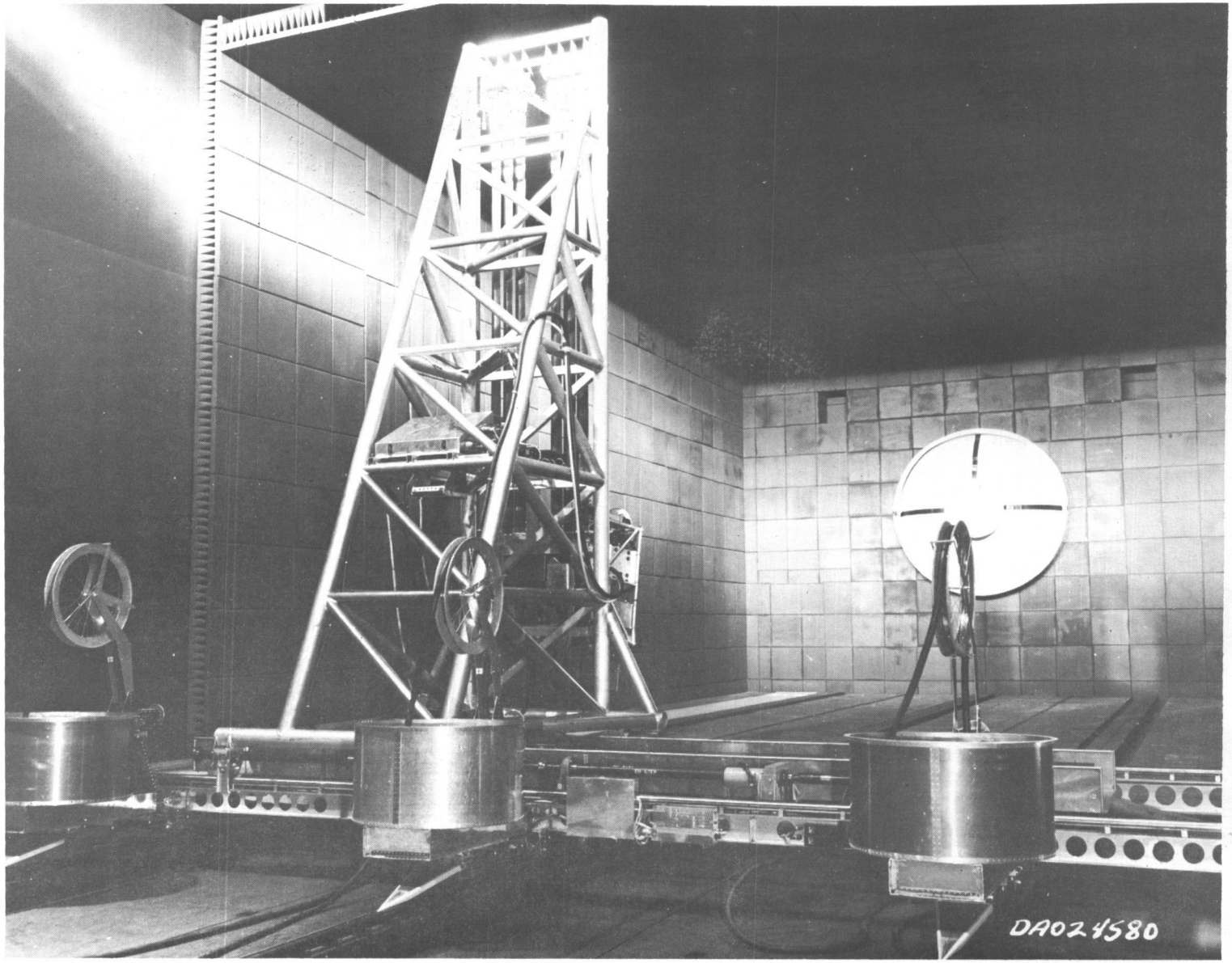

Figure 11.-Moving Base Carriage

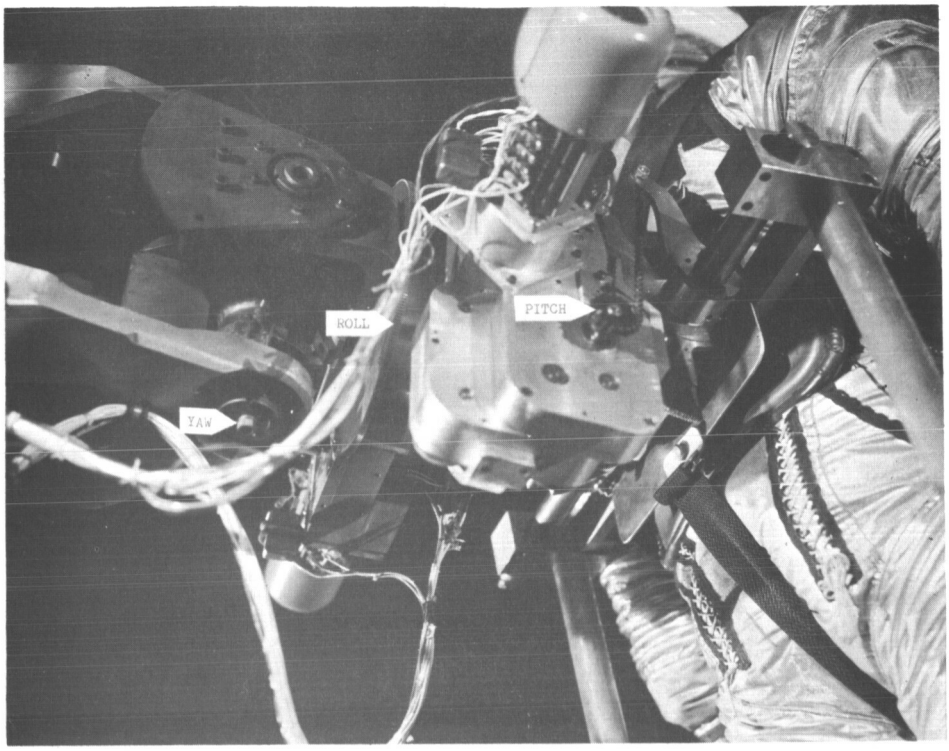

Figure 12.-Attitude Gimbal System

Figure 13.-Test Subject on SOS Demonstrating Self-Induced Rotations

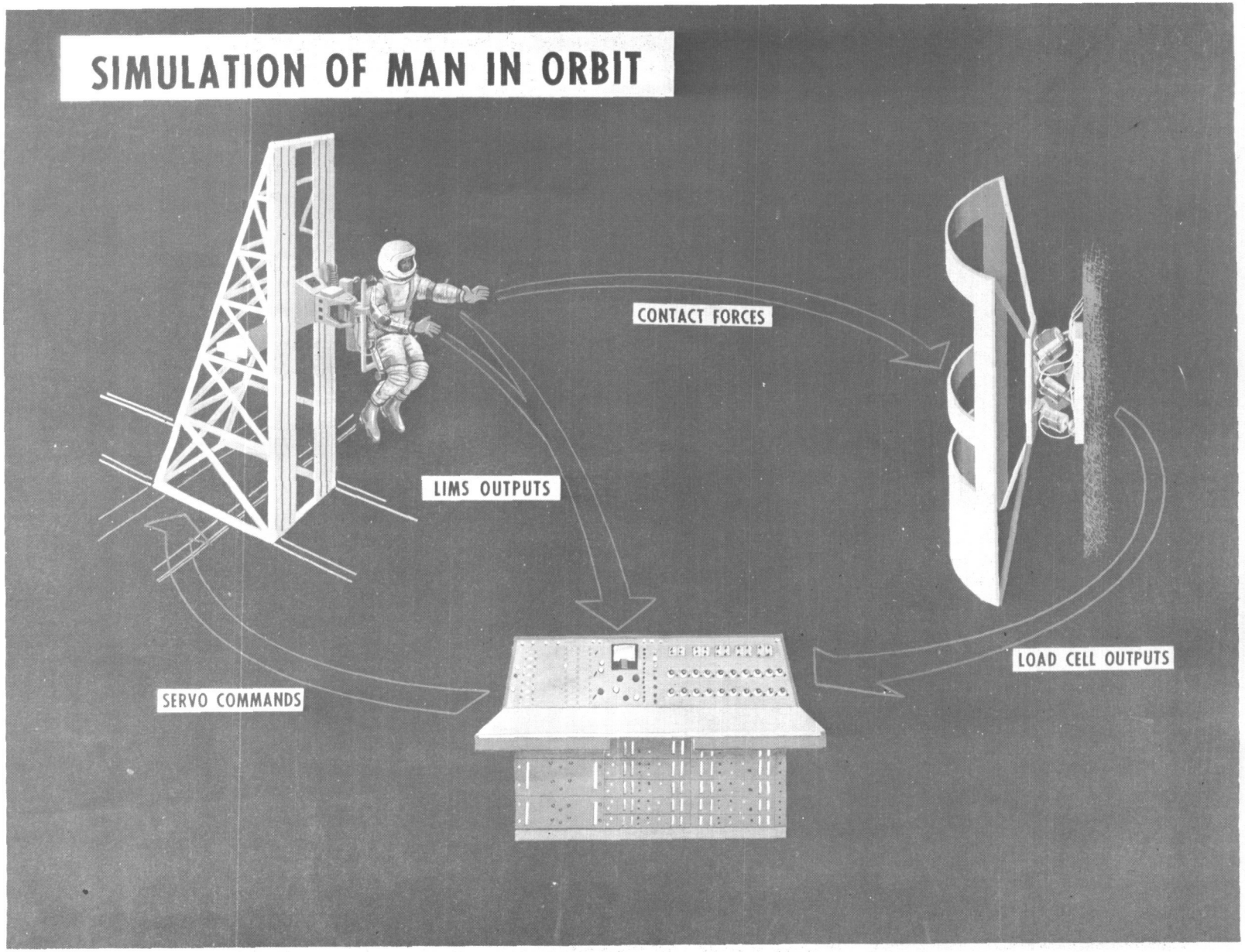

Figure 14.-Simulation of Man in Orbit

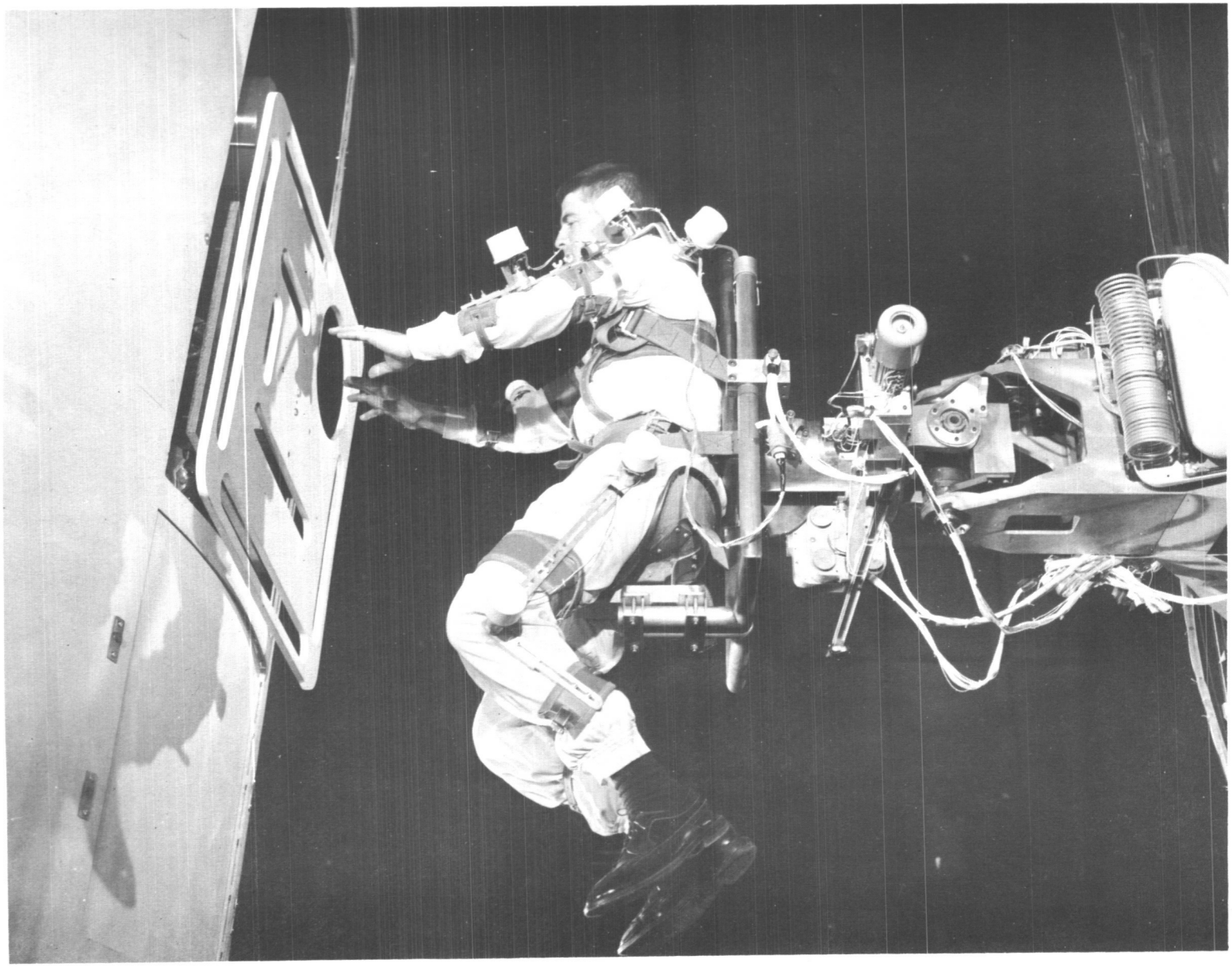

Figure 15.-Free Soaring Simulation

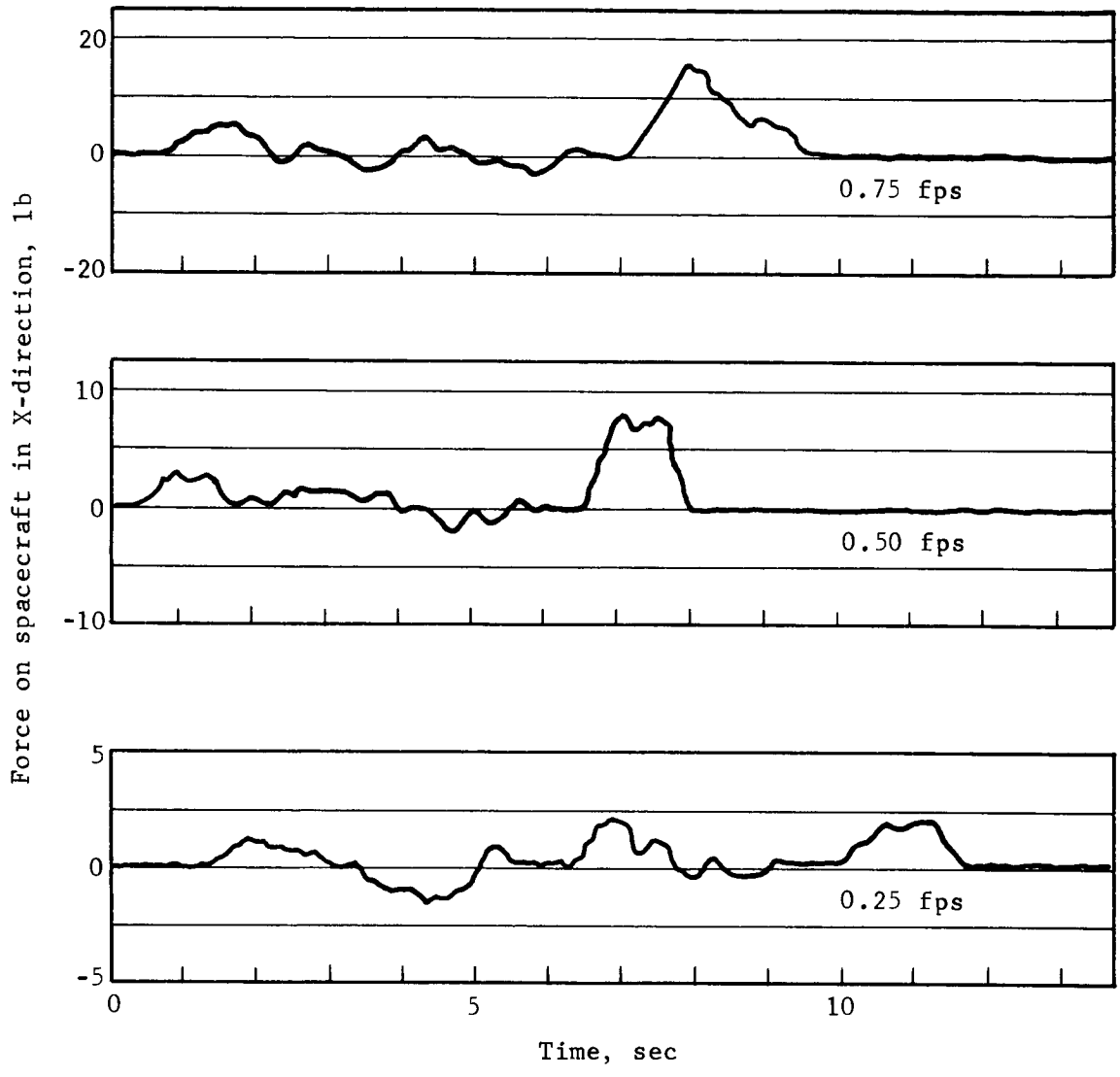

Figure 16.-Free Soaring Force Spectra

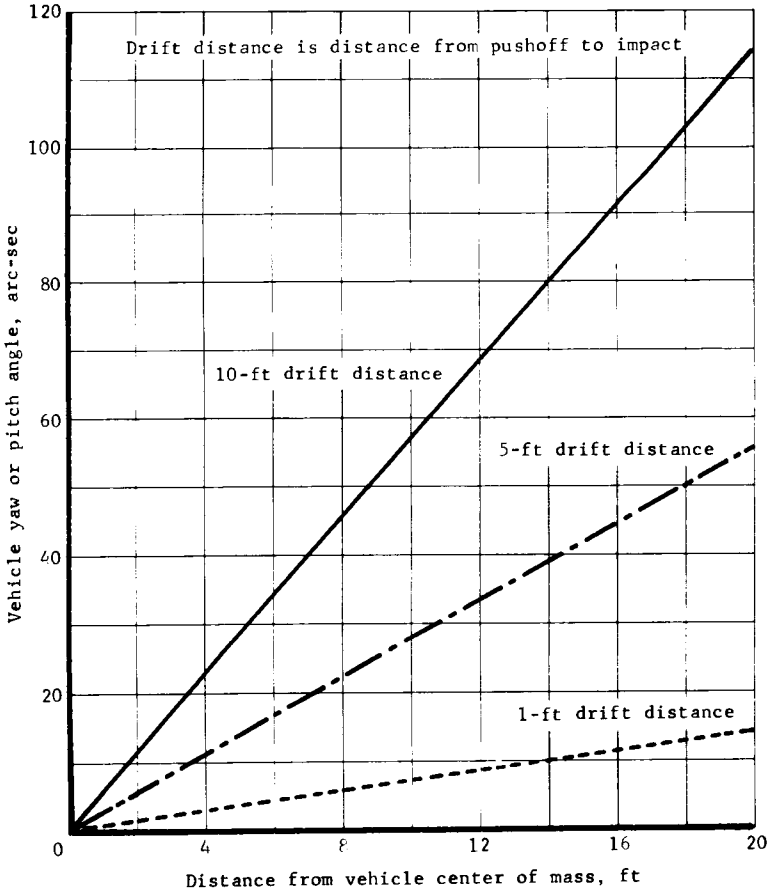

Figure 17.-Spacecraft Disturbances due to Free Soaring, Pushoff at 0.25 fps

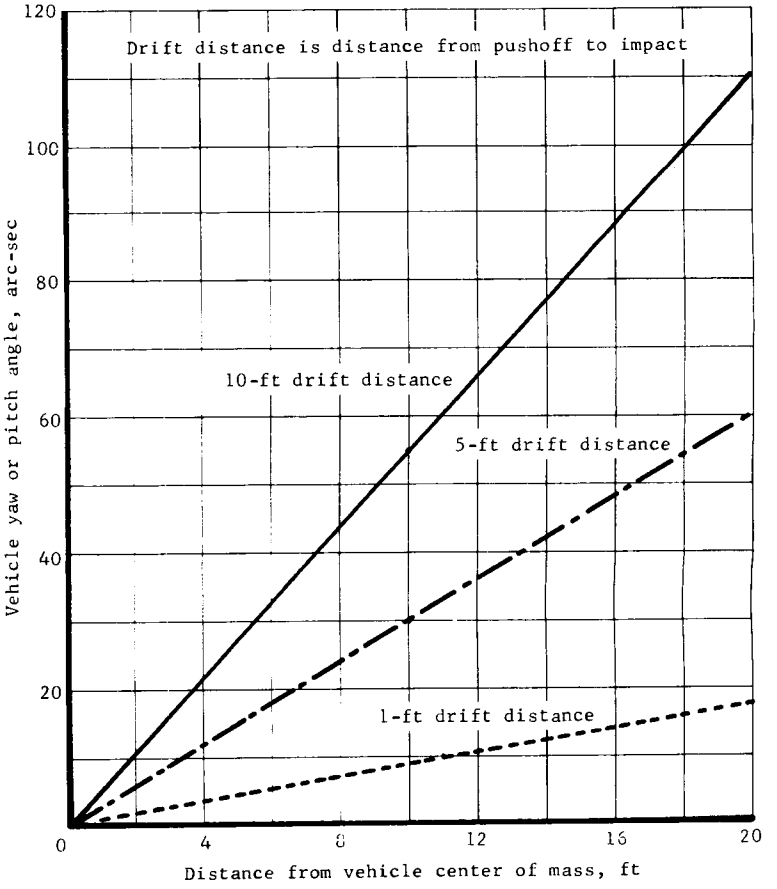

Figure 18.-Spacecraft Disturbances due to Free Soaring, Pushoff at 0.50 fps

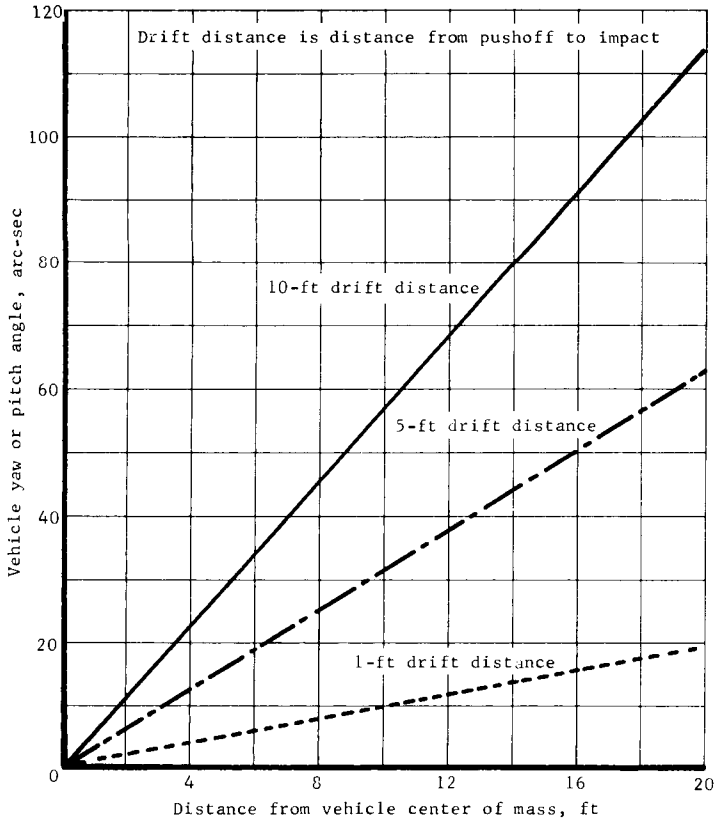

Figure 19.-Spacecraft Disturbances due to Free Soaring Pushoff at 0.75 fps

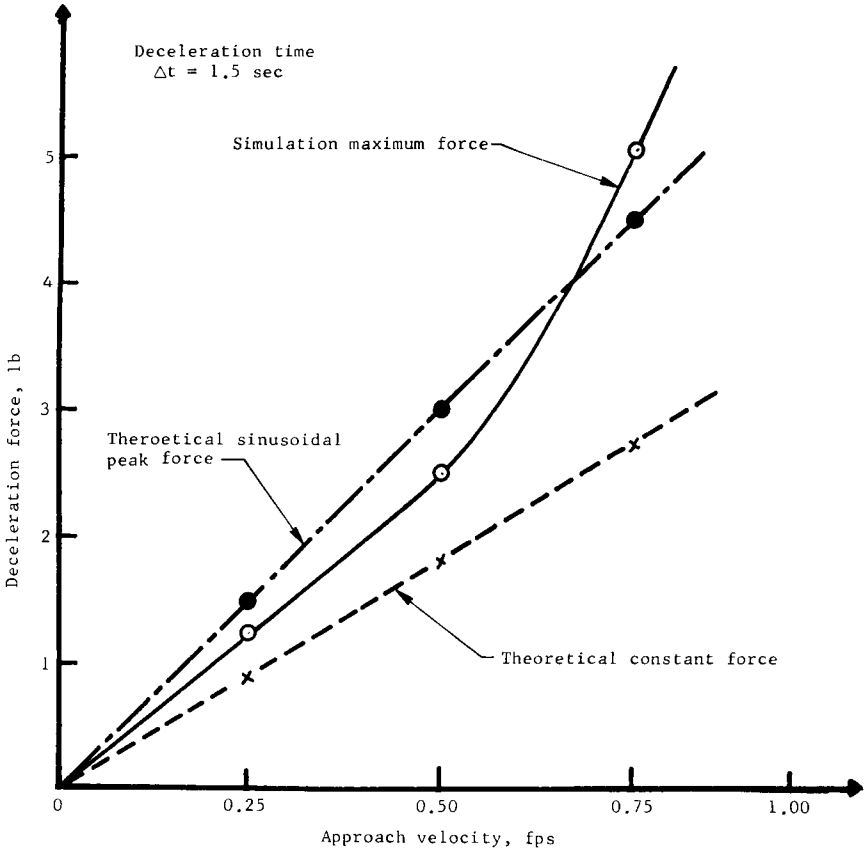

Figure 20.-Free Soaring Impact Forces

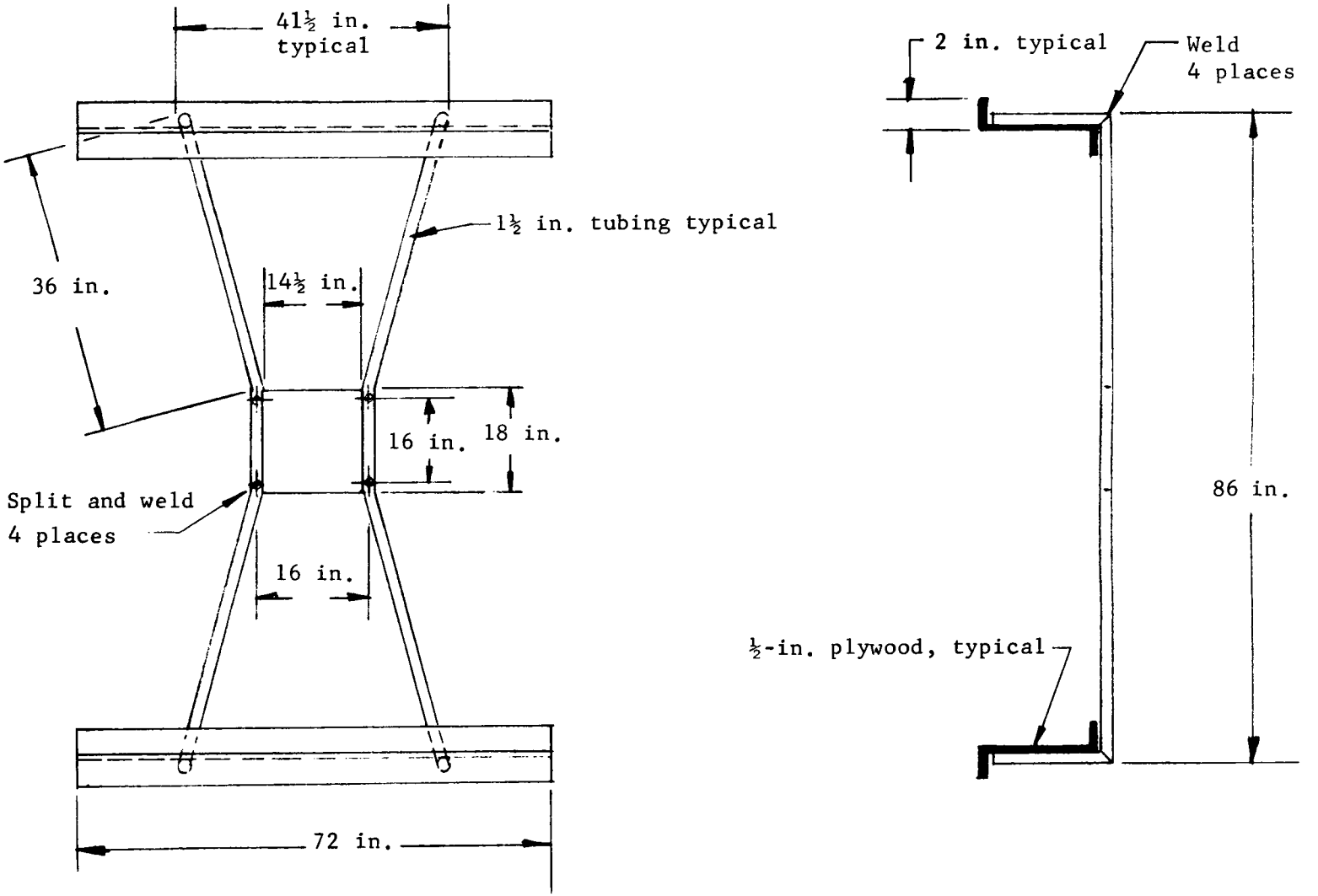

Figure 21.-Guided Soaring Mockup

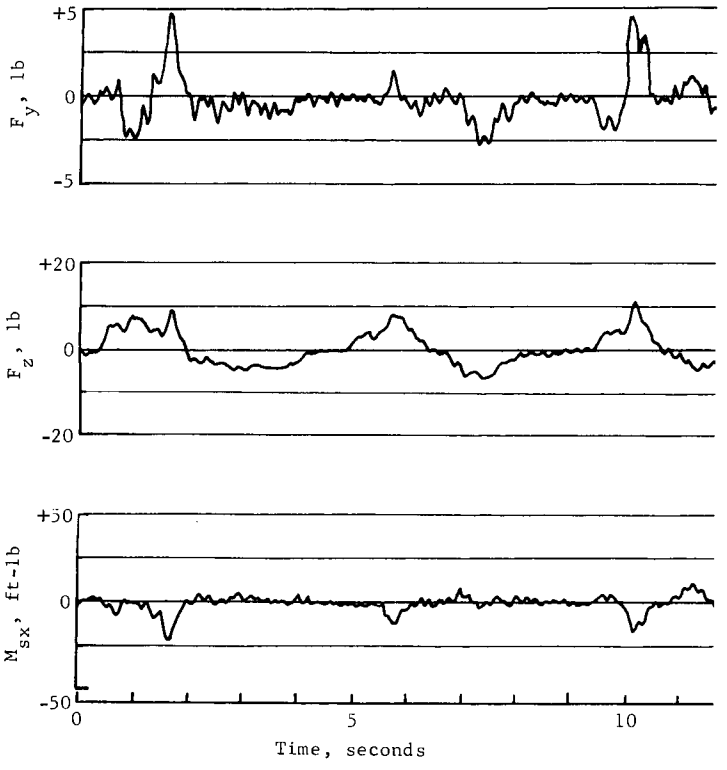

Figure 22.-Guided Soaring Disturbance Spectra

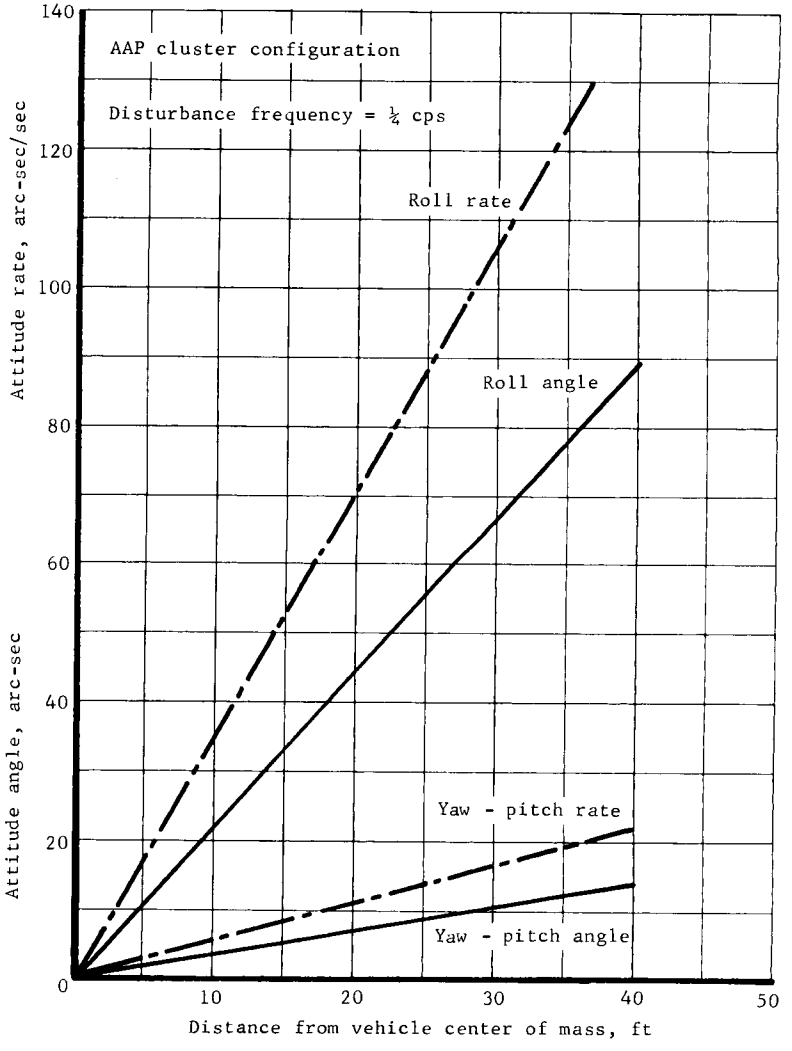

Figure 23.-Vehicle Attitude and Rate Disturbances due to Guided Soaring

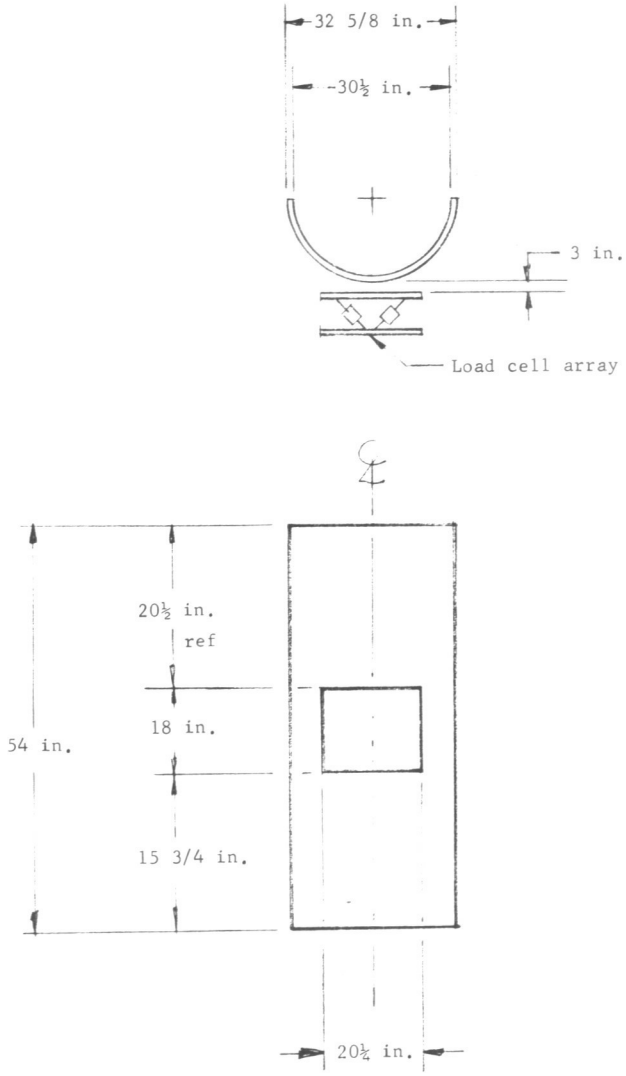

Figure 24.-CSM Hatch and Tunnel Mockup

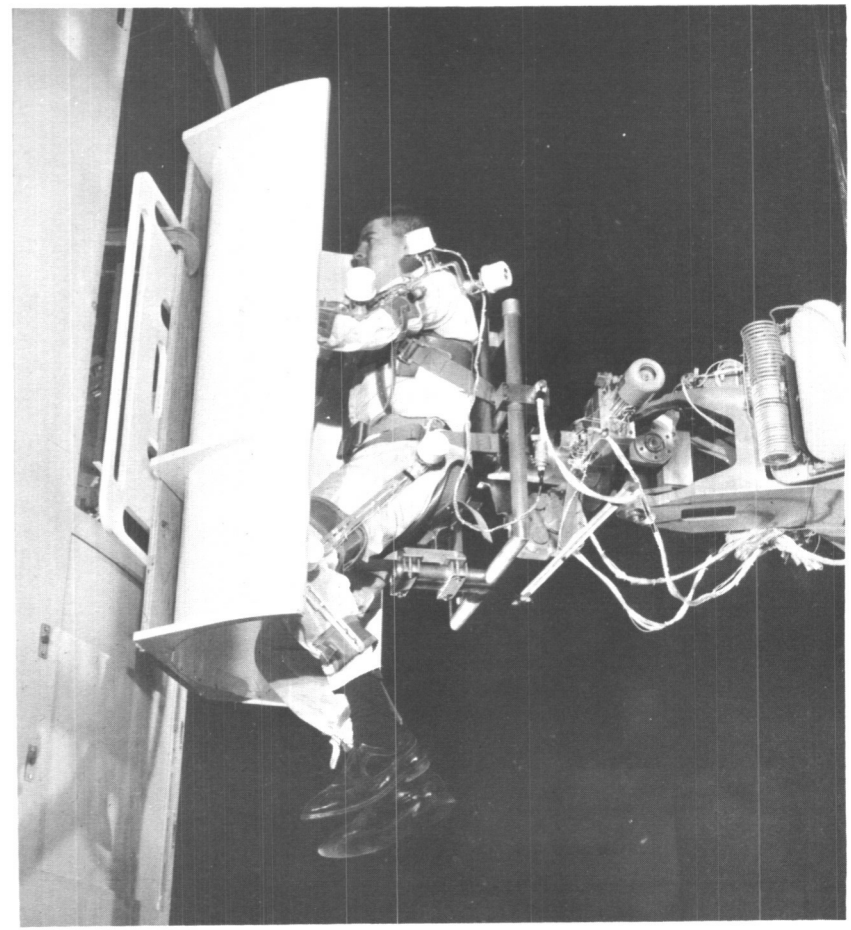

Figure 25.-Tunnel Transfer Simulation

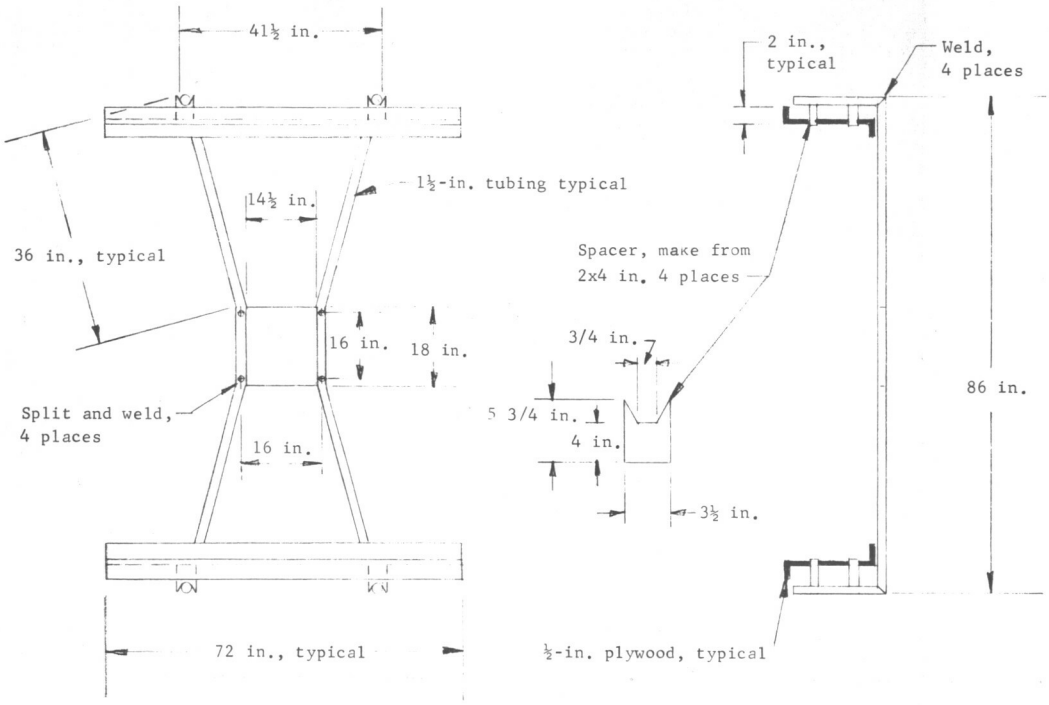

Figure Compressive Walking Mockup

Figure 26.-Compressive Walking Mockup

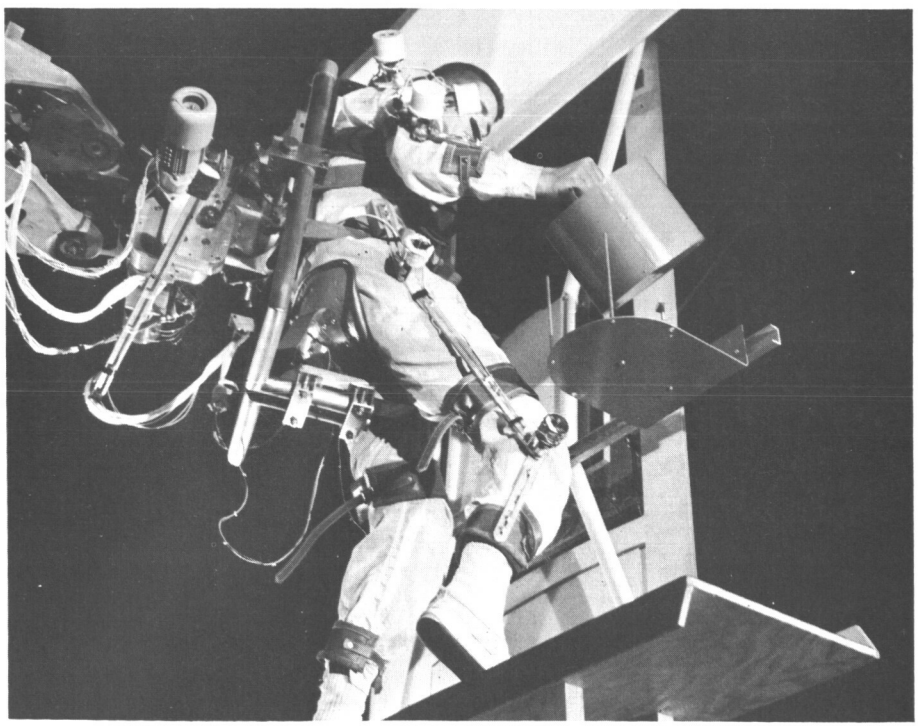

Figure 27.-Adhesive Walking, Canister Removal Simulation

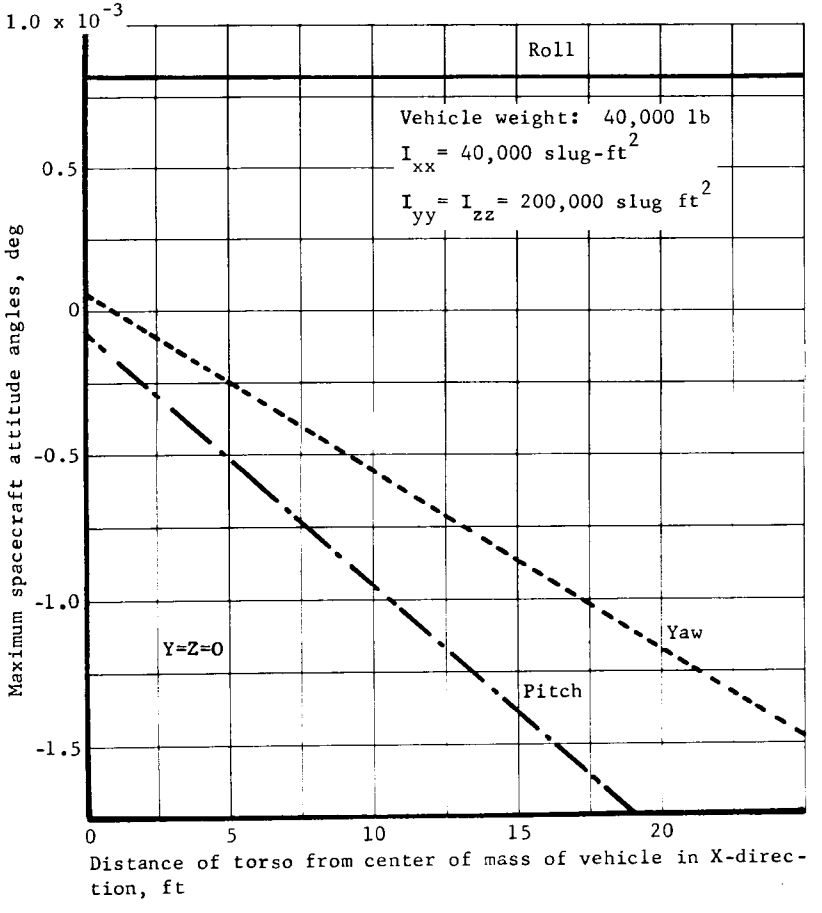

Figure 28.-Spacecraft Attitude Disturbance due to Simple Arm Motion Midway between Sagittal and Frontal Plane, Test Vehicle

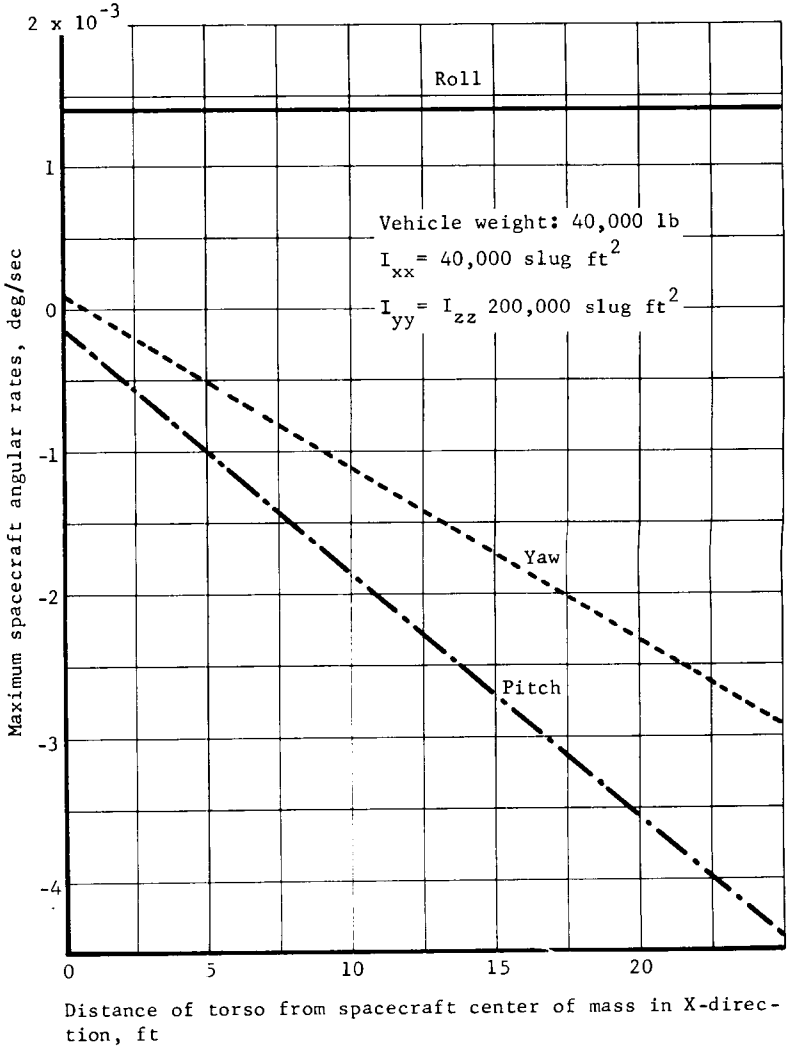

Figure 29.-Simple Spacecraft Rate Disturbance due to Simple Arm Motion Midway between Sagittal and Frontal Plane, Test Vehicle

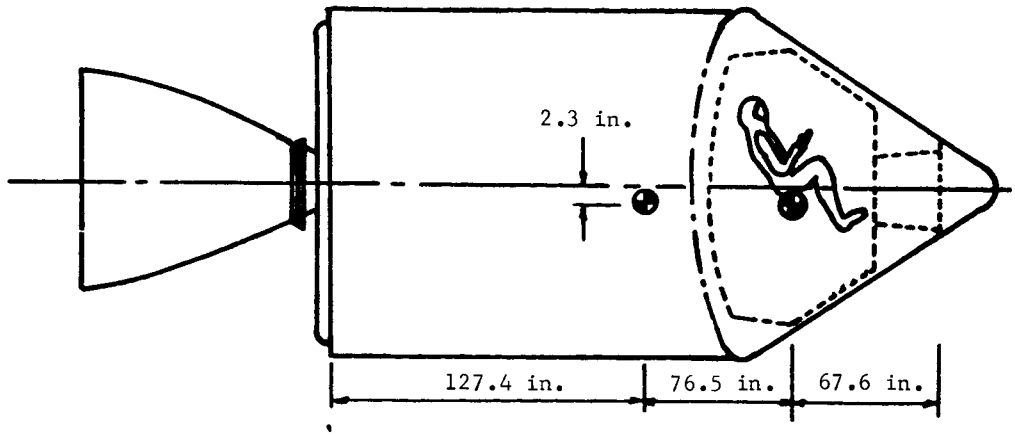

Weight, lb - 24,860

Location of center-of-mass, in. - (127.4 - 2.3, 7.1)

Inertia, slug ft^2 - (13,862; 46,870; 47,840)

Figure 30.-Apollo Command/Service Module, Configuration 1

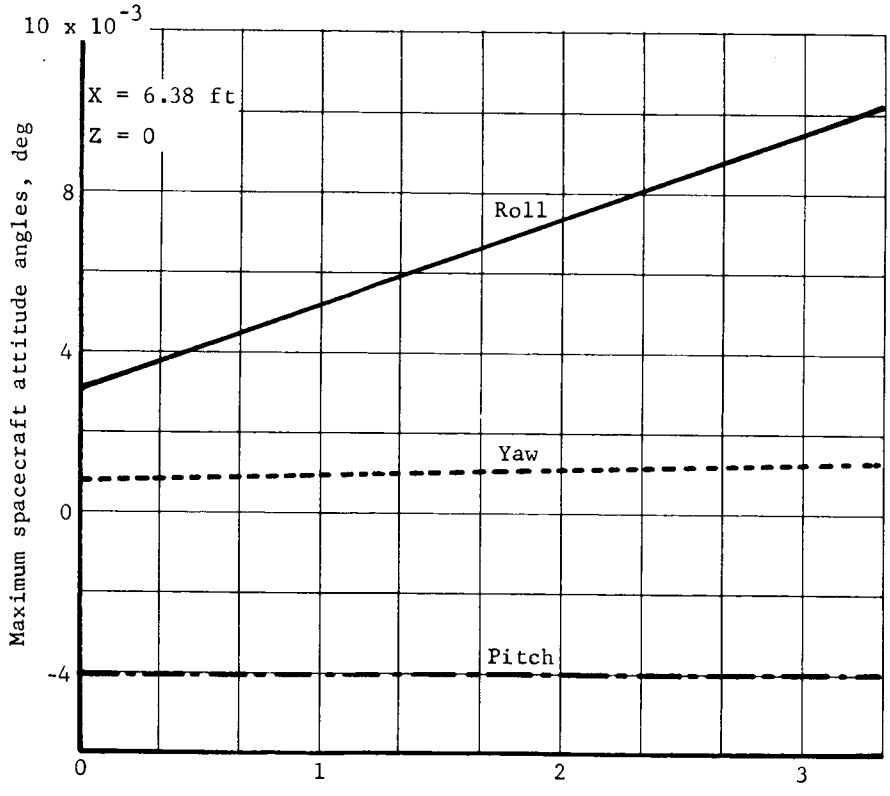

Figure 31.-Spacecraft Attitude Disturbance due to Simple Arm Motion Midway between Sagittal and Frontal Plane, Configuration 1

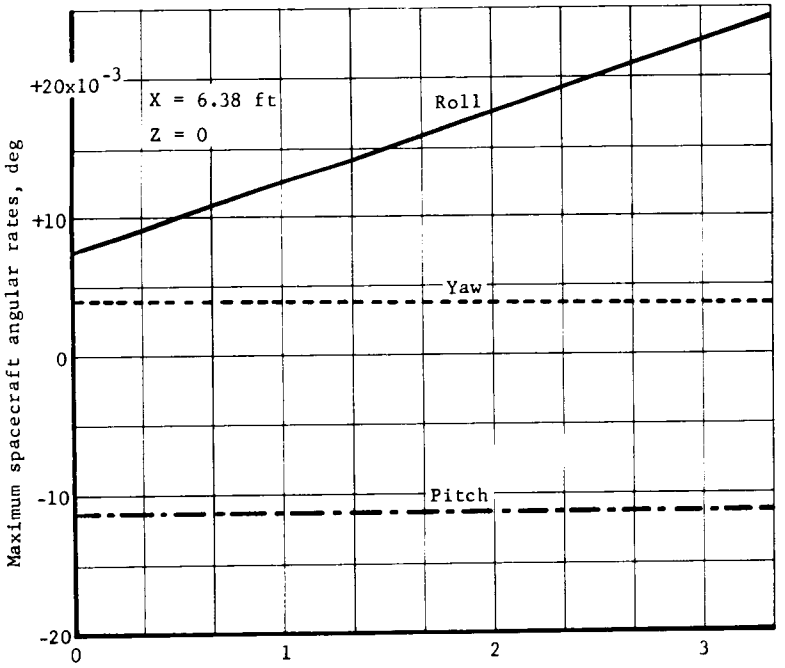

Figure 32.-Spacecraft Rate Disturbance due to Simple Arm Motion Midway between Sagittal and Frontal Plane, Configuration 1

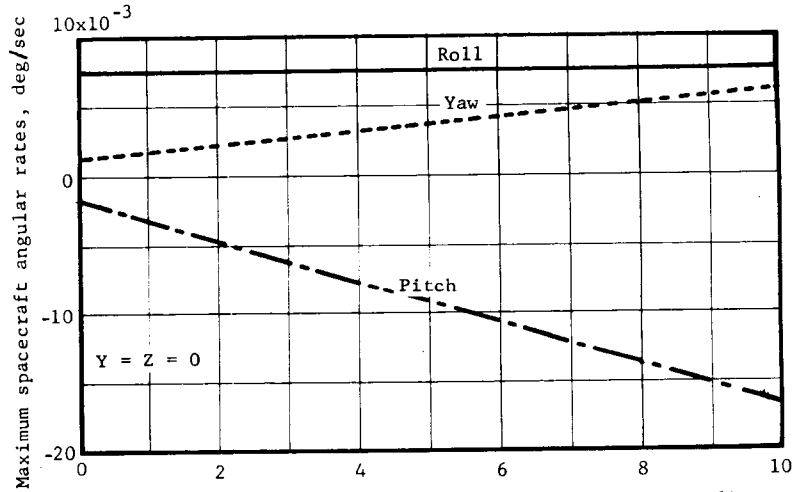

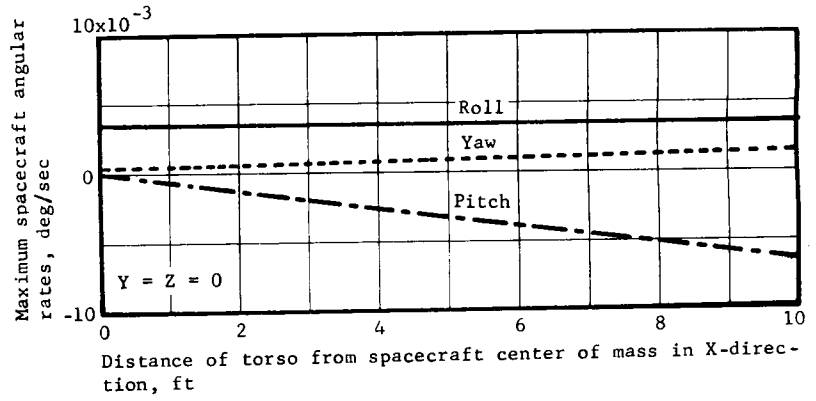

Figure 33.-Spacecraft Disturbances, Simple Arm Motion Midway between Sagittal and Frontal Plane, Configuration 1

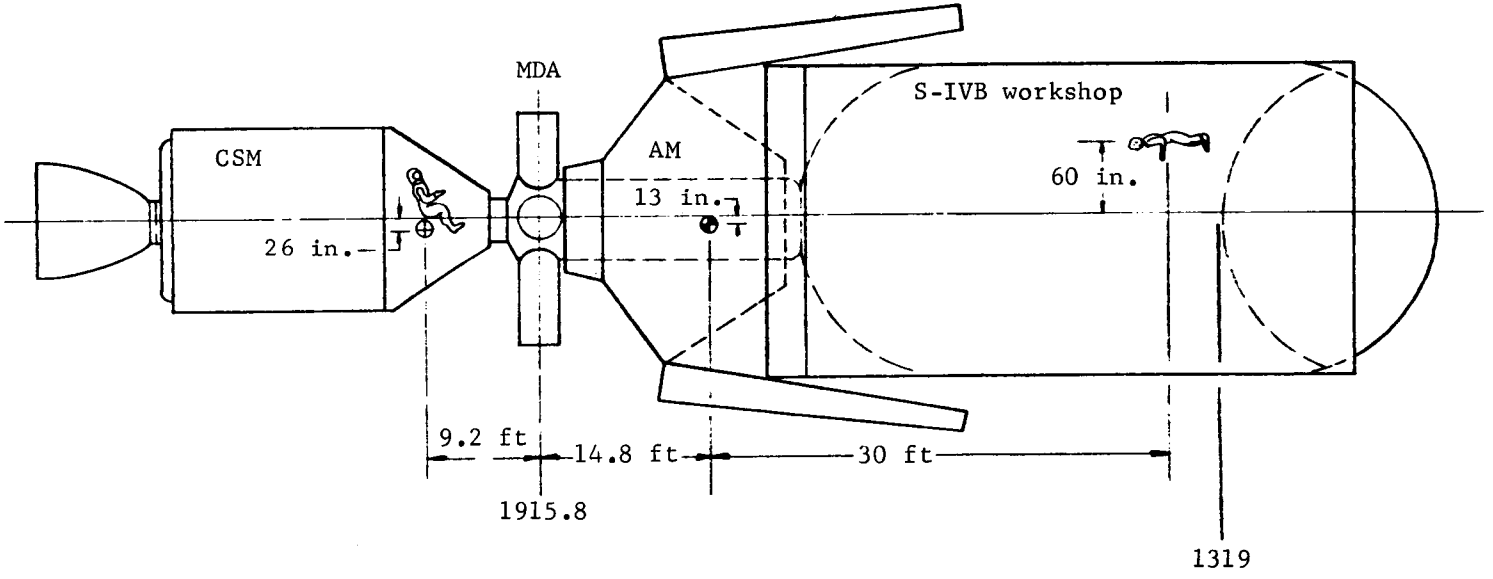

Figure 34.-Orbital Vehicle Configuration Flight 1/2, Configuration 2

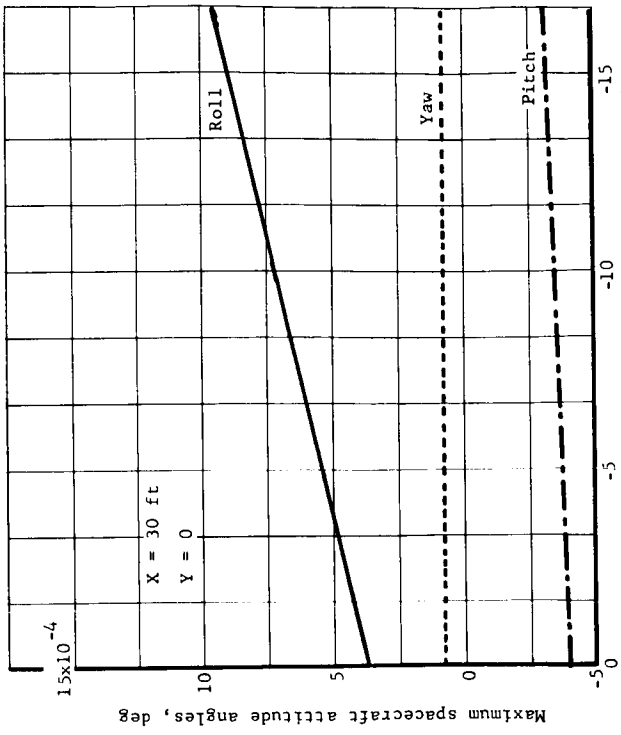

Figure 36.-Spacecraft Attitude Disturbance due to Simple Arm Motion Midway between Sagittal and Frontal Plane, Configuration 2

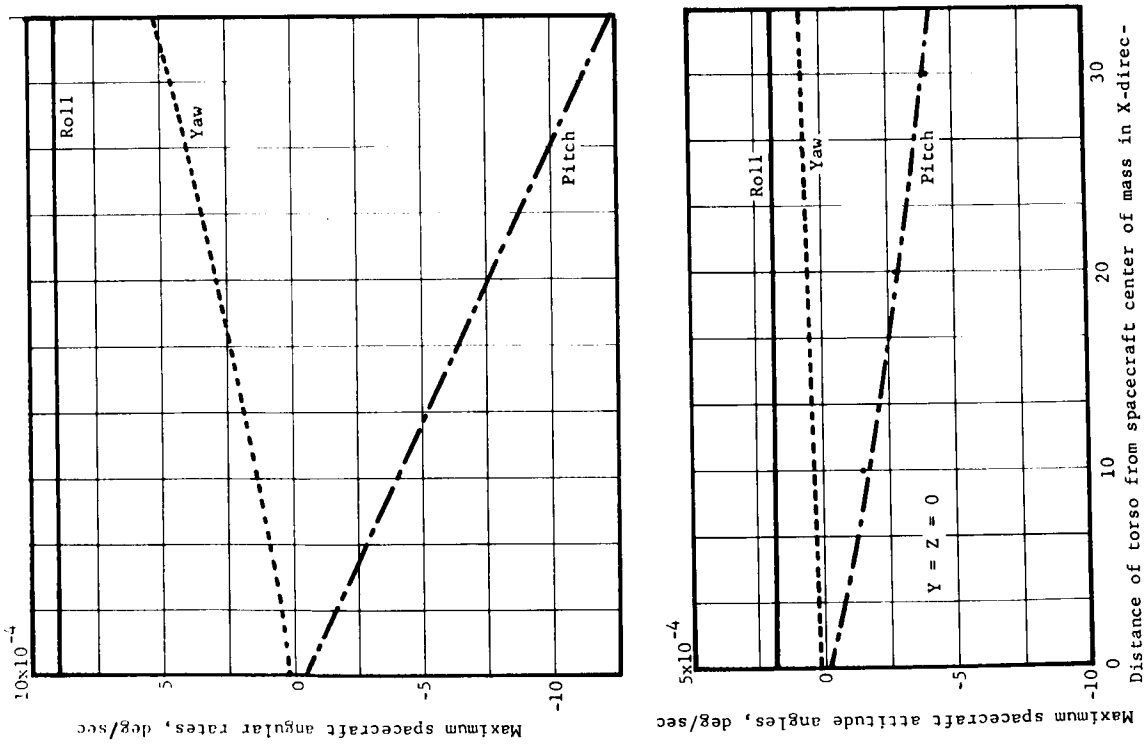

Figure 35.-Spacecraft Disturbances due to Simple Arm Motion Midway between Sagittal and Frontal Plane, Configuration 2

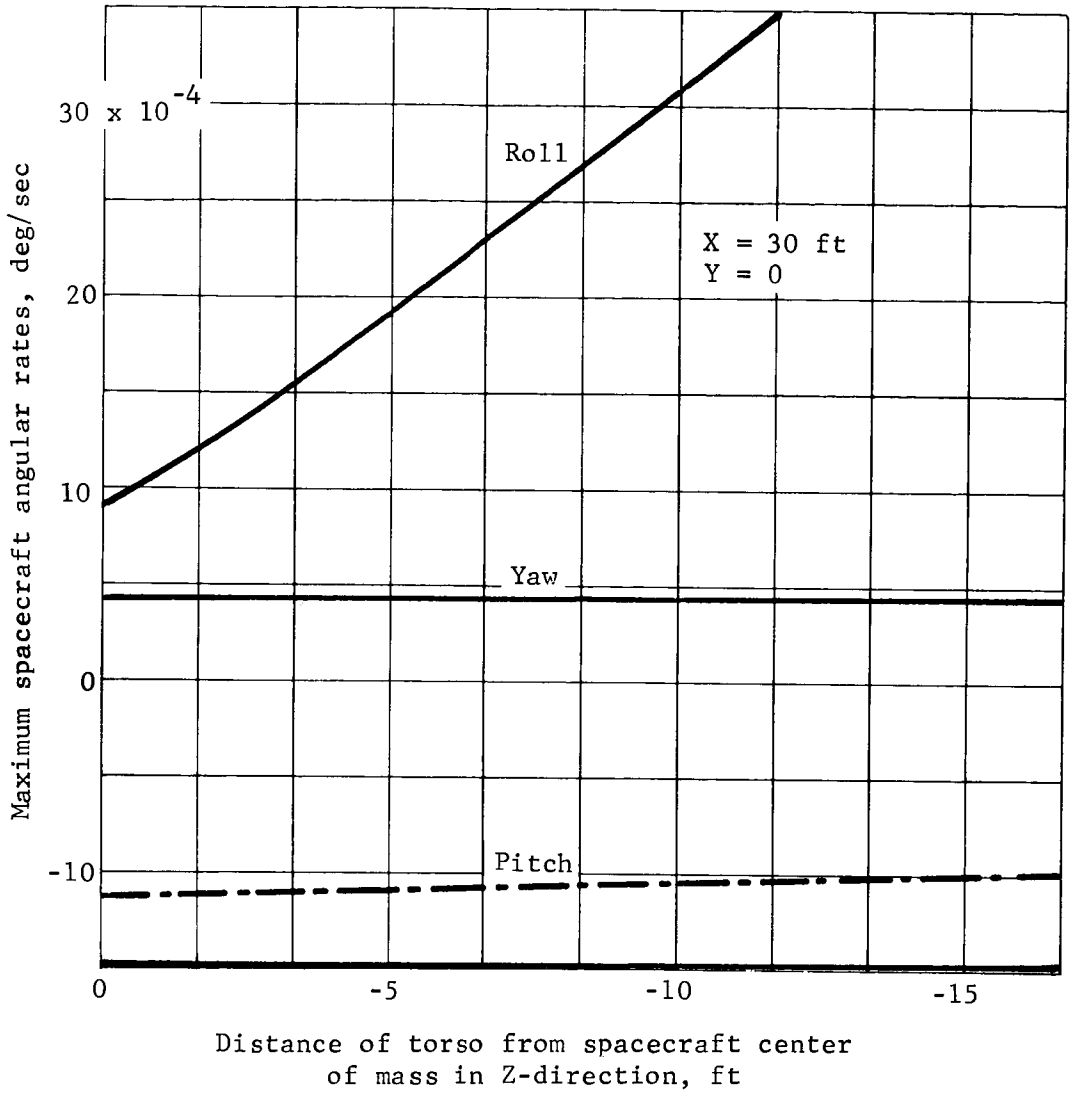

Figure 37.- Spacecraft Rate Disturbance due to Simple Arm Motion Midway between Sagittal and Frontal Plane, Configuration 2

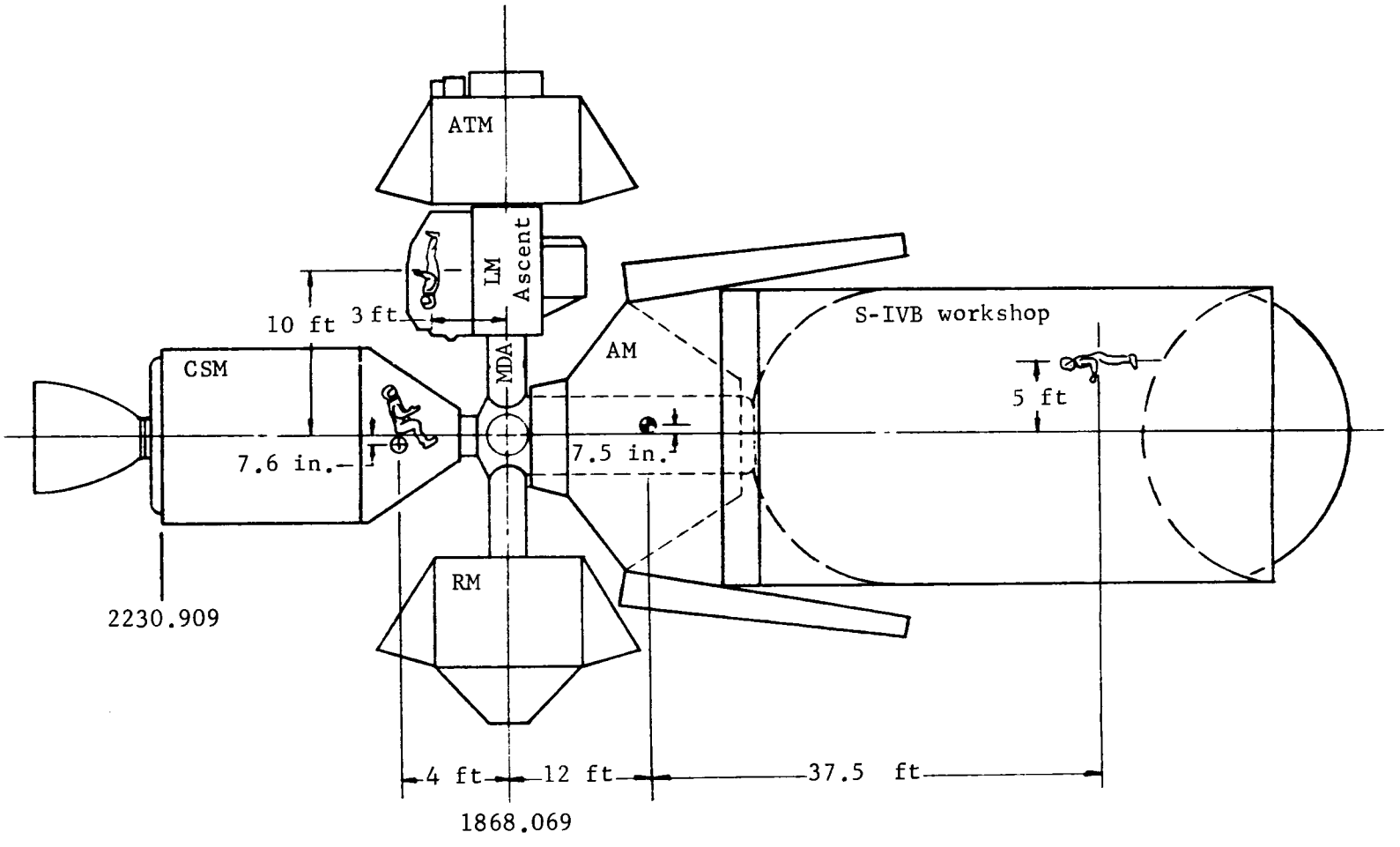

Figure 38.- Orbital Vehicle Configuration (Cluster) Flight 3/4, Configuration 3

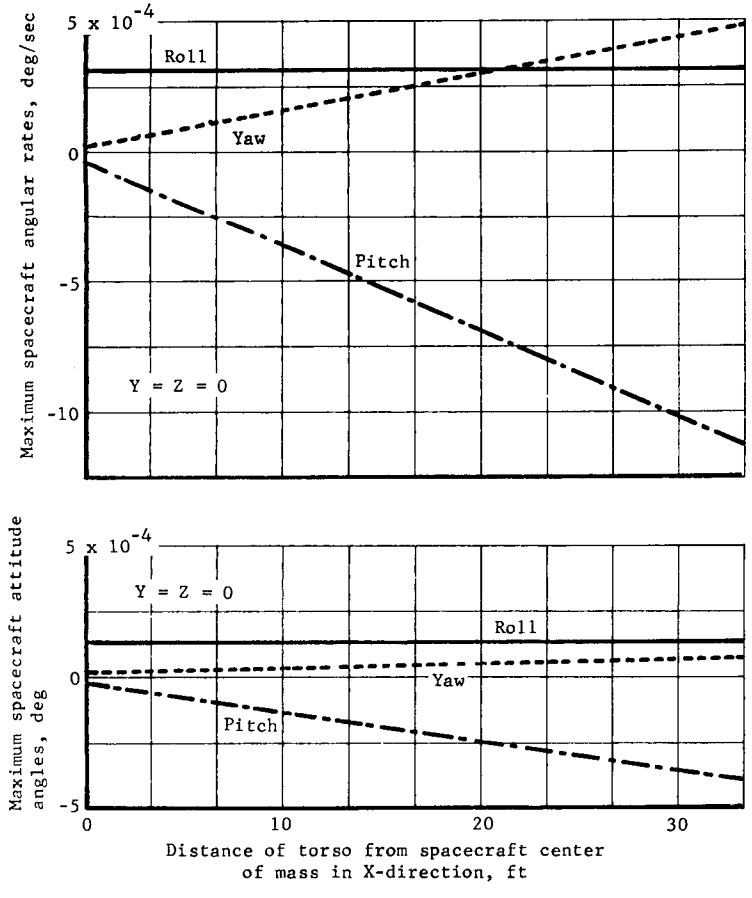

Figure 39.- Spacecraft Disturbances due to Simple Arm Motion Midway between Sagittal and Frontal Plane, Configuration 3

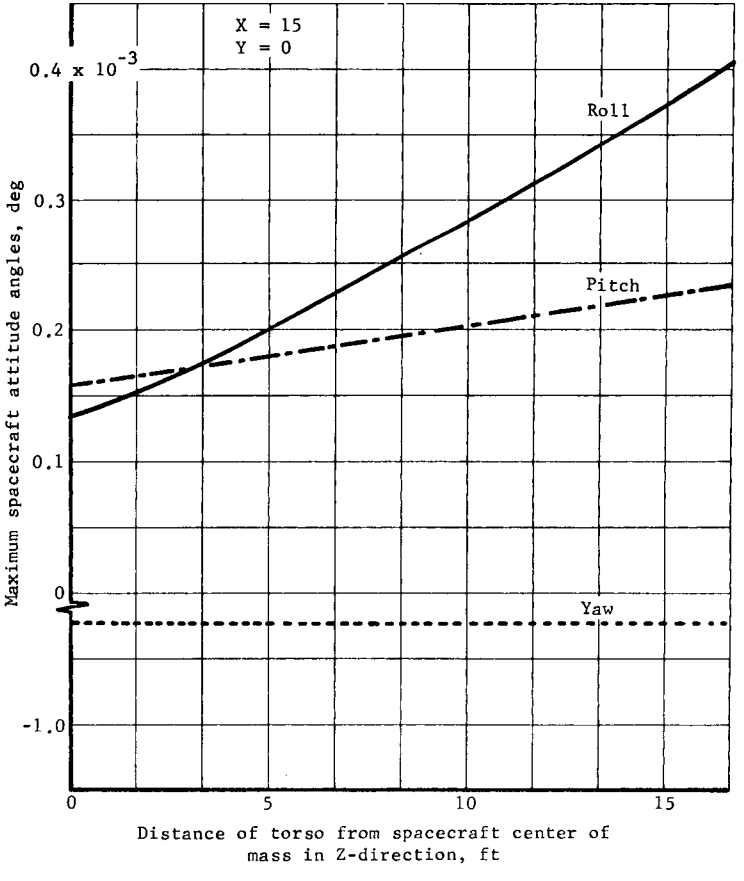

Figure 40.- Spacecraft Attitude Disturbances due to Simple Arm Motion Midway between Sagittal and Frontal Plane, Configuration 3

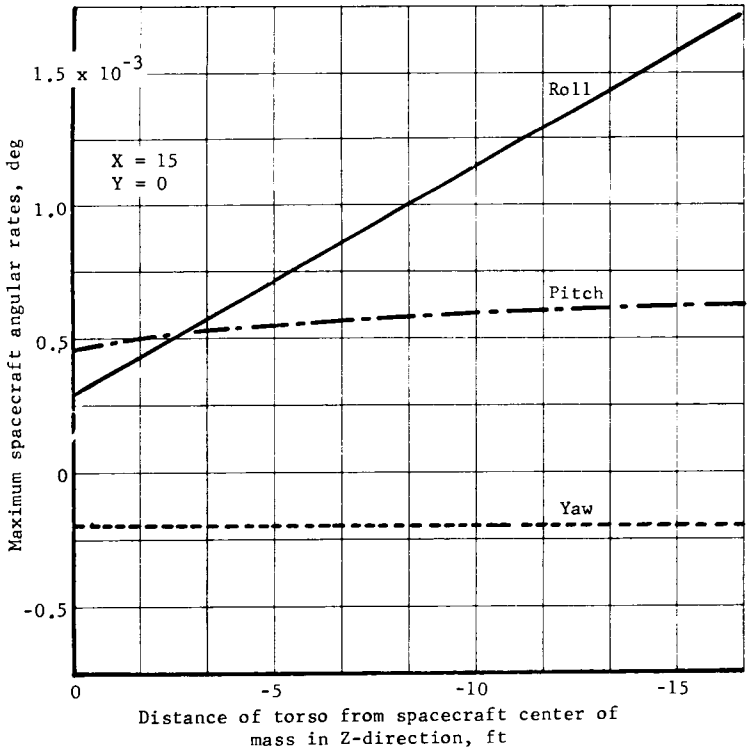

Figure 41.- Spacecraft Rate Disturbances due to Simple Arm Motion Midway between Sagittal and Frontal Plane, Configuration 3

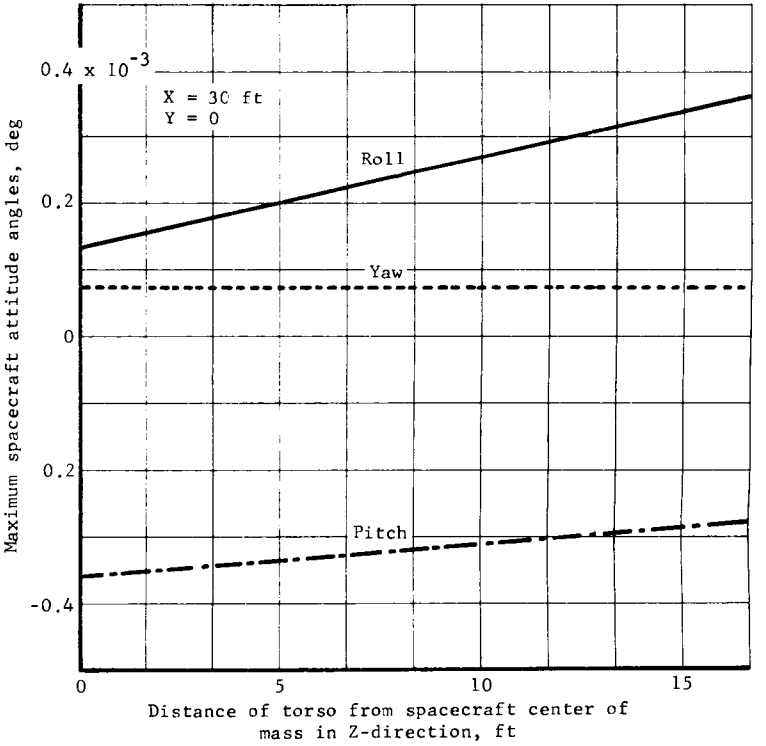

Figure 42.- Spacecraft Attitude Disturbances due to Simple Arm Motion Midway between Sagittal and Frontal Plane, Configuration 3

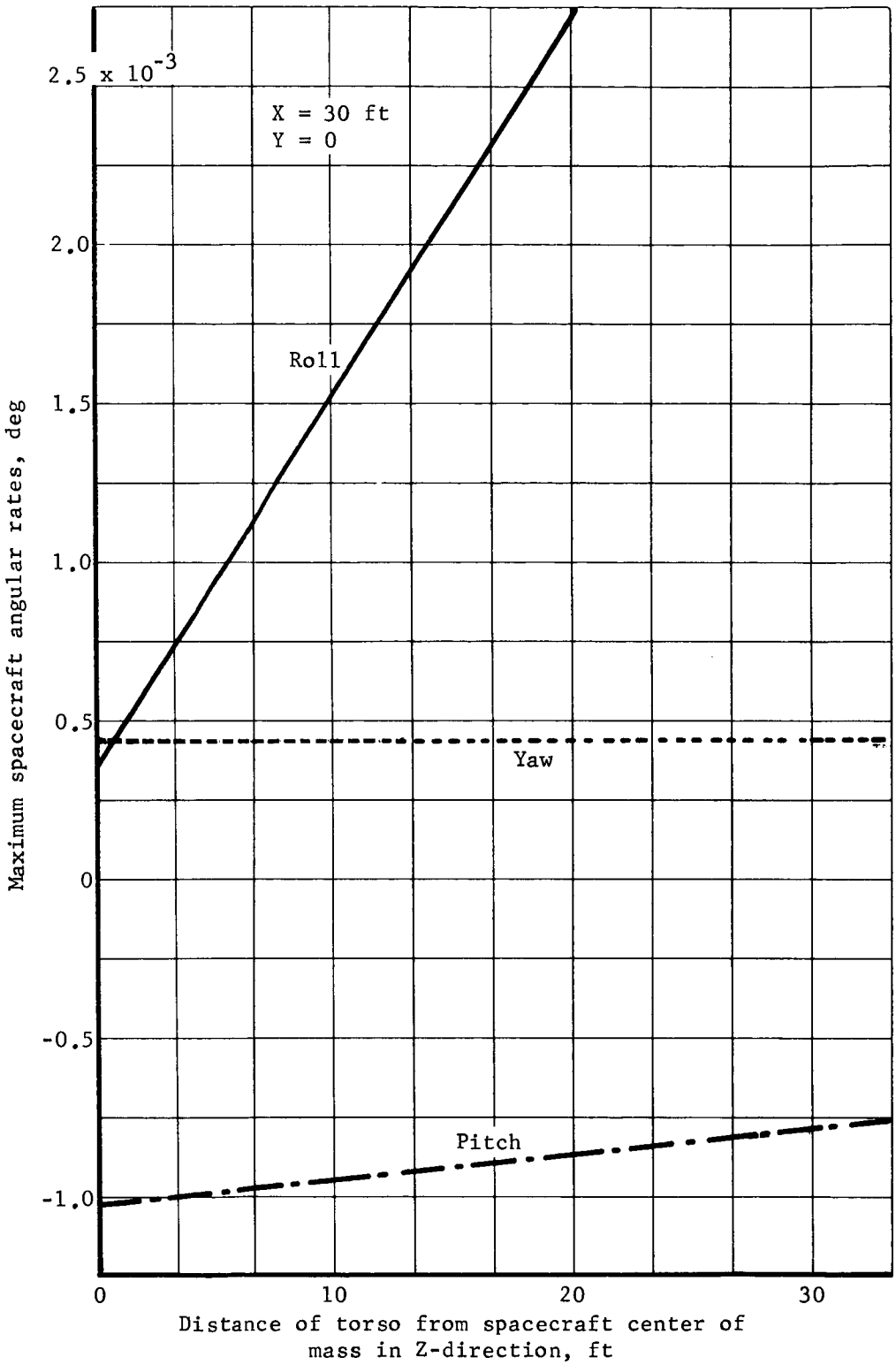

Figure 43.- Spacecraft Rate Disturbances due to Simple Arm Motion Midway between Sagittal and Frontal Plane, Configuration 3

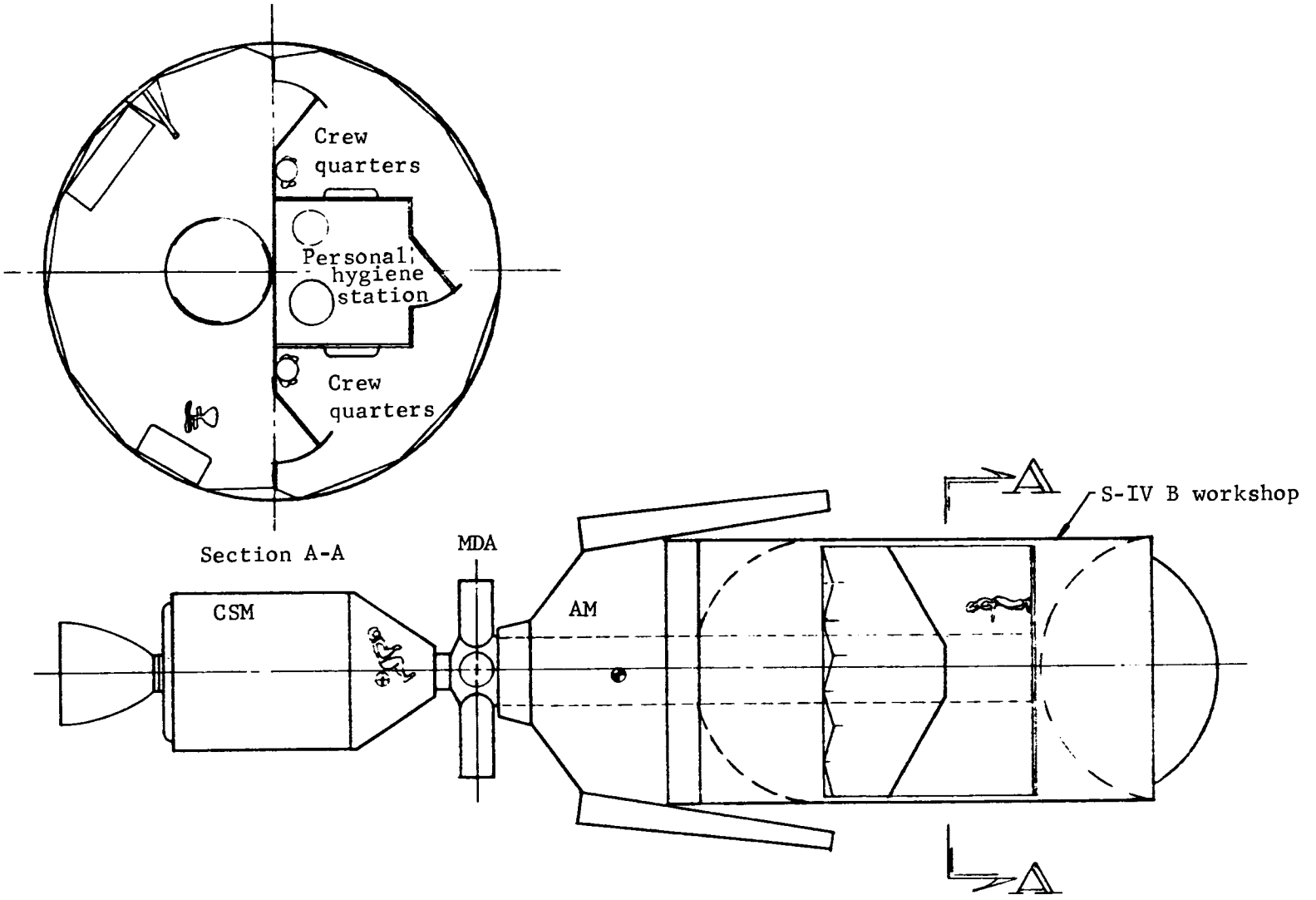

Figure 44.-Inboard Profile of Orbital Vehicle Configuration Flight 1/2

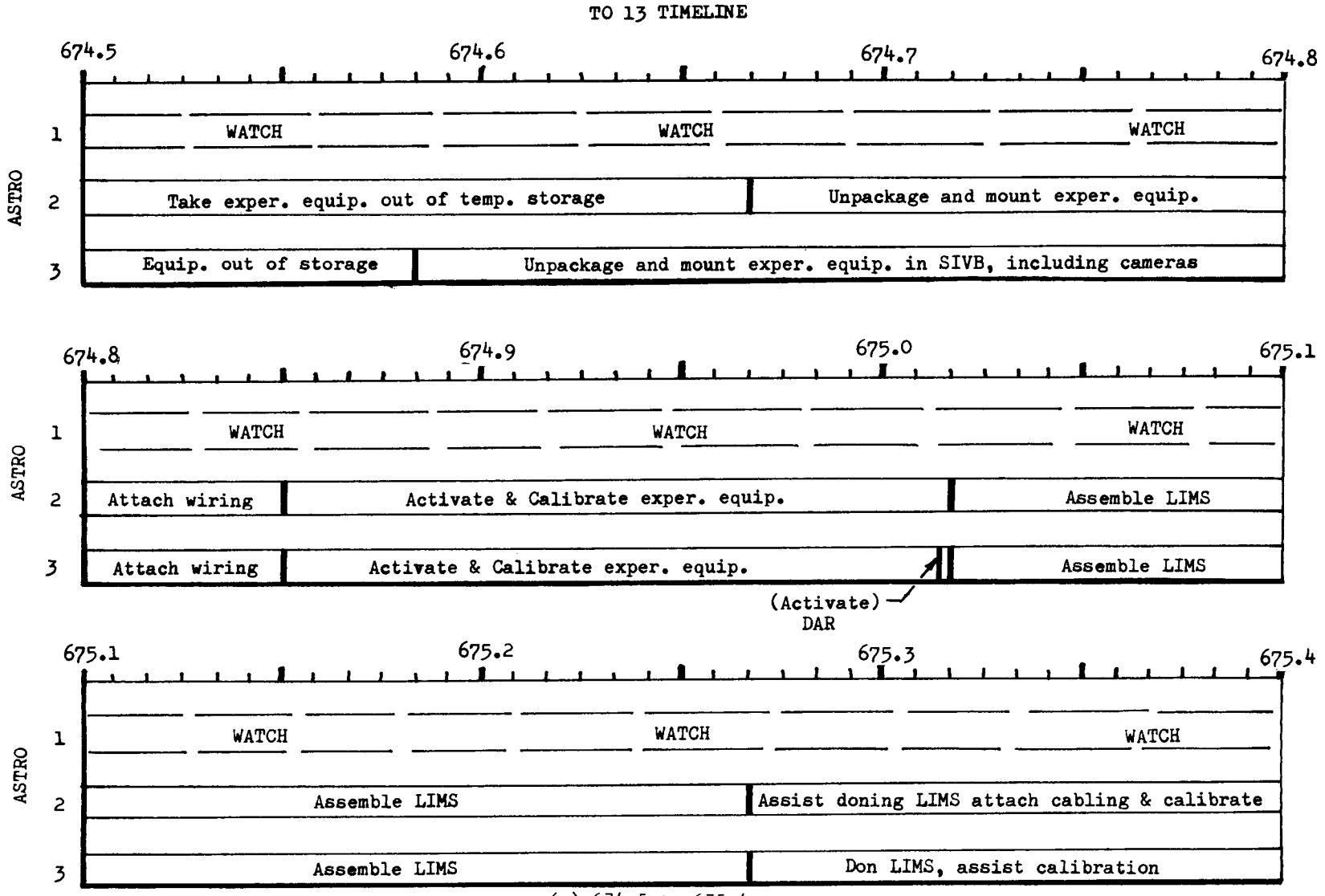

(a) 674.5 to 675.4

Figure 45.-Preliminary Experiment TO13 Timeline

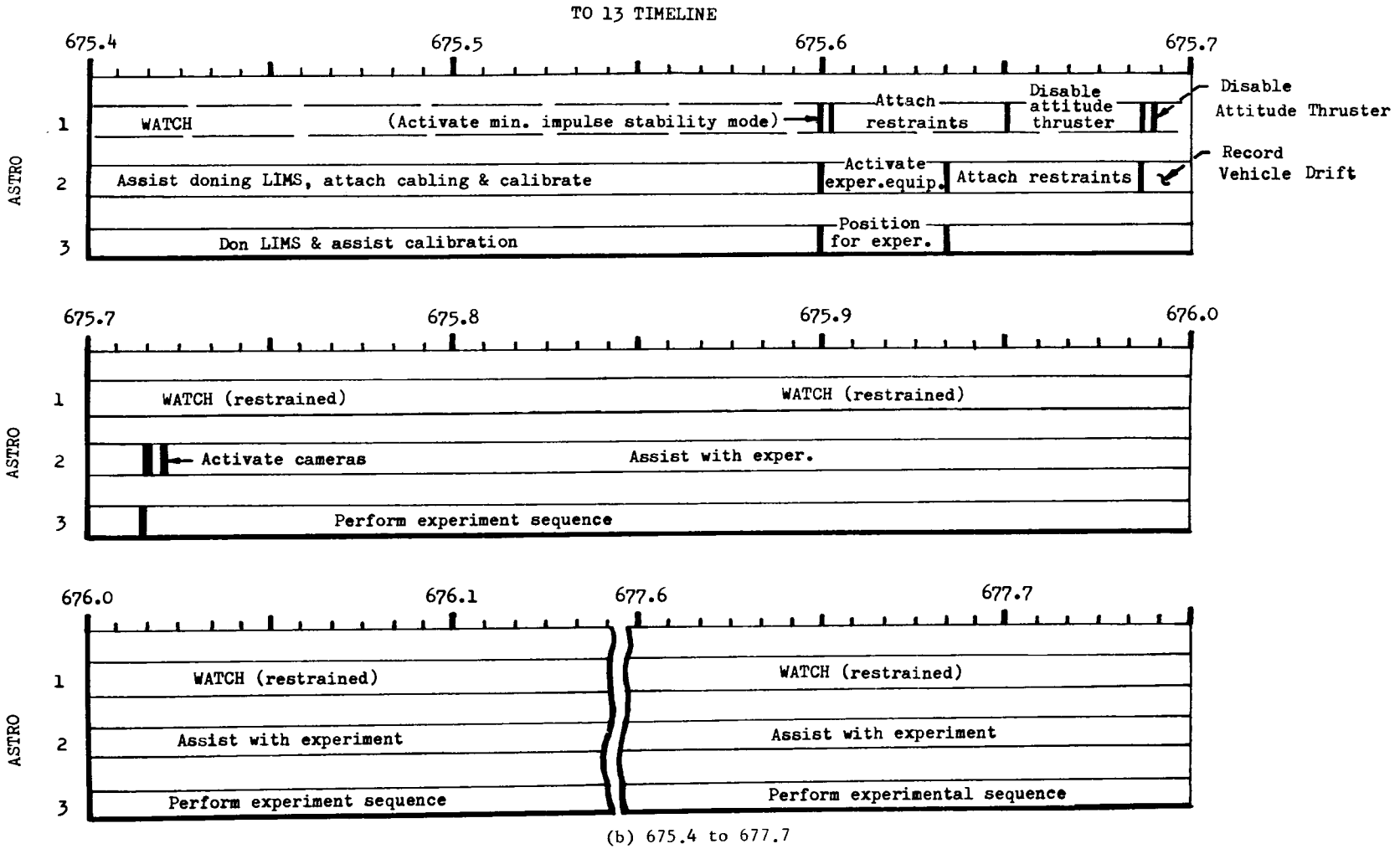

(b) 675.4 to 677.7

Figure 45.-Continued.

TO 13 TIMELINE

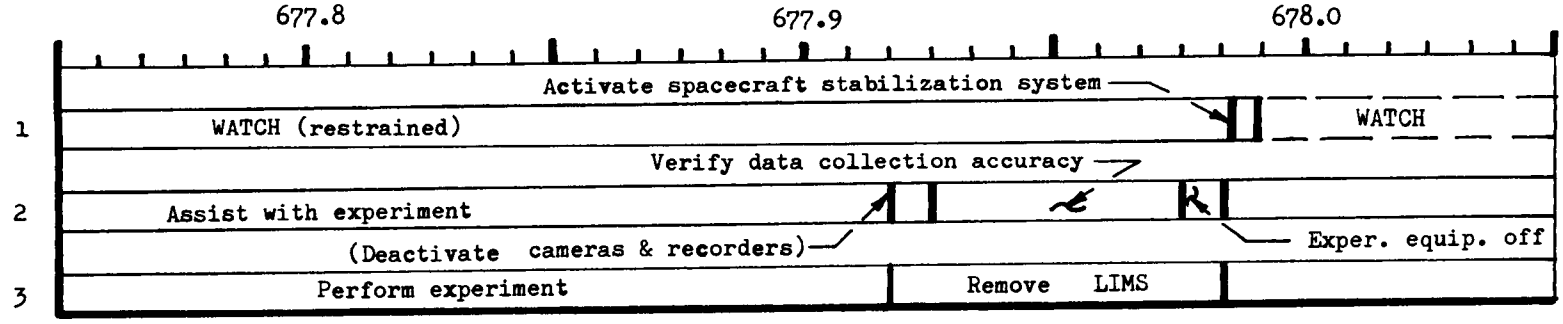

(c) 677.8 to 678.0

Figure 45.-Concluded.

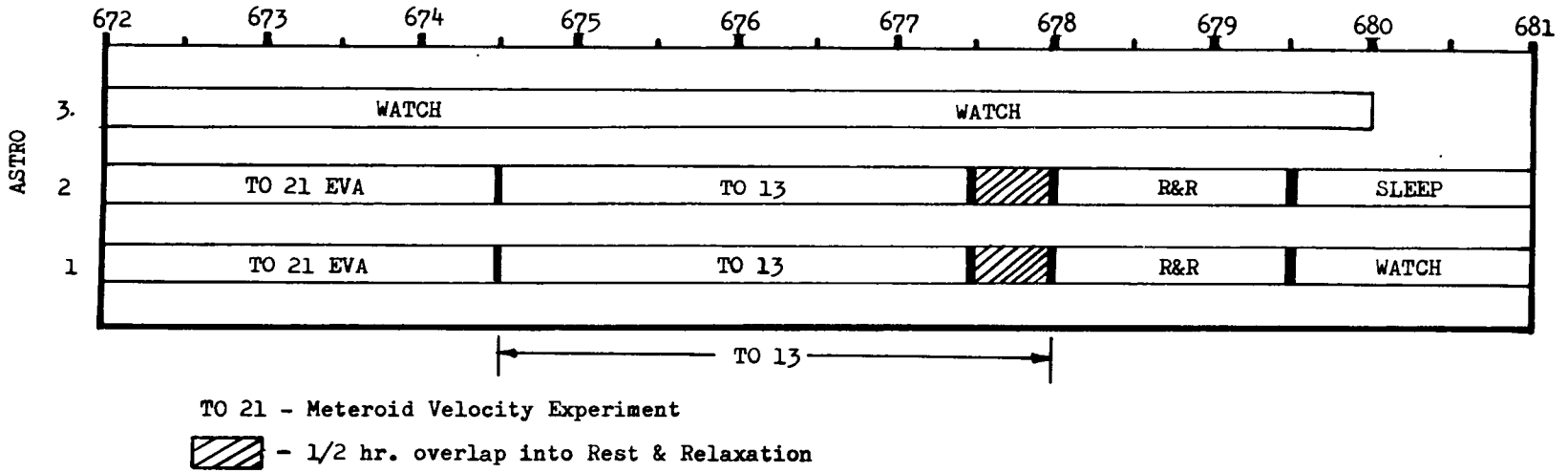

Figure 46.-Flight AAP 2, T013 Experiment Compatibility Timeline, Day 29

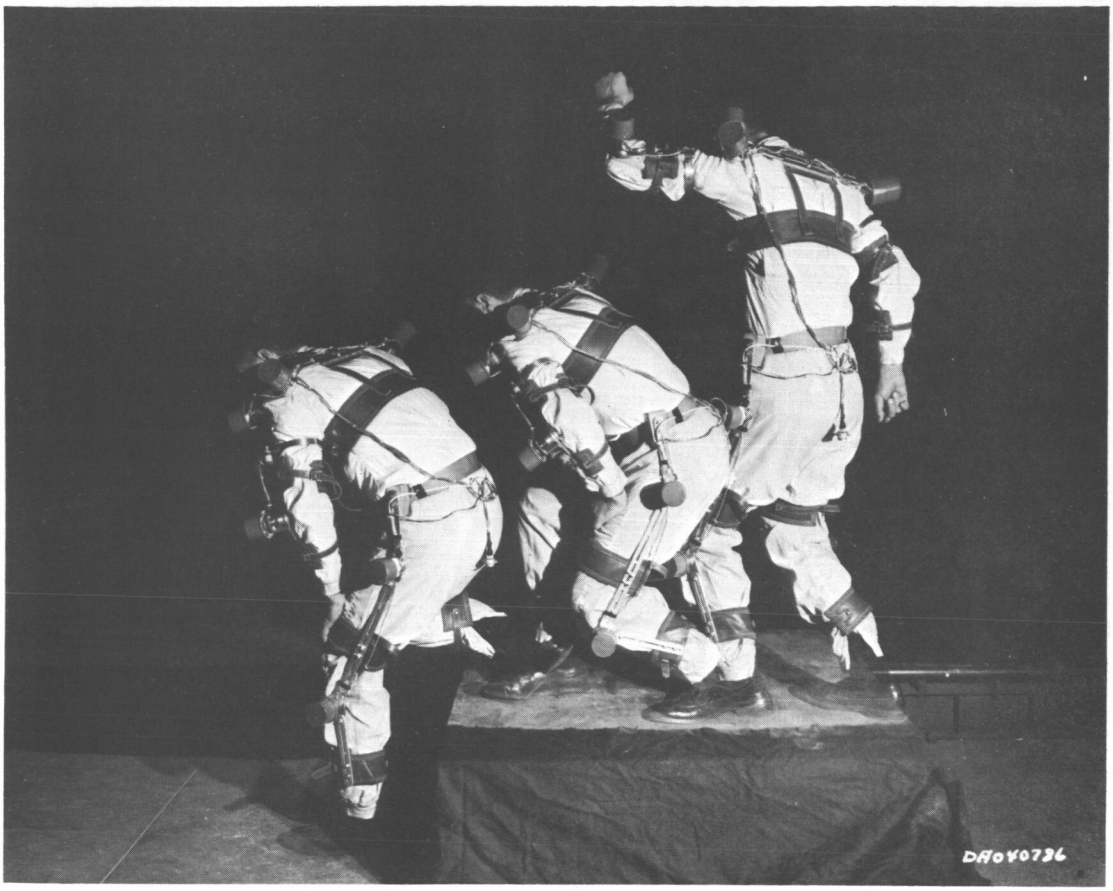

Figure 47.-LIMS Mobility

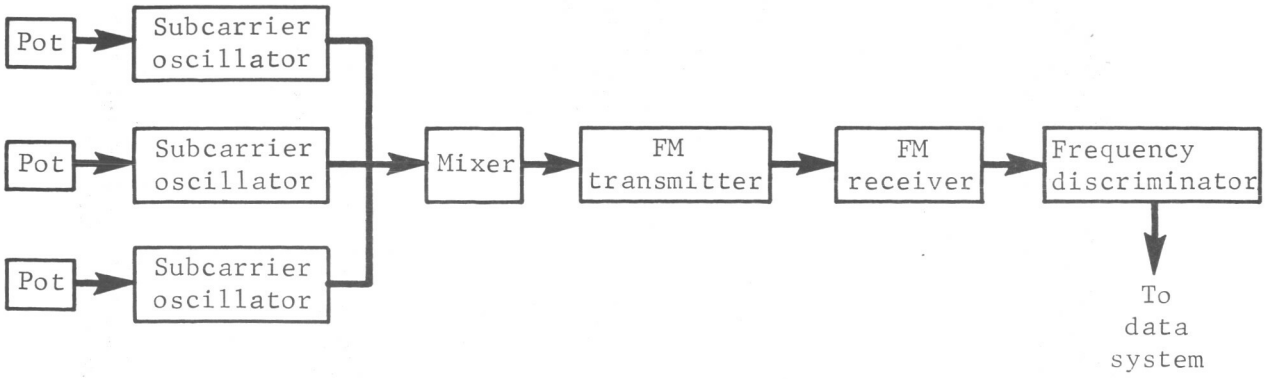

Figure 48.-FM/FM Telemetry System

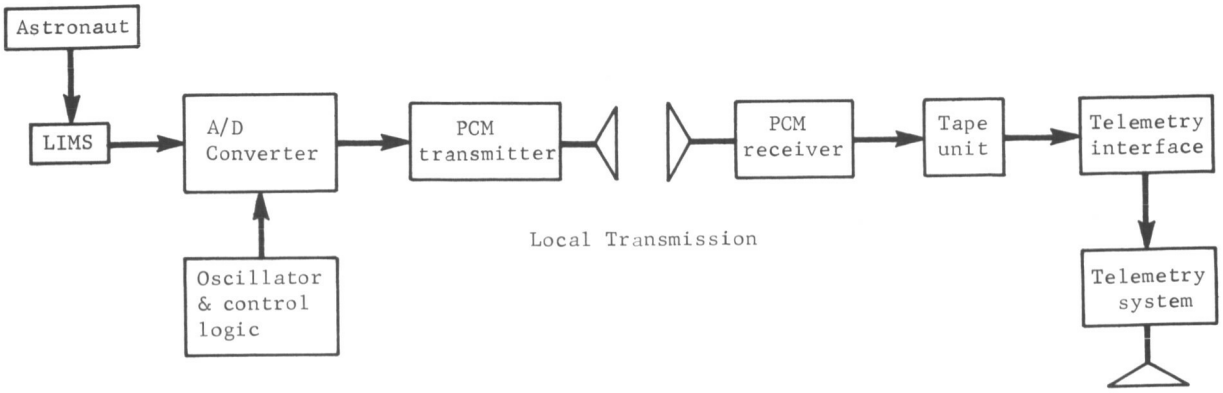

Figure 49.-PCM System

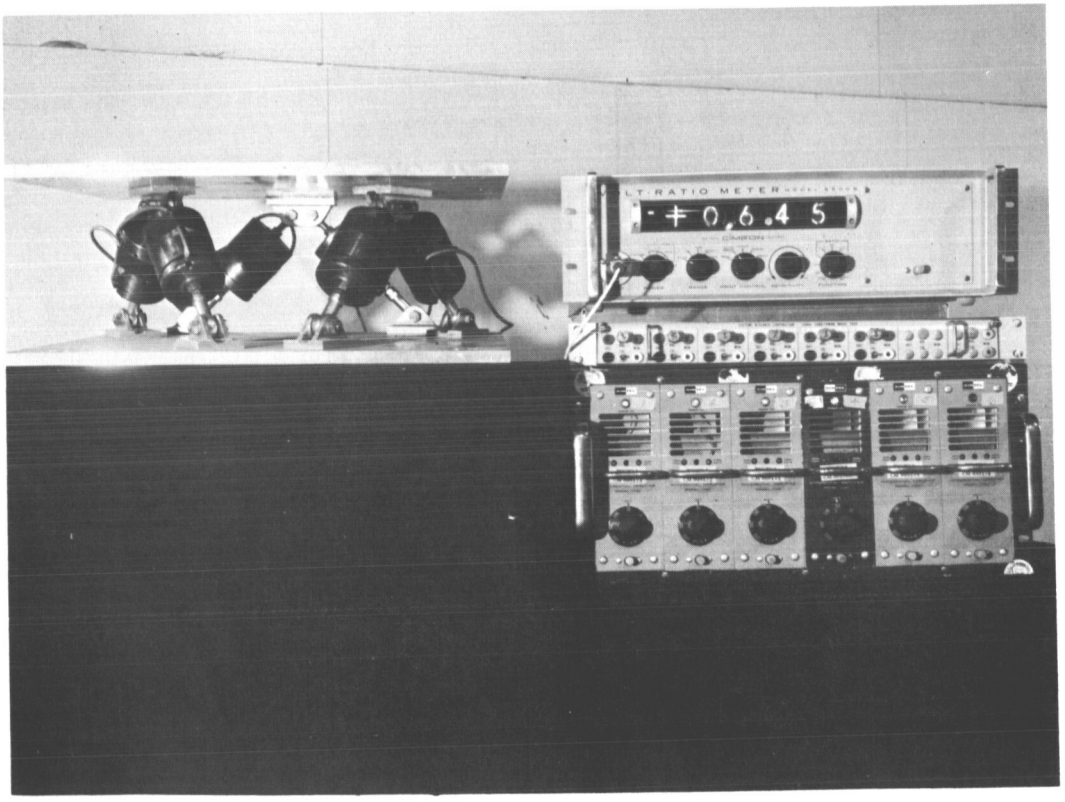

Figure 50.-Load Cell Array and Amplifiers

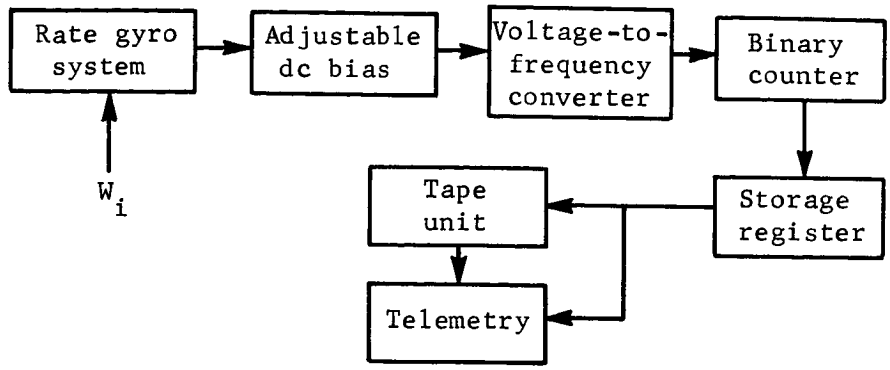

Figure 51.-Rate Gyro System

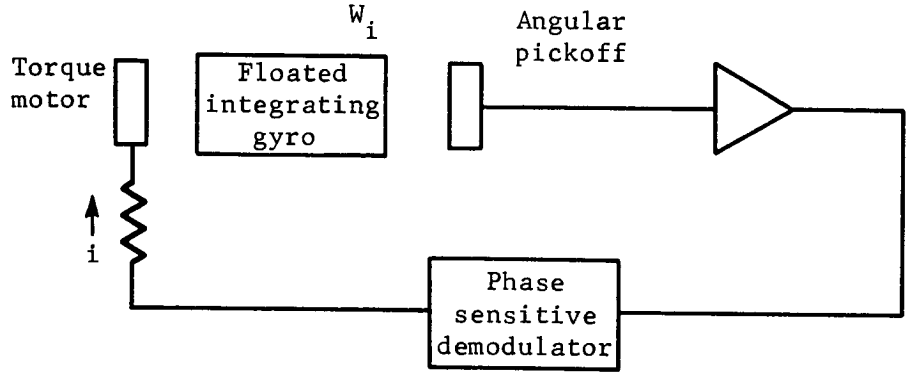

Figure 52.-Rate Gyro Loop

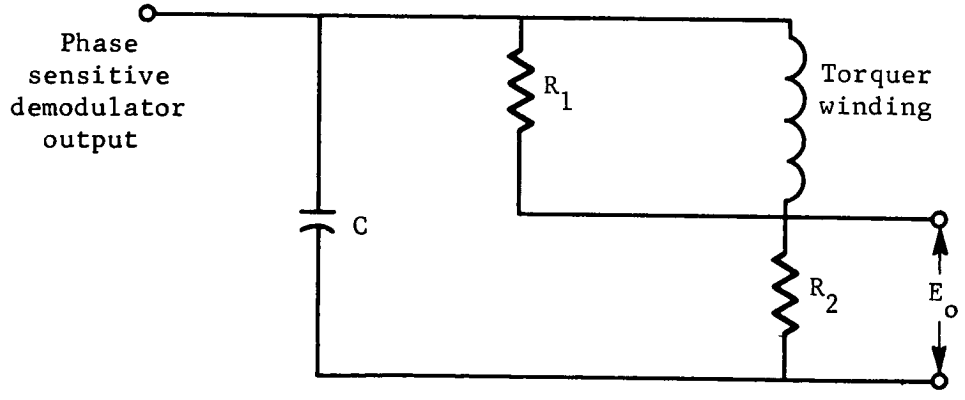

Figure 53.-Rate Gyro Output Circuit

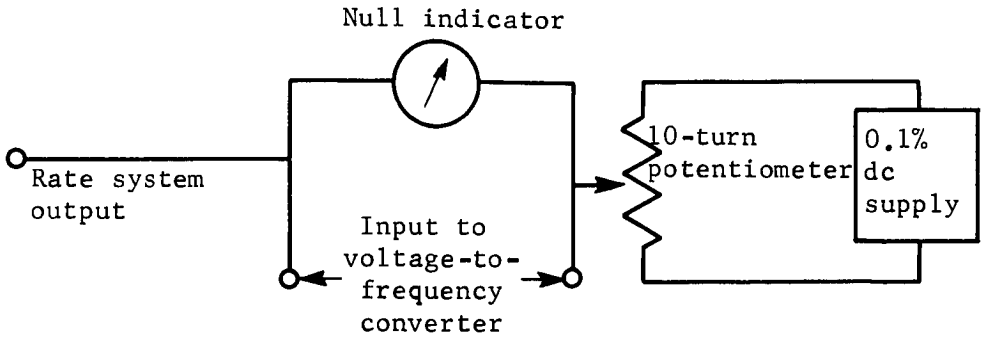

Figure 54.-Adjustable dc Bias

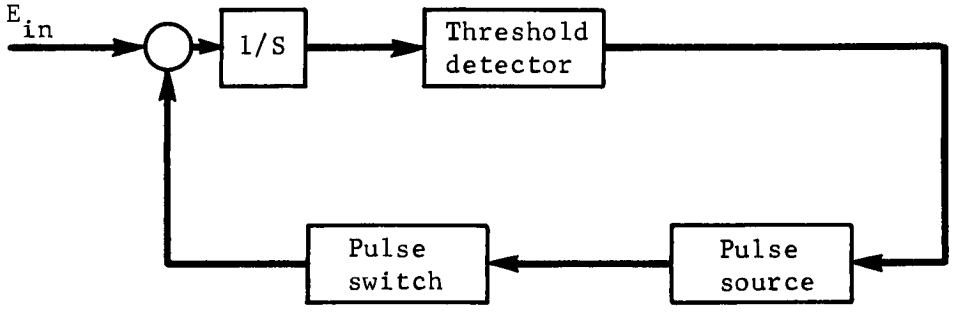

Figure 55.-Voltage-to-Frequency Converter

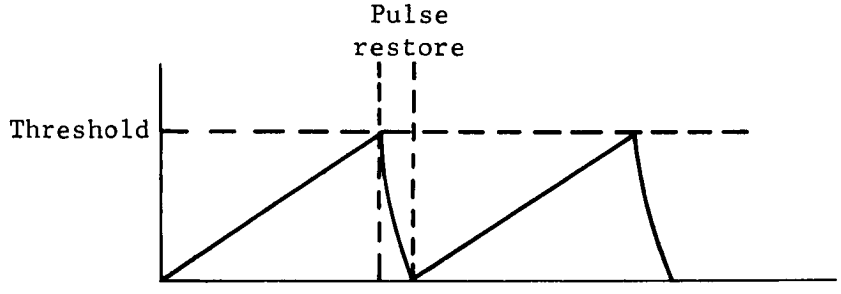

Figure 56.-Integrator Output

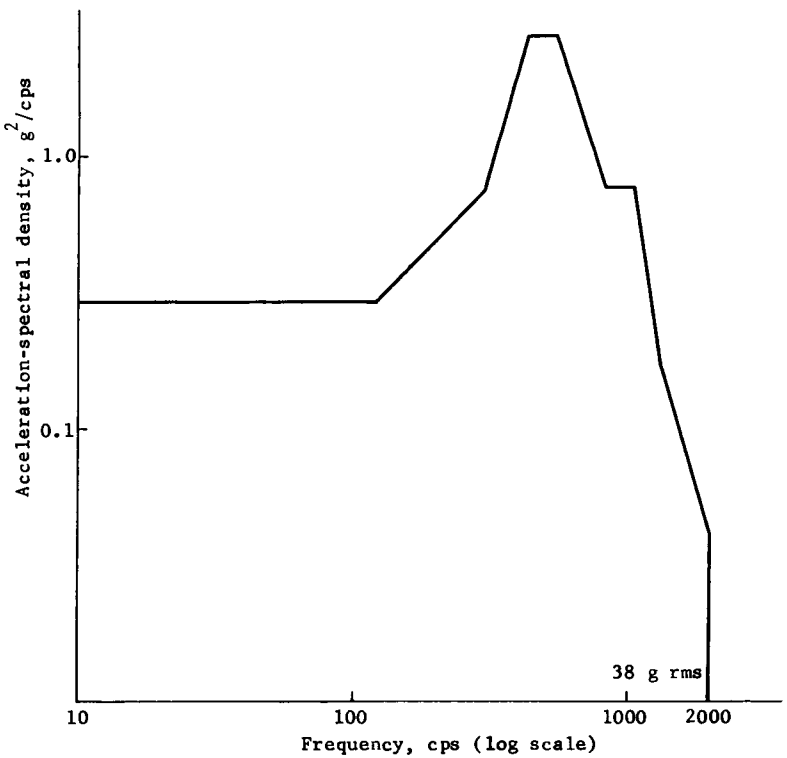

Figure 57.-Random Vibration Spectrum, Rate Gyro System

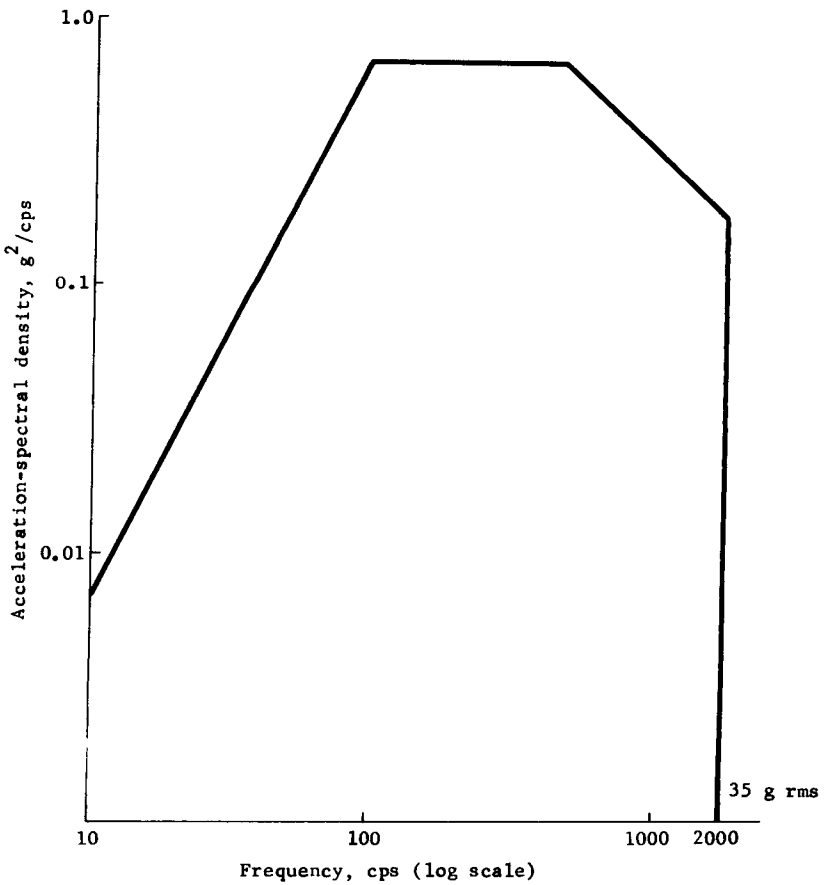

Figure 58.-Random Vibration Spectrum, Command Module

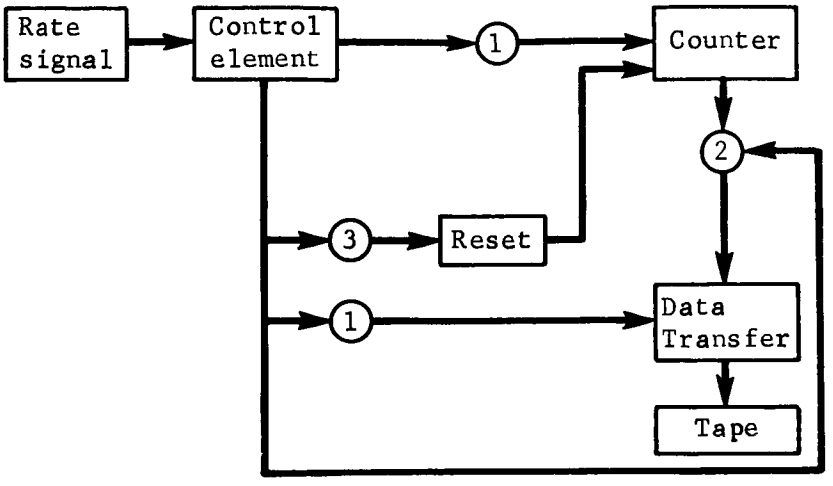

Figure 59.-Digital Output Diagram

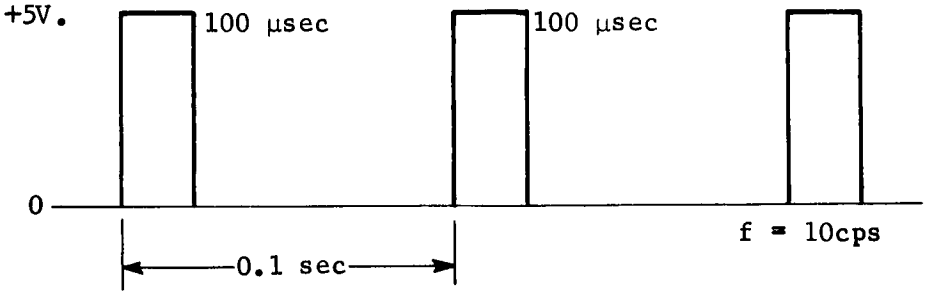

Figure 60.-Control Element Output

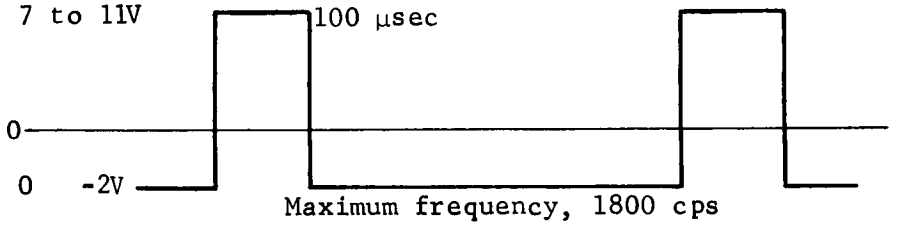

Figure 61.-Pulse Wave Form

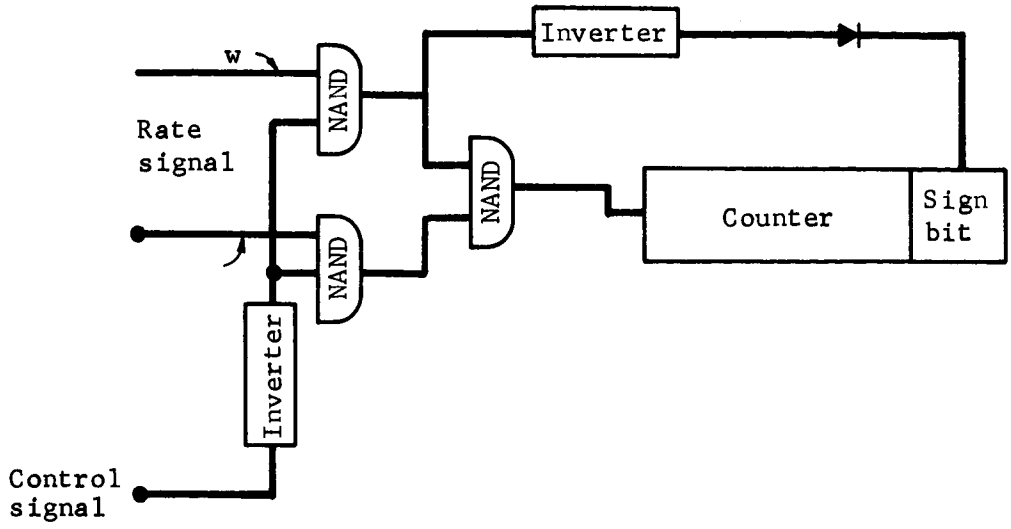

Figure 62.-Counter Logic Nine-Bit Counter

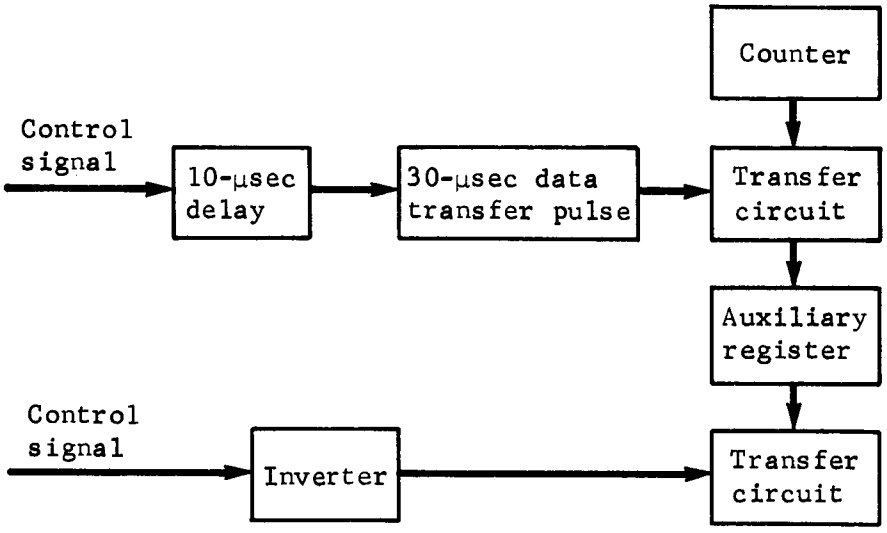

Figure 63.-Data Transfer Block Diagram

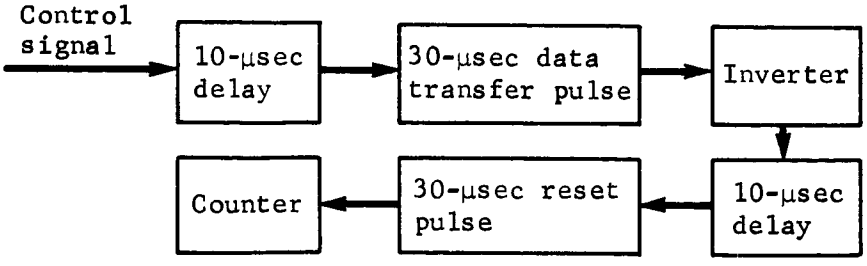

Figure 64.-Counter Reset Block Diagram

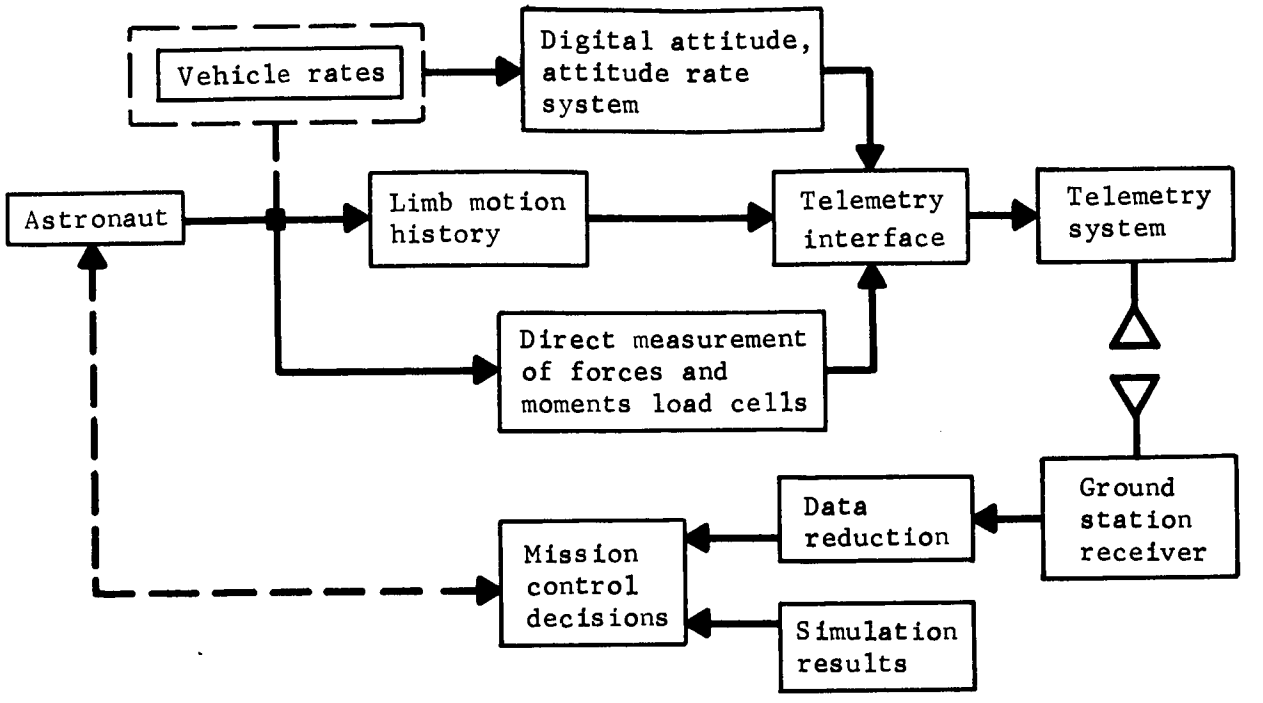

Figure 65.-Total Instrumentation Scheme

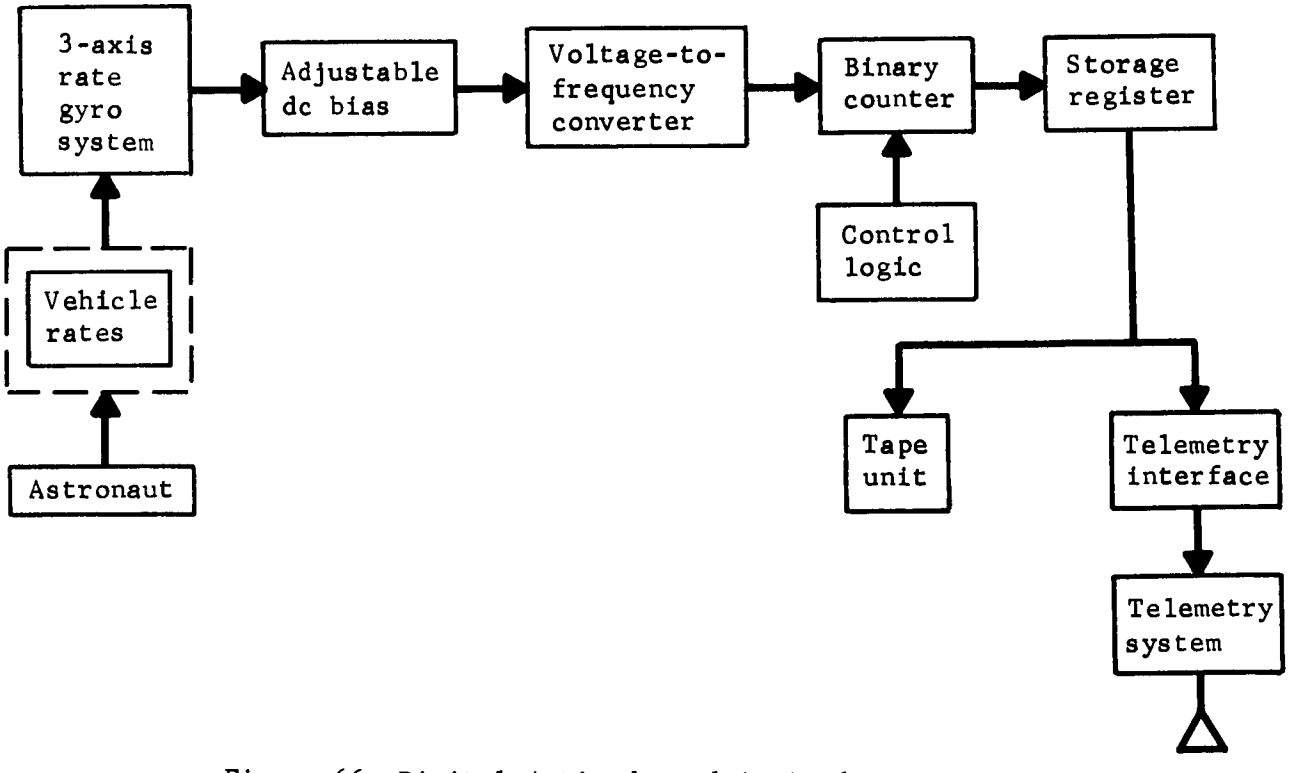

Figure 66.-Digital Attitude and Attitude Rate System

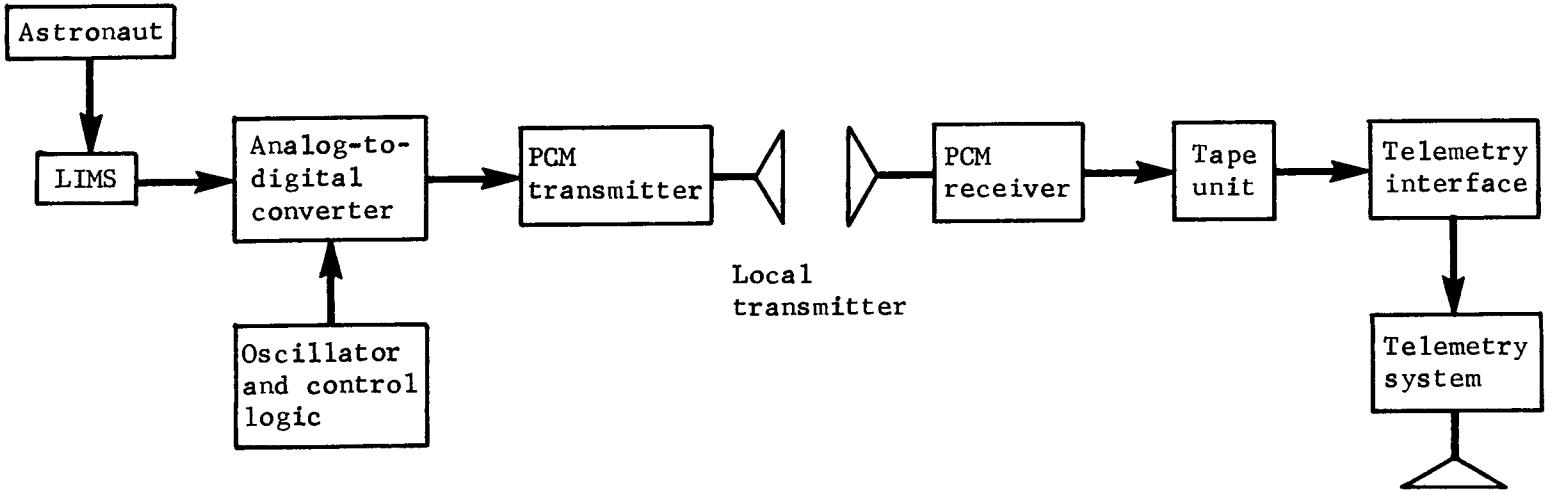

Figure 67.-Limb Motion Sensor (LIMS) System

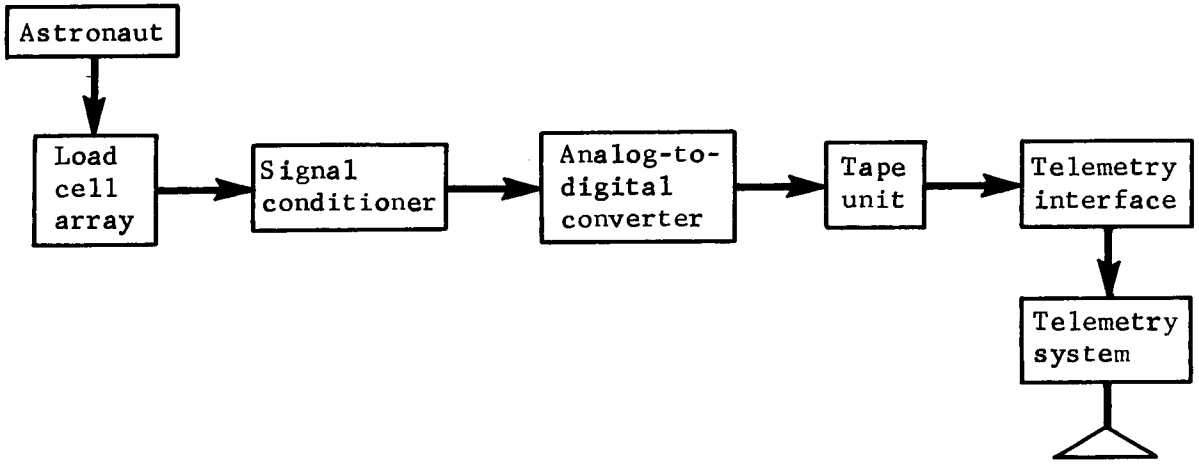

Figure 68.-Direct Measurement of Forces and Moments Block Diagram

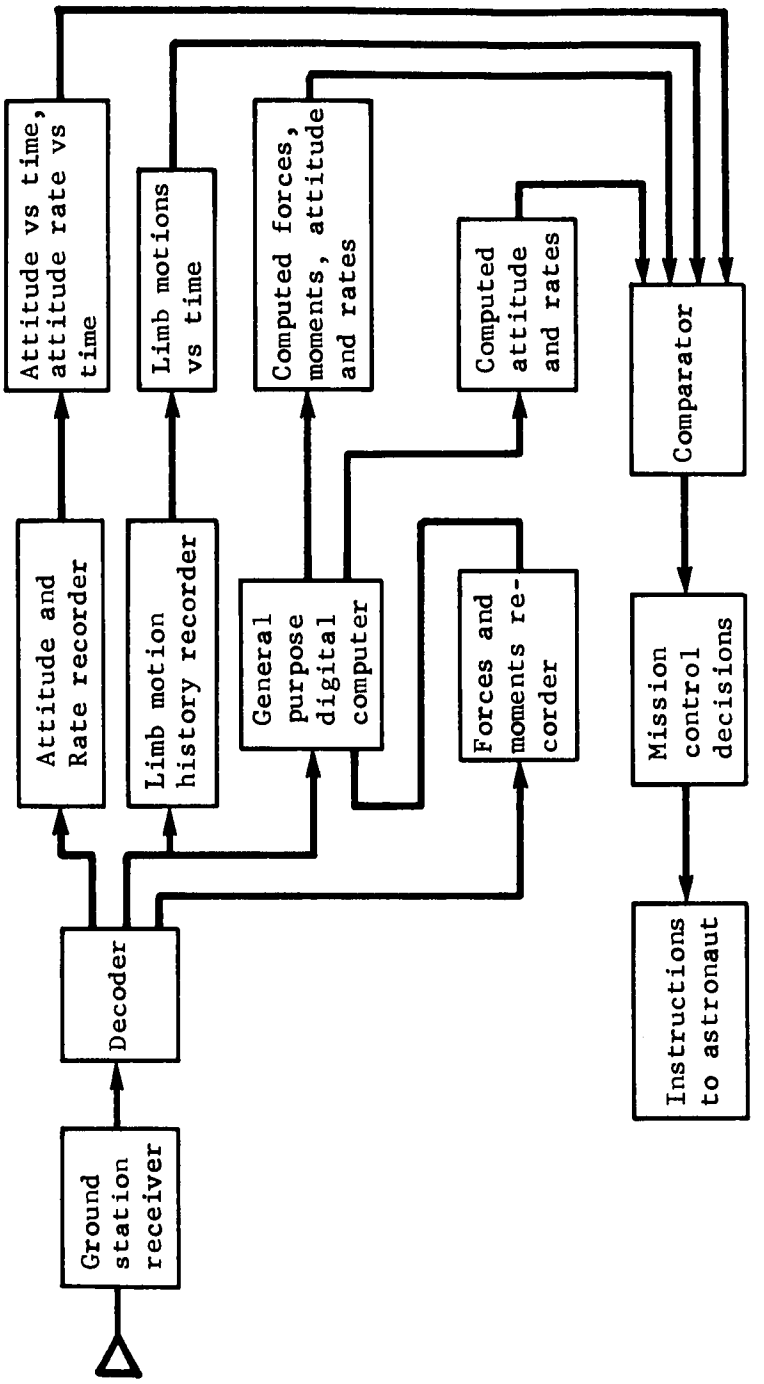

Figure 69.-Ground Support Equipment

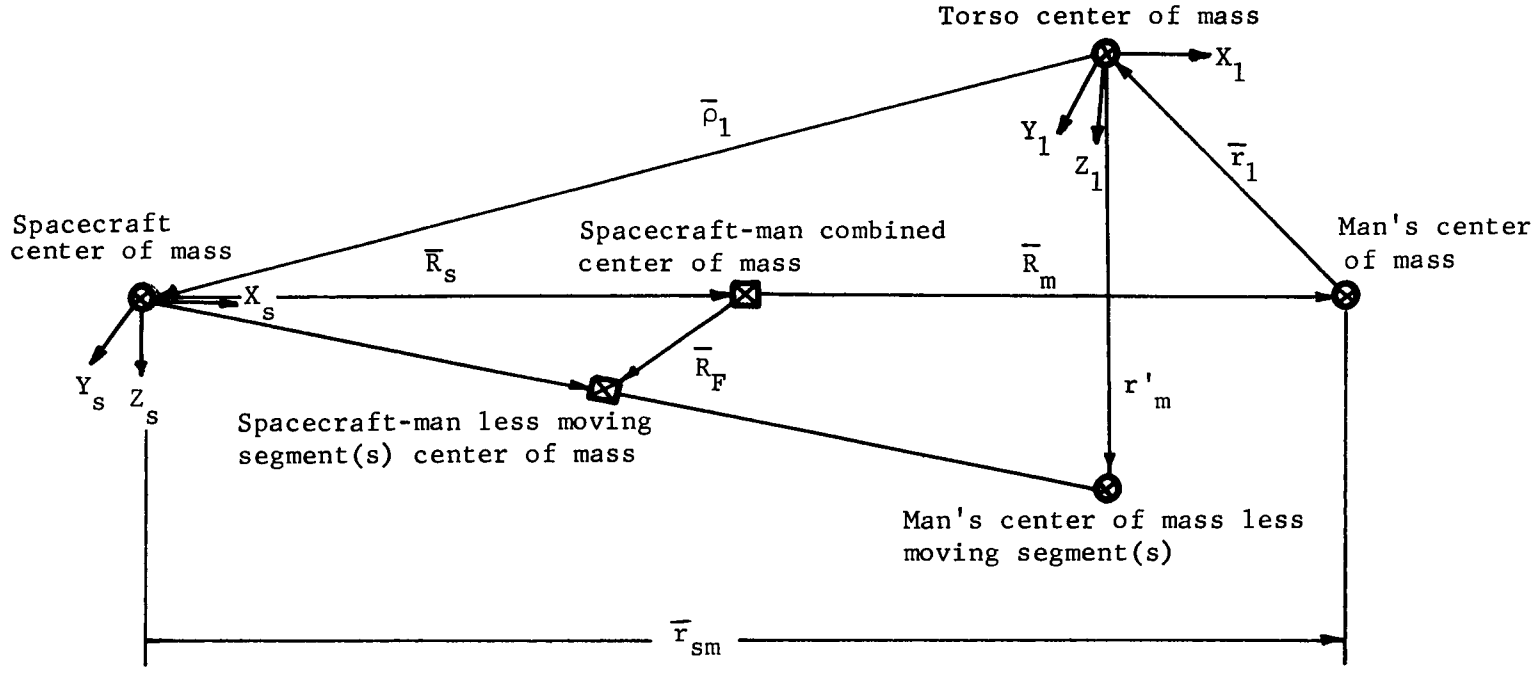

Figure A-1.-Reference Axes System

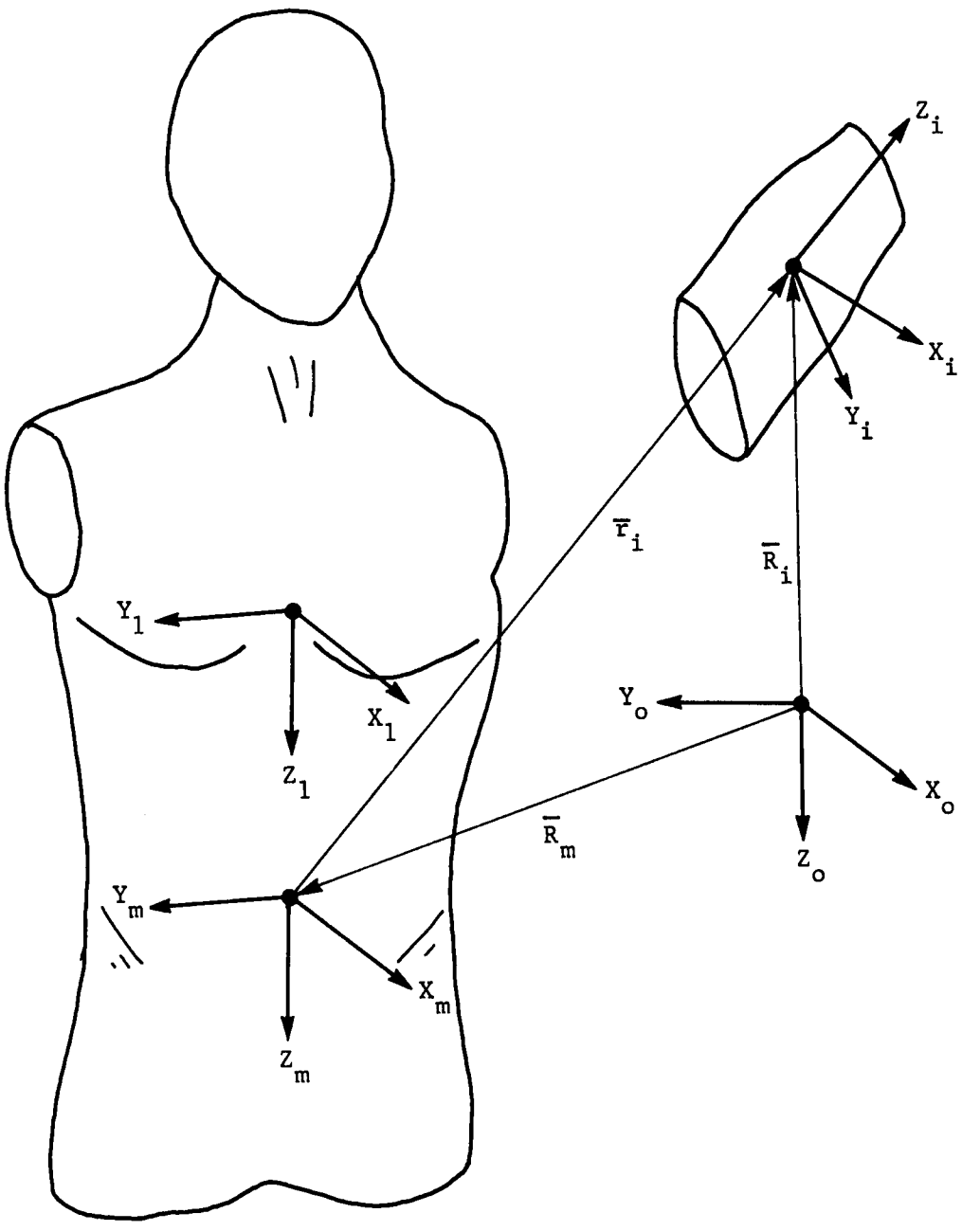

Figure A-2.-Segment Coordinate Systems

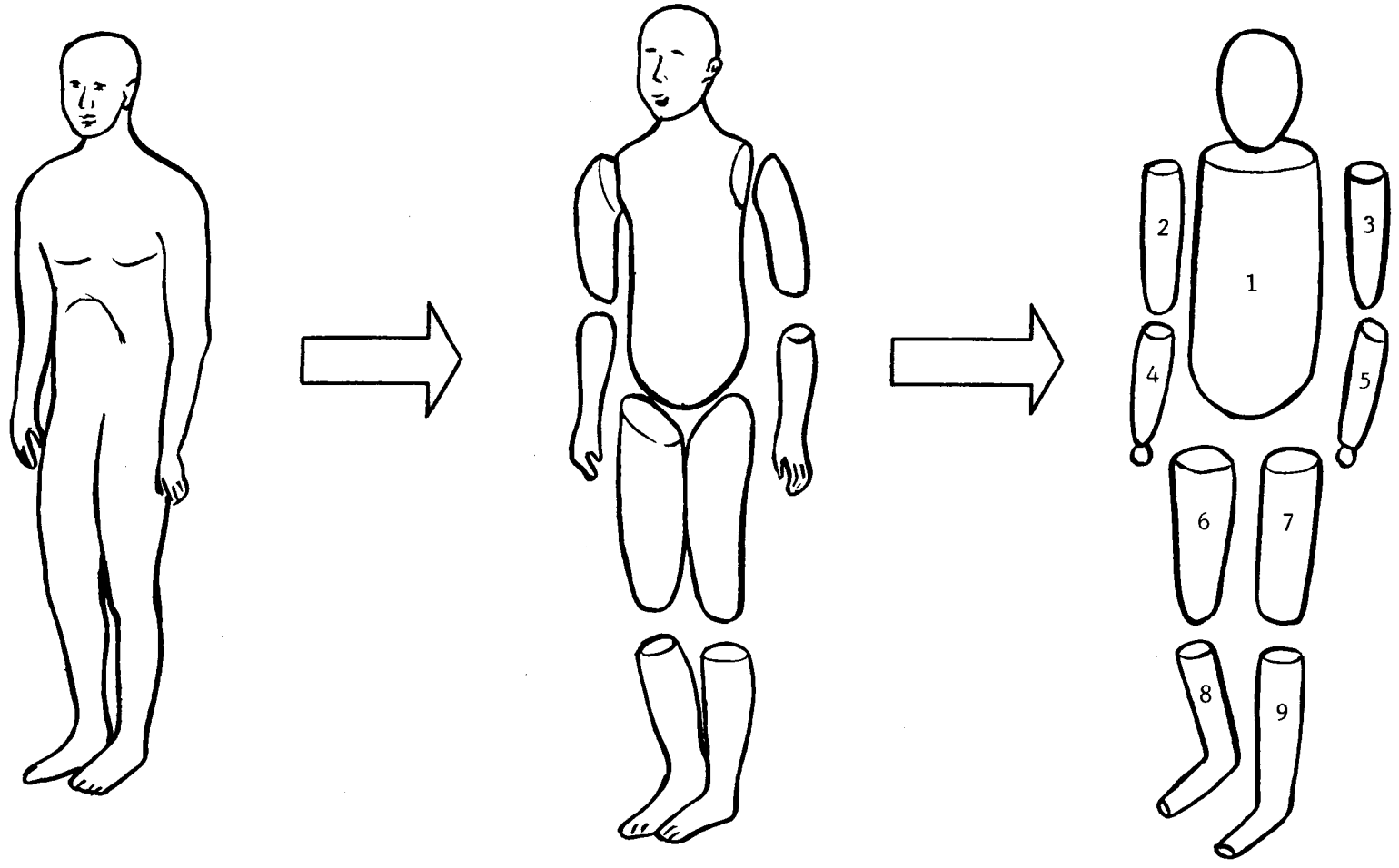

Figure A-3.-Mathematical Model of Man

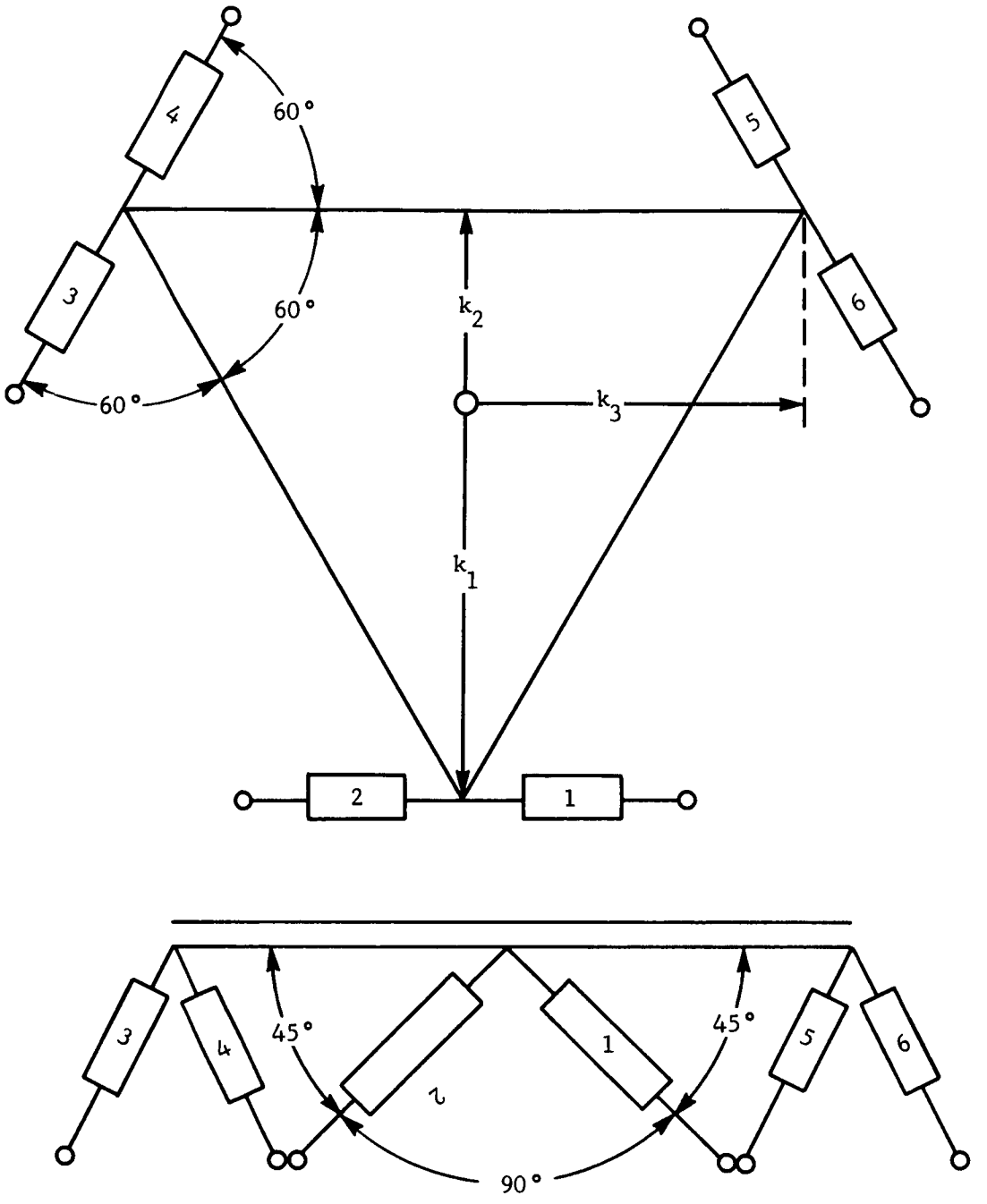

Figure A-4.-Load Cell Array Configuration

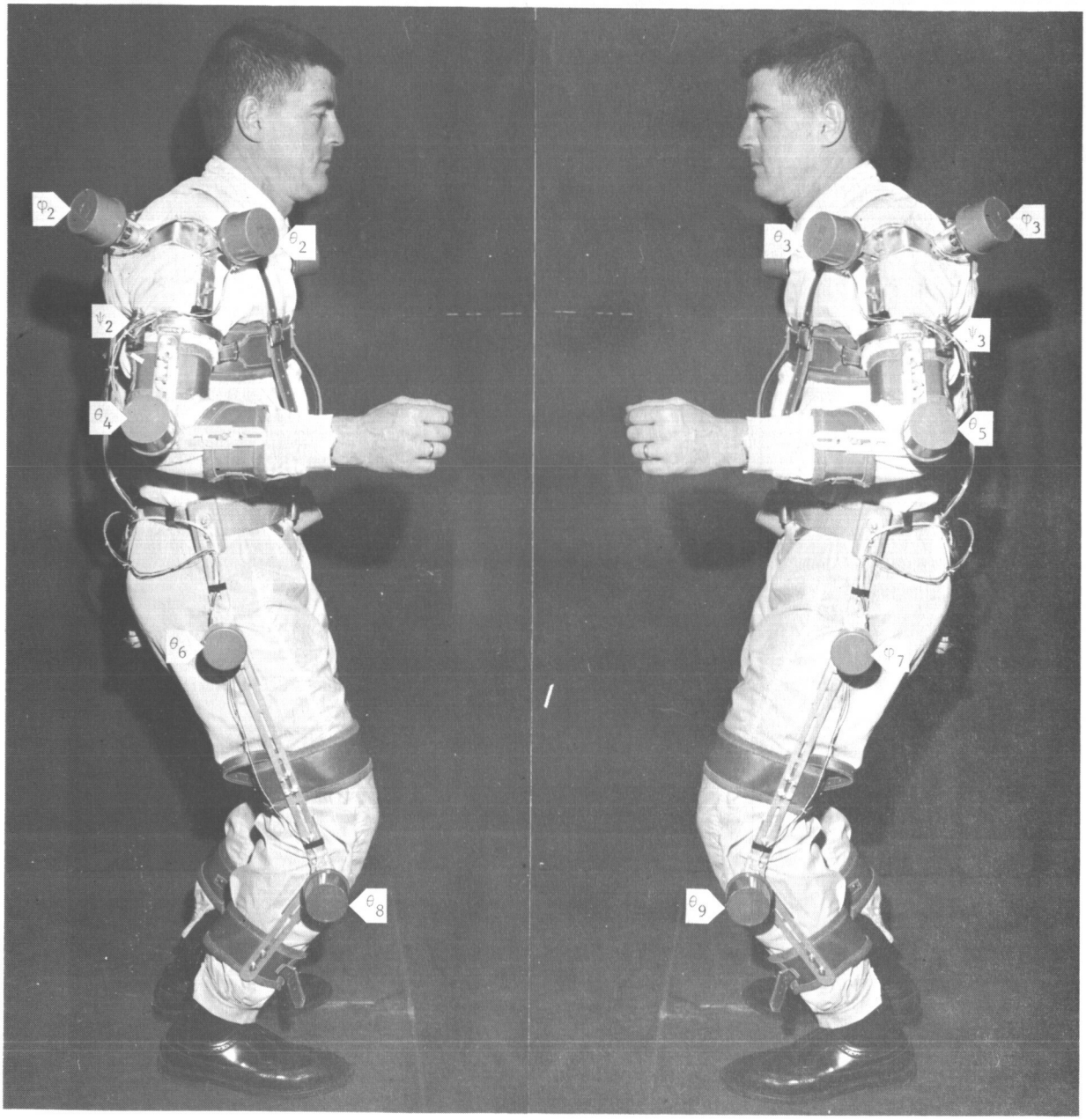

Figure A-5.-LIMS Potentiometer Designation

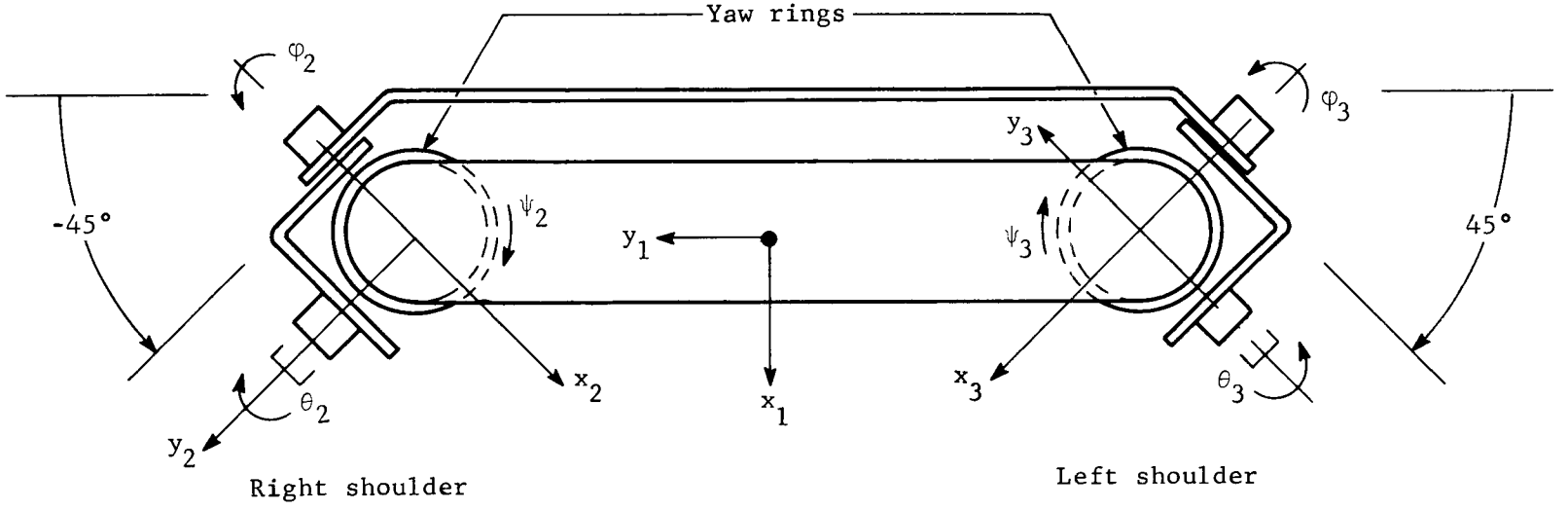

Figure A-6.-LIMS Shoulder Joint

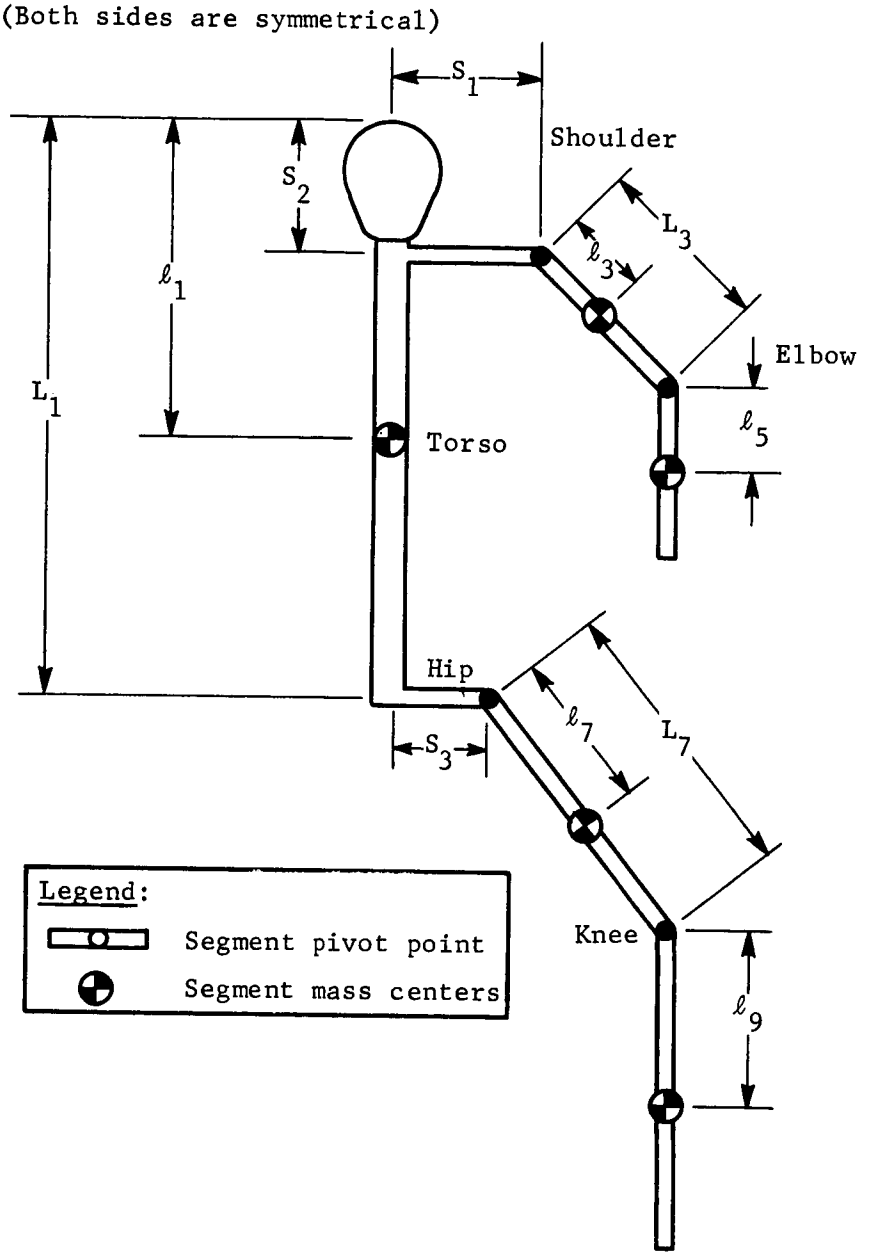

Figure A-7.-Segmental Model of Man

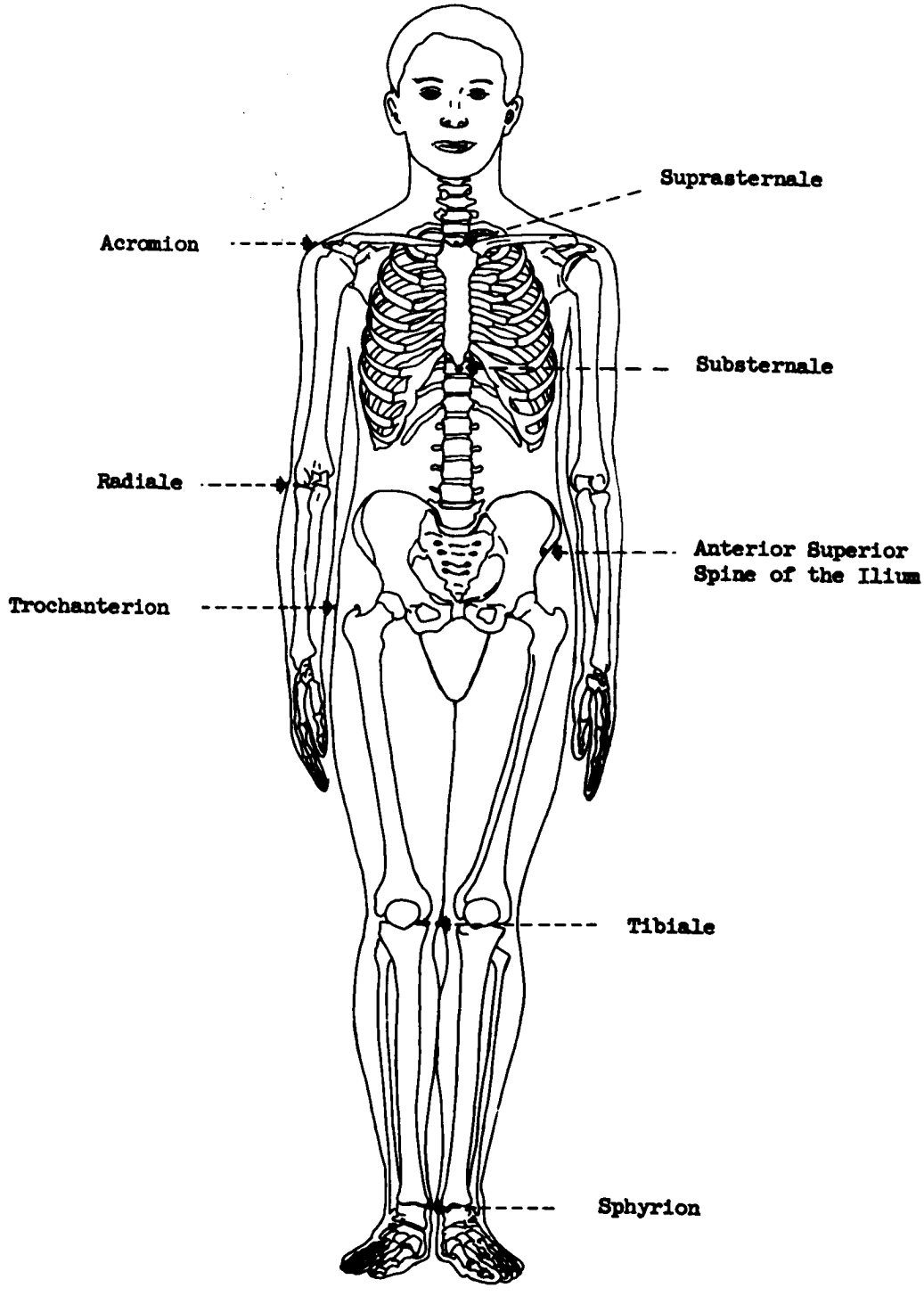

Fig. G-1.-Skeletal Anthropometric Points